Utrecht University
Faculty of Physics and Astronomy

The influence of impurities on equilibrium crystal shapes

Martin Bootsma

January 2001

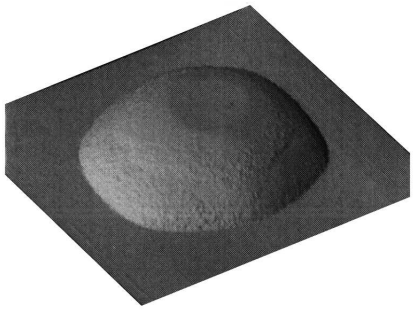

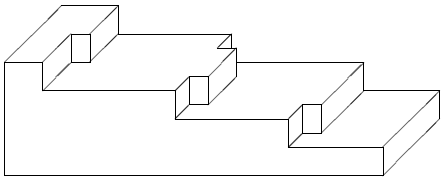

Report number: ITF-UU-2001/02
Supervisor: Prof. dr. H. van Beijeren
Institute for Theoretical Physics

The influence of impurities on equilibrium crystal shapes [1]

Martin Bootsma
Institute for Theoretical Physics, University of Utrecht
Princetonplein 5, 3584 CC Utrecht, The Netherlands

January 24, 2001

[1]Report number: ITF-UU-2001/02

Abstract

This thesis presents some aspect of the free energy of a step on a crystal. In particular, it deals with the width dependence of the free energy if the crystal contains impurities and the equilibrium crystal shape that arises from it.

Contents

Chapter 1

Introduction

In daily life, most of the things we get in touch with, are not in equilibrium, and we should be glad of that. Let's explain this statement. A system in equilibrium has the lowest free energy as possible. In the case of a metal object of a fixed number of atoms, the lowest free energy coincides with that configuration of the atoms with the lowest sum of the crystal free energy and the surface free energy. For a fixed number of atoms there is therefore only one equilibrium state. This means that an iron tool of a fixed mass, can only be in one form if it is in equilibrium, and therefore there would be no iron tools. Happily in daily life the temperature to cross the energy barrier between the actual configuration and the configuration with the lowest free energy is too high.

Nevertheless this doesn't mean that the equilibrium crystal shape (ECS) isn't important. Although it's rather difficult to bring a crystal in equilibrium (see [1] and references therein), the ECS contains information about various parameters. But let us describe first how an ECS can be constructed theoretically. Suppose we have a droplet of lead and we suppose that there are no forces working on it. As said before, in the equilibrium state the free energy is minimal. If the problem would be rotationally symmetric, this would mean that the the lead droplet wants to minimize its surface area and therefore the lead would organize in a sphere. But the world isn't that easy. Lead atoms are organized in a lattice structure. Therefore the surface free energy depends on the orientation of the surface. If we know for a macroscopically flat surface the surface tension, which is orientation dependent, the equilibrium crystal shape is given through the Wulff construction [2],[3]. Therefore we would like to know the surface free energy for all orientations. Suppose we have a surface which makes a tiny angle with respect to a facet, such an interface is called a vicinal interface. (A facet is an interface which is macroscopically flat, usually its orientation coincides with an axis of symmetry of the lattice.) If we look microscopically at such a vicinal surface, we see the following: At zero temperature the vicinal surface will look like a stair with regular distances between the steps, see Figure 1.1. This is the ground state. At higher temperatures there will be thermally induced fluctuations around the ground state and the stairs will exhibit kinks, see Figure 1.2. There is a temperature at which the fluctuations will be so frequent, that one cannot recognize the steps anymore. This is called the roughening

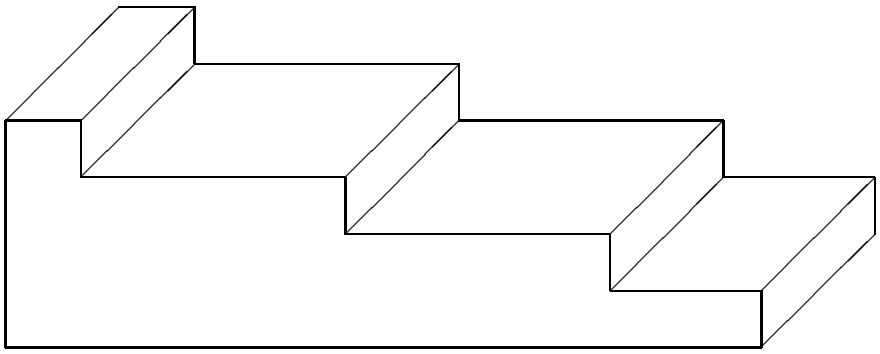

Figure 1.1: ground state of a vicinal surface

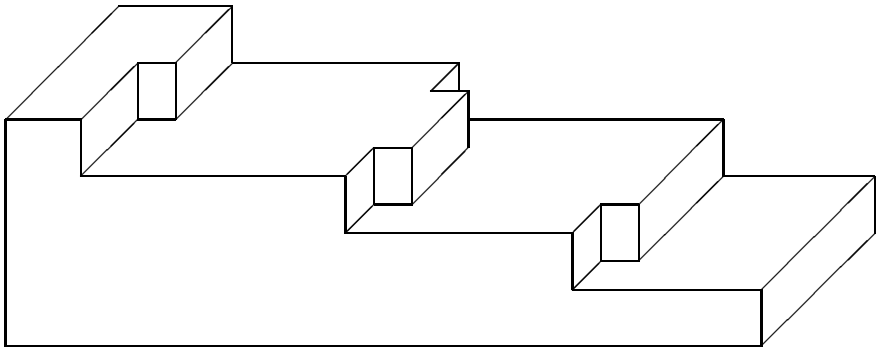

Figure 1.2: steps on a vicinal surface with thermally induced kinks

transition [2]. An interesting quantity to look at is the step free energy, the free energy to create a step. The step free energy will be temperature dependent, and at and above the roughening temperature it will be zero. It's therefore very useful to look at step free energy, which we will do both numerically and analytically.

If we add impurities to the system, the situation will be some more complicated. Where in the impurity free case the ground state of a step is a straight line at zero temperature, this is no longer the case with impurities. The step will develop kinks to encounter energetically favorable impurities and to avoid unfavorable ones. Furthermore one can imagine that the step free energy will depend on the mean distance between two steps. If the mean distance is very large, the steps will not see each other and they can form those kinks that minimize their own step free energy. If the mean distance between two steps is rather small, the paths of the step will be restricted by its neighboring steps. If a neighboring step goes through an energetically favorable step, the step itself cannot, because that would mean that there is locally a step of atomic height two. Such a kink of two lattice units is not forbidden, but it is energetically so unfavorable, that such a kink will appear very rarely.

The theory predicts an $\frac{1}{L^2}$-dependence in the step free energy, with L the mean distance between two steps, if there are no impurities in the system, while the theory predicts in the continuum limit an $\frac{1}{L}$-dependence if there are impurities. Especially we are interested in the transition from an impurity free case to a lattice with impurities.

I would like to thank my supervisor, prof. dr. H. van Beijeren, for his guidance during the time is was working on this subject. Furthermore I would like to thank the other graduate students at the institute for the nice atmosphere in our room. Finally, I would like to thank my family for their support.

Chapter 2

Theory

2.1 introduction

In statistical mechanics the fundamental quantity is the partition function Z. It is defined as $Z = \sum_{\{\mathbf{s}\}} e^{-\beta\mathcal{H}[s]}$, where $\{\mathbf{s}\}$ is the set of all possible configurations of the system, $\mathcal{H}[s]$ is the Hamiltonian of the system and β is $\frac{1}{k_B T}$ where k_B is the Boltzmann constant and T is the temperature. The factor $e^{-\beta\mathcal{H}[s]}$ is the Boltzmann factor of the configuration s and it is related to the partition function by the probability to be in state s: $P(s) = \frac{e^{-\beta\mathcal{H}[s]}}{Z}$. From the partition function we can in principle calculate all the interesting quantities of the system. For instance the average energy of the system is given by: $U = k_B T^2 \frac{\partial \log Z}{\partial T}$.

An example of such a system is a lattice with on each point on the lattice a particle. For simplicity we give the particle only one property, its magnetic spin. If we assume that the particles interact, but the interaction is only dependent on the orientation of the two spins and their relative distance, we have a simple model for a magnet.

The situation becomes more complex if we do not know all the properties of the system. Suppose that we add some impurities to the system, which change the interactions between the particles. If the experimental times of observation are much larger than the typical times of fluctuations, (in the example of the ferro-magnet both fluctuations in the spins and fluctuations in the impurities), the system is called annealed and we can calculate the partition function as described above, where the summation goes also over all the possible realizations of the impurities.

The other limit is the case where the experimental times of observation are much smaller than the typical time of fluctuation in the impurities, the impurities are frozen or quenched.

Suppose we add some impurities to this system. This will change the interactions between the particles. In general the Hamiltonian of the quenched system will depend on the kind of impurities, which are added to the system, the location of the impurities at the moment that the system was frozen and of course also on the orientations of the spins. Therefore $\mathcal{H} = \mathcal{H}_J[S]$ where S stands for the orientations of the spins and J for

the couplings between the particles, which depend on the impurities.

If we know the exact configuration of the impurities, we can in principle calculate all the interesting quantities with the aid of the partition function, for that particular configuration of the impurities. For instance the mean free energy per particle is given by:

$$\frac{f_J}{N} = -\frac{1}{\beta N} \log \left\{ \sum_{\{\mathbf{s}\}} e^{-\beta \mathcal{H}_J[s]} \right\} \tag{2.1}$$

For many pure systems it is possible to calculate the partition function in the thermodynamical limit, that means $N \to \infty$.

If we don't know the exact configuration of the impurities, we can only base our calculations on the distribution function of the impurities, $P[J]$. Even if we do know the exact configuration of the impurities this is often the best we can do. If we want to calculate the mean free energy, we have to determine $\langle f \rangle$ where $\langle\rangle$ stands for averaging over all the possible configurations of the impurities. The problem with this quantity is the fact that we have to take the logarithm of the partition function before we average over the impurities. In contradiction to the annealed case, in which the times of observation are much larger than the typical times of fluctuations and we would like to determine $\log \langle Z \rangle$, this problem cannot be solved by standard methods from statistical mechanics. (Although the replica trick, see below, may have become a standard method in the past years.)

Therefore we use the replica trick, which allows us to calculate the system with quenched impurities anyway. We look at a new physical system that consists of n copies (replicas) of the old system. The partition function of the new system is given by Z_N^n, where Z_N is the partition function of the old system of N particles. We define a new quantity:

$$\Phi_N(n) = \frac{1}{N} \log \langle Z_N^n \rangle \tag{2.2}$$

Suppose we can calculate $\langle Z_N^n \rangle$ for each $n \in \mathbb{N}$ in the limit $N \to \infty$. Now we come to the tricky part of the replica method. Suppose we can continue the quantity Φ_N^n for each $n \in \mathbb{R}$. Then we have that:

$$\lim_{n \to 0} \frac{d}{dn} \Phi_N(n) = \frac{1}{N} \langle \log Z_N \rangle = -\frac{\beta}{N} \langle f_N \rangle \tag{2.3}$$

In the previous formula there is still an N present, so we are not yet working in the thermodynamic limit. For the majority of the models known, the partition function can only be calculated in the thermodynamical limit, and therefore it can only be continued to non-integer n in the thermodynamical limit. Therefore for such models the replica method only allows us to calculate:

$$\lim_{n \to 0} \frac{d}{dn} \{ \lim_{N \to \infty} \Phi_N(n) \} \tag{2.4}$$

If we can reverse the order of the two limits, we can calculate the mean free energy per particle in the thermodynamic limit. The order of the two limits can be reversed if we have a system in equilibrium where the spin interactions have a short range, see [4] and section 2.9.

Note: The replica method was historically first defined in the following equivalent way: $\lim_{n\to 0} \frac{\langle Z_N^n\rangle - 1}{n}$ instead of $\lim_{n\to 0} \frac{d}{dn}\Phi_N(n)$.

2.2 The Sherrington-Kirkpatrick model

To show how the replica method works, we will discuss the most famous model in which the replica trick is needed, the Sherrington-Kirkpatrick model (S-K model) see [5] and [6]. We will also discuss a problem which arises if we solve the S-K model. (See also [7] and [8]).

The S-K model is a model for spin glasses. Spin glasses are magnetic materials, in which the interaction between spins is sometimes ferromagnetic (the spins want to align, $J > 0$), and sometimes anti-ferromagnetic ($J < 0$). In the S-K model the distribution function for the coupling J between two spins is identical for each pair of spins. Therefore the range of interaction is infinite in this model. The Hamiltonian of this model is given by:

$$\mathcal{H}_J[\mathbf{s}] = -\sum_{(ij)} J_{i,j} s_i s_j - \sum_i h s_i \tag{2.5}$$

The first summation is over all pairs of spins, $1 \leq i < j \leq N$, and h is an external magnetic field. Further we have that $s_i = \pm 1$ and the $J_{i,j}$'s are Gaussian distributed with as distribution function:

$$f(J_{i,j}) = \sqrt{\frac{N}{2\pi J^2}} \exp\left[-\frac{N(J_{ij} - \frac{J_0}{N})^2}{2J^2}\right] \tag{2.6}$$

From the distribution function it follows that $E[J_{ij}] = \frac{J_0}{N}$ and $E\left[J_{ij}^2\right] = \frac{J^2}{N} + \frac{J_0^2}{N^2}$, where E stands for the expectation value. For simplicity we assume that there is no external magnetic field, so $h = 0$. We also assume that there is no preference for the ferro- or anti-ferro magnetic case, thus $J_0 = 0$. In this context we will apply the replica method.

This gives for the expectation of the partition function:

$$\langle Z_N^n\rangle = \int d\mathbf{J} f(\mathbf{J}) \sum_{\{\mathbf{s}\}} \exp\left[\sum_{a=1}^{n} \beta \sum_{(ij)} J_{ij} s_i^a s_j^a\right] \tag{2.7}$$

where $f(\mathbf{J})$ stands for $\prod_{(ij)} f\left(J_{(ij)}\right)$ and $d\mathbf{J}$ stands for $\prod_{(ij)} dJ_{ij}$. With the identity

$$\int_{-\infty}^{+\infty} \exp\left[-\alpha x^2 + \beta x\right] dx = \sqrt{\frac{\pi}{\alpha}} \exp\left[\frac{\beta^2}{4\alpha}\right] \tag{2.8}$$

the expectation of the partition function can be written as

$$\langle Z_N^n \rangle = \sum_{\{\mathbf{s}\}} \exp\left[\sum_{(ij)} \frac{\beta^2 J^2}{2N} (\sum_{a=1}^{n} s_i^a s_j^a)^2\right] \tag{2.9}$$

Reversing the order of summation in the exponent gives (see appendix):

$$\langle Z_N^n \rangle = \exp\left[\frac{\beta^2 J^2 n(N-n)}{4}\right] \sum_{\{\mathbf{s}\}} \exp\left[\frac{\beta^2 J^2}{2N} \sum_{(ab)} (\sum_{i=1}^{N} s_i^a s_i^b)^2\right] \tag{2.10}$$

Now we will rewrite $\langle Z_N^n \rangle$, and therefore we need two identities: The first is:

$$\int_{-\infty}^{+\infty} dQ_{ab} \exp\left[-\frac{\beta^2 J^2 N}{2} Q_{ab}^2 - \beta^2 J^2 (\sum_{i=1}^{N} s_i^a s_i^b) Q_{ab}\right] = \sqrt{\frac{2\pi}{\beta^2 J^2 N}} \exp\left[\frac{\beta^2 J^2}{2N} (\sum_{i=1}^{N} s_i^a s_i^b)^2\right] \tag{2.11}$$

where we used (2.8). The second is:

$$\sum_{\{\mathbf{s}\}} \exp\left[\sum_{(ab)} c_{ab} \sum_{i=1}^{N} s_i^a s_i^b\right] = \left(\sum_{\{\mathbf{S}\}} \exp\left[\sum_{(ab)} c_{ab} S_a S_b\right]\right)^N \tag{2.12}$$

where the first summation, $\sum_{\{\mathbf{s}\}}$, goes over all the 2^{nN} configurations of the spin variables s_i^a and the second summation, $\sum_{\{\mathbf{S}\}}$, goes over the 2^n configurations of the spin variables S_a which are ± 1 and c_{ab} is a constant dependent on a en b. See the appendix for the proof of equation (2.12). With the aid of (2.11) and (2.12) the expectation of the partition function can be written as:

$$\langle Z_N^n \rangle = \exp\left[\tfrac{\beta^2 J^2 n(N-n)}{4}\right]$$
$$\int \prod_{(ab)} \left(dQ_{ab} \sqrt{\tfrac{\beta^2 J^2 N}{2\pi}}\right) \exp\left[-\tfrac{\beta^2 J^2 N}{2} \sum_{(ab)} Q_{ab}^2\right] \left(\sum_{\{\mathbf{S}\}} \exp\left[\textstyle\sum_{(ab)} \beta^2 J^2 S_a S_b Q_{ab}\right]\right)^N$$

where we have omitted the last minus sign in the the exponent, which is allowed because we sum over all possible spin configurations and the spin variables only take the values ± 1. Now we are able to calculate $\Phi(n) := \lim_{N\to\infty} \Phi_N(n) := \lim_{N\to\infty} \frac{1}{N} \log \langle Z_N^n \rangle$

$$\Phi(n) = \tfrac{\beta^2 J^2 n}{4} + \lim_{N\to\infty} \tfrac{1}{N} \log \tag{2.13}$$
$$\left\{ \int \prod_{(ab)} \left(dQ_{ab} \sqrt{\tfrac{\beta^2 J^2 N}{2\pi}} \right) \exp\left[-\tfrac{\beta^2 J^2 N}{2} \sum_{(ab)} Q_{ab}^2 \right] \left(\sum_{\{\mathbf{S}\}} \exp\left[\sum_{(ab)} \beta^2 J^2 S_a S_b Q_{ab} \right] \right)^N \right\}$$

This can be written as:

$$\Phi(n) = \frac{\beta^2 J^2 n}{4} + \lim_{N\to\infty} \frac{1}{N} \log \left\{ \int \prod_{(ab)} \left(dQ_{ab} \sqrt{\frac{\beta^2 J^2 N}{2\pi}} \right) \exp\left[-N A[\mathbf{Q}] \right] \right\} \tag{2.14}$$

where

$$A\left[\mathbf{Q}\right] = \frac{\beta^2 J^2}{2} \sum_{(ab)} Q_{ab}^2 - \log \left\{ \sum_{\{\mathbf{S}\}} \exp\left[\beta^2 J^2 \sum_{(ab)} S_a S_b Q_{ab} \right] \right\} \tag{2.15}$$

Note that $A[\mathbf{Q}]$ is independent of N. For large N the integral in (2.14) will be dominated by the minimal value of $A[\mathbf{Q}]$. Therefore we are interested in those Q_{ab}'s with:

$$\frac{\partial A}{\partial Q_{ab}} = 0 \tag{2.16}$$

This is equivalent with:

$$Q_{ab} = \frac{\sum_{\{\mathbf{S}\}} S_a S_b \exp\left[\beta^2 J^2 \sum_{(\tilde{a}\tilde{b})} S_{\tilde{a}} S_{\tilde{b}} Q_{\tilde{a}\tilde{b}} \right]}{\sum_{\{\mathbf{S}\}} \exp\left[\beta^2 J^2 \sum_{(\tilde{a}\tilde{b})} S_{\tilde{a}} S_{\tilde{b}} Q_{\tilde{a}\tilde{b}} \right]} = \langle S_a S_b \rangle \tag{2.17}$$

where $\langle\rangle$ stands for the expectation with respect to the Hamiltonian $-\beta J^2 \sum_{(ab)} S_a S_b Q_{ab}$ Because the original equations were symmetric in the replicas, we expect that the solution is also symmetric in the replicas. In the minimum we have therefore $Q_{ab} = q \quad \forall a < b$, see [5]. Because of the dominance of the term with $Q_{ab} = q$ we have

$$\begin{aligned} \Phi(n) &= \frac{\beta^2 J^2 n}{4} + \lim_{N\to\infty} \frac{1}{N} \log \left\{ \exp\left[-N A\left[\mathbf{Q}\right] \right] \right\} \Big|_{Q_{ab}=q} \\ &= \frac{\beta^2 J^2 n}{4} - A\left[\mathbf{Q}\right] \Big|_{Q_{ab}=q} \end{aligned} \tag{2.18}$$

We now try to find an expression for $\Phi(n)$. For that purpose we write:

$$\sum_{\{\mathbf{S}\}} \exp\left[\beta^2 J^2 \sum_{(ab)} S_a S_b Q_{ab}\right] = \sum_{\{\mathbf{S}\}} \exp\left[\beta^2 J^2 q \sum_{(ab)} S_a S_b\right]$$
$$= \sum_{\{\mathbf{S}\}} \exp\left[\frac{\beta^2 J^2 q}{2}\left(\sum_{a=1}^{n} S_a\right)^2\right] \exp\left[-\frac{\beta^2 J^2 q n}{2}\right] \quad (2.19)$$

with the aid of (2.8) this can be written as:

$$\exp\left[-\frac{\beta^2 J^2 q n}{2}\right] \sum_{\{\mathbf{S}\}} \int_{-\infty}^{+\infty} dx \sqrt{\frac{1}{2\pi}} \exp\left[-\frac{1}{2}x^2 + \beta J \sqrt{q} x \sum_{a=1}^{n} S_a\right] \quad (2.20)$$

Now the sum over the spins can be calculated with the use of the following formula ($\lambda = \beta J \sqrt{q} x$):

$$\sum_{\{\mathbf{S}\}} \exp\left[\lambda \sum_{a=1}^{n} S_a\right] = \left(e^{\lambda} + e^{-\lambda}\right)^n = (2\cosh\lambda)^n \quad (2.21)$$

Thus (2.20) can be written as:

$$\exp\left[-\frac{\beta^2 J^2 q n}{2}\right] \int_{-\infty}^{+\infty} dx \sqrt{\frac{1}{2\pi}} \exp\left[-\frac{1}{2}x^2\right] \left(2\cosh\left[\beta J x \sqrt{q}\right]\right)^n \quad (2.22)$$

With the formulas (2.14), (2.15), (2.18) and the previous reasoning we have:

$$\Phi(n) = \frac{\beta^2 J^2 n}{4}\left(1 - 2q - (n-1)q^2\right) + \quad (2.23)$$
$$\log\left\{\int_{-\infty}^{+\infty} dx \sqrt{\frac{1}{2\pi}} \exp\left[-\frac{1}{2}x^2\right] \left(2\cosh\left[\beta J x \sqrt{q}\right]\right)^n\right\}$$

Here we can take the derivative with respect to n in n=0

$$\left.\frac{d}{dn}\Phi(n)\right|_{n=0} = \frac{\beta^2 J^2}{4}(1 - 2q + q^2) + \frac{\int_{-\infty}^{+\infty} dx \sqrt{\frac{1}{2\pi}} \exp\left[-\frac{1}{2}x^2\right] \log\left(2\cosh\left[\beta J x \sqrt{q}\right]\right)}{\int_{-\infty}^{+\infty} dx \sqrt{\frac{1}{2\pi}} \exp\left[-\frac{1}{2}x^2\right]}$$

and we get for the average free energy per particle (see (2.3)):

$$\frac{\langle f \rangle}{N} = -\frac{\beta J^2}{4}(1-q)^2 - \frac{1}{\beta} \int_{-\infty}^{+\infty} dx \sqrt{\frac{1}{2\pi}} \exp\left[-\frac{1}{2}x^2\right] \log\left(2\cosh\left[\beta J x \sqrt{q}\right]\right) \quad (2.24)$$

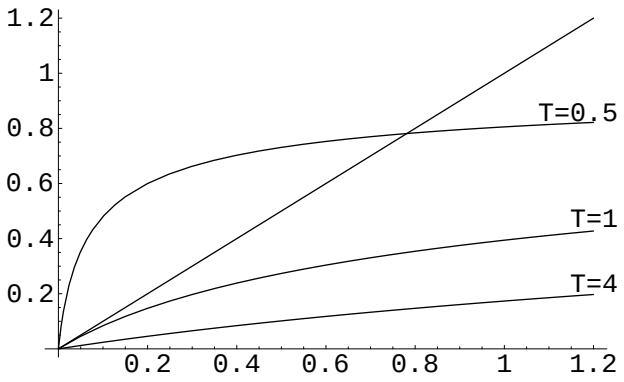

Figure 2.1: Plot of $\int_{-\infty}^{+\infty} dx \sqrt{\frac{1}{2\pi}} \exp\left[-\frac{1}{2}x^2\right] \tanh^2\left[\beta J x \sqrt{q}\right]$ as a function of q for T=4, 1 and 0.5 and the diagonal.

Now we only need to calculate q. According to (2.17) we have:

$$q = \langle S_a S_b \rangle = \frac{1}{\beta^2 J^2} \frac{\partial}{\partial Q_{ab}} \log \left\{ \sum_{\{\mathbf{S}\}} \exp \left[\beta^2 J^2 \sum_{(ab)} S_a S_b Q_{ab} \right] \right\} \tag{2.25}$$

With the previous formulas and the sum over the equivalent replicas we get:

$$\frac{n(n-1)}{2} \beta^2 J^2 q = \frac{\partial}{\partial q} \log \left\{ \exp\left[-\frac{\beta^2 J^2 q n}{2} \right] \int_{-\infty}^{+\infty} dx \sqrt{\frac{1}{2\pi}} \exp\left[-\frac{1}{2}x^2 \right] \left(2\cosh\left[\beta J x \sqrt{q}\right] \right)^n \right\}$$

After taking the $n \to 0$ limit, we get:

$$q = 1 - \frac{1}{\beta J \sqrt{q}} \int_{-\infty}^{+\infty} dx \sqrt{\frac{1}{2\pi}} \exp\left[-\frac{1}{2}x^2 \right] x \tanh\left[\beta J x \sqrt{q}\right]$$

Now perform partial integration to obtain:

$$q = \int_{-\infty}^{+\infty} dx \sqrt{\frac{1}{2\pi}} \exp\left[-\frac{1}{2}x^2 \right] \tanh^2\left[\beta J x \sqrt{q}\right] \tag{2.26}$$

This implicit expression for q is the best we can get. Formulas (2.24) and (2.26) are known as the "replica-symmetric" solution of the SK-model. There are two different temperature regions to look at. If $T > 1$, the only solution of (2.26) is the trivial one, $q = 0$, for $T < 1$ there is also a non-trivial solution, see Figure 2.1.

Unfortunately there are some problems with this model. When we try to calculate the entropy per site, $s(T) = -\frac{\partial f}{\partial T}$, it can be shown that $s(0) = -\frac{k_B}{2\pi}$ which is a negative

value. This is impossible because the entropy is a positive quantity because at zero temperature it is defined as the logarithm of the the number of configurations with energy equal to E_{min} . (An exact calculation of the value $\frac{\partial f}{\partial T}$ in T=0 is quite difficult, but to show that the entropy of the replica symmetric solution of the SK-model for zero temperature is negative is not so hard. For small T the tanh in the implicit definition of q is almost equal to one except when x is very small. Therefore the right hand side of equation (2.26) is 1 minus a small area. One can easily show that the area is proportional with $1/\sqrt{q}$ This gives that $q = 1 - \alpha T$ with α a constant. With this result the computation of the entropy for T=0 is straightforward.)

The problem of the negative entropy demands a completely new approach. Namely the concept of replica symmetry breaking. This will be explained in section 2.9

2.3 The model of Kardar

In this section we want to look at the system which we used for our numerical simulations. It is a model that Kardar describes in [9], which is based on the article of Kardar and Nelson [10]. We follow Kardar's calculation in [9], keeping close to his notation. We have a square lattice. On each site of the lattice we define a height of integer value. Now we demand that the left edge of the system is one unit of height lower than the right edge. Therefore we force a step on the system. From now on we restrict ourselves to the one-dimensional solid on solid (SOS) approximation which restricts the allowed step configurations. This approximation excludes overhangs in the sense that only transverse and forward displacements of the steps are allowed. This approximation is correct in the anisotropic limit, which means that parallel bonds are energetically highly unfavorable. Furthermore we exclude closed loops of steps, which create adatomic island or adatomic vacancies. In this case the position of the step can be described by a function $x(t)$ where t is the coordinate parallel to the step and x is the position of the step perpendicular to the step direction. Furthermore we assume that all the transverse bonds have energy K, and that the energy of the parallel bonds are all independent random variables $\mu(x,t)$. Here we have included the factor β in the coefficients μ and K. (So $\mu(x,t) = \beta\mu'(x,t)$ and $K = \beta K'$ with $\mu'(x,t)$ and K' temperature $-$ independent.) The partition function for the step can now be calculated with the aid of transfer matrices at position t:

$$\langle x|\mathcal{F}(t)|x'\rangle = \exp\left[-\mu(x,t) - K|x - x'|\right]$$

If $K \gg 1$, kinks in the step are rare, especially kinks larger than 1, see Figure 2.3. Therefore we can expand $\langle x|\mathcal{F}(t)|x'\rangle$ in $\gamma := e^{-K}$

$$\langle x|\mathcal{F}(t)|x'\rangle = \exp\left[-\mu(x,t)\right]\left\{\delta_{x,x'} + \gamma\left(\delta_{x,x'+1} + \delta_{x,x'-1}\right) + \mathcal{O}(\gamma^2)\right\}$$

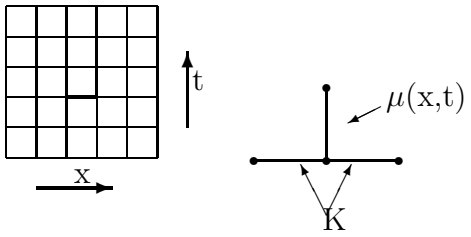

Figure 2.2: A step on the lattice with a kink of length 1

One has that:

$$\sum_{x'} \{\delta_{x,x'} + \gamma\left(\delta_{x,x'+1} + \delta_{x,x'-1}\right)\} f(x') = f(x) + \gamma f(x-1) + \gamma f(x+1)$$
$$\approx f(x) + \gamma\left(f(x) - f'(x) + \frac{1}{2}f''(x)\right) + \gamma\left(f(x) + f'(x) + \frac{1}{2}f''(x)\right)$$
$$= f(x) + 2\gamma f(x) + \gamma f''(x) = \left\{1 + 2\gamma + \gamma\frac{\partial^2}{\partial x^2}\right\} f(x)$$

where we have gone to a continuum limit in the x-direction. Therefore we can write the transfer matrix as:

$$\begin{aligned}\langle x|\mathcal{F}(t)|x'\rangle &= \langle x|\exp\left[-\mu(x,t)\right]\left\{1 + 2\gamma + \gamma\tfrac{\partial^2}{\partial x^2}\right\}|x\rangle \\ &\approx \langle x|\exp\left[-\mu(x,t)\right]\exp\left[2\gamma + \gamma\tfrac{\partial^2}{\partial x^2}\right]|x\rangle \\ &= \langle x|\exp\left[-\mu(x,t) + 2\gamma + \gamma\tfrac{\partial^2}{\partial x^2}\right]|x\rangle := \langle x|\exp\left[-\mathcal{H}(t)\right]|x\rangle\end{aligned} \tag{2.27}$$

and therefore the transfer matrix can be written as:

$$\mathcal{F}(t) = \exp\left[-\mu(x,t) + 2\gamma + \gamma\frac{\partial^2}{\partial x^2}\right] = \exp\left[-\mathcal{H}(t)\right] \tag{2.28}$$

In fact this isn't entirely correct, because $\mu(x,t)$ and $\frac{\partial^2}{\partial x^2}$ do not commute. This problem can be solved by averaging over the impurities. Because the impurities are randomly chosen from a Gaussian distribution we expect that $\left\langle \frac{\partial^2 \mu(x,t)}{\partial x^2} \right\rangle$ is zero, and therefore $\left[\frac{\partial^2}{\partial x^2}, \mu(x,t)\right]$=0.This allows us to write the two exponents as one, see [11], but according to equation (2.29) we have to replace $\mu(x,t)$ by $\mu - \frac{1}{2}\sigma^2$.

Because we want to know the quantity $\langle f \rangle \sim \langle \log Z \rangle$ we use the replica trick. (see section 2.1). Therefore we want to do the previous reasoning for n copies of the system, so with n steps (interfaces). Suppose we have a Gaussian distribution of $\mu(x,t)$ with average μ and variance σ^2. (Because we have $\mu(x,t) = \beta\mu'(x,t)$, the Gaussian distribution is in fact temperature-dependent.) Before we calculate the transfer matrix

we look at the following identity which we shall need: (where m is the number of steps that cross a particular bond)

$$\langle \exp\left[-m\mu(x,t)\right]\rangle = \int_{-\infty}^{+\infty} \frac{dy}{\sqrt{2\pi\sigma^2}} \exp\left[-\frac{(y-\mu)^2}{2\sigma^2}\right] \exp\left[-my\right]$$

when we use formula (2.8) we get:

$$\langle \exp\left[-m\mu(x,t)\right]\rangle = \exp\left[-\left(\mu - \frac{1}{2}\sigma^2\right)m + \frac{1}{2}\sigma^2 m(m-1)\right] \tag{2.29}$$

If we examine this result we can conclude the following: Averaging over the randomness gives an effective value for the energy of an interface to cross a bond, of $\mu - \frac{1}{2}\sigma^2$. But we also get an attraction between two steps which cross the same bond, of magnitude σ^2, because there are $\frac{1}{2}m(m-1)$ different pairs one can select from m different elements. Now we can calculate the expectation of the n-replica-transfer matrix, where $\{x\}$ stands for $\{x_1(t), x_2(t), \cdots, x_n(t)\}$and the big $\langle\rangle$ stands for averaging over the randomness.

$$\left\langle \langle\{x\}|\mathcal{F}(t)|\{x'\}\rangle \right\rangle = \exp\left[-n\left(\mu - \frac{1}{2}\sigma^2\right) + \sigma^2 \sum_{(ab)} \delta\left(x_a - x_b\right) - K\sum_{a=1}^{n} |x_a - x'_a|\right]$$

Expanding in $\gamma = e^{-K}$ and taking the continuum-limit we get:

$$\mathcal{F}(t) = \exp\left[-n\left(\mu - \frac{1}{2}\sigma^2 - 2\gamma\right) + \gamma\sum_{a=1}^{n}\frac{\partial^2}{\partial x^2} + \sigma^2\sum_{(ab)}\delta\left(x_a - x_b\right)\right] := \exp\left[-\mathcal{H}_n(t)\right] \tag{2.30}$$

Now we have solved the problem of averaging at the expense of interactions between the replicas.

For an infinite system the partition function will depend only on the largest eigenvalue of the transfer matrix, see [12]. Therefore for a system of length T, with $T \gg 1$ the following approximation is valid: $\langle Z_n\rangle \sim \exp[-E_n T]$ with E_n the ground-state energy of the Hamiltonian in (2.30). The equation $\mathcal{H}\Psi = E\Psi$ cannot be solved by direct manipulations. We have to use a guess for the ground state solution and we take the Bethe-ansatz (see chapter 3). For n=2 we want to solve:

$$\begin{gathered}\mathcal{H}_2\Psi(x_1,x_2) = \\ \left(2\mu - \sigma^2 - 4\gamma - \gamma\left(\tfrac{\partial^2}{\partial x_1^2} + \tfrac{\partial^2}{\partial x_2^2}\right) - \sigma^2\delta(x_1 - x_2)\right)\Psi(x_1,x_2) = E_2\Psi(x_1,x_2)\end{gathered} \tag{2.31}$$

The Bethe-ansatz, [13], says: Try $\Psi_0 \sim \exp\left[-\kappa\left|x_1 - x_2\right|\right]$. Here again we have included the temperature dependence in κ ($\kappa = \beta\kappa'$). This function is a solution of the problem, and because it has no zero points, it is the ground state. We want a smooth solution

and therefore we demand that the derivatives and the δ-function in the Hamiltonian cancel each other at $x_1 = x_2$. This gives the equation:

$$4\kappa\gamma = \sigma^2 \tag{2.32}$$

The same can be done for other n: The Bethe-ansatz now gives the following solution: (see chapter 3)

$$\Psi_0 \sim \exp\left[-\kappa \sum_{(ab)} |x_a - x_b|\right] \tag{2.33}$$

Again we get (2.32) if we want to remove the discontinuities. (2.32) can be interpreted as follows.Write

$$l_d := \kappa^{-1} = \frac{4\gamma}{\sigma^2} \tag{2.34}$$

l_d is a length-scale. We see that l_d is proportional to γ. Therefore l_d is small when the step is stiff ($K \gg 1$). Because we used a continuum approximation, we need that the lattice spacing is much smaller than l_d. Therefore the continuum approximation is only valid if K is not too large. It looses its validity for low temperature or if transverse bonds have high energy, see section 4.1.4.

$|x_a - x_b|$ can be written as $+$ or $-(x_a - x_b)$. Let's assume the following ordering of the x_a's. $x_1 > x_2 > \ldots > x_n$. With this ordering we can write $\kappa \sum_{(ab)} |x_a - x_b|$ as $\sum_{a=1}^{n} \kappa_a x_a$ where $\kappa_a = (n + 1 - 2a)\kappa$. When 2 particles cross each other they exchange their kinetic energy, because the kinetic energy of particle i is determined by the number of $+$ signs in the expansion of $\sum_{(ab)} |x_a - x_b|$ to x_i. Therefore for every permutation of the particles the total kinetic energy is the same and we can write:

$$\mathcal{H}_n \Psi_0 = \left(\left(\mu - \frac{1}{2}\sigma^2 - 2\gamma\right) n - \gamma \sum_{a=1}^{n} \kappa_a^2\right) \Psi_0$$

With the identities

$$\sum_{a=1}^{n} a = \frac{n(n+1)}{2} \quad \text{and} \quad \sum_{a=1}^{n} a^2 = \frac{1}{3}n^3 + \frac{1}{2}n^2 + \frac{1}{6}n, \tag{2.35}$$

which can be proven by induction, we can write the ground-state-energy as:

$$E_n = \left(\mu - \frac{1}{2}\sigma^2 - 2\gamma\right) n - \frac{1}{3}\gamma\kappa^2 n\left(n^2 - 1\right) \tag{2.36}$$

Because of the special form of the partition function $\langle Z^n \rangle \sim \exp[-E_n T]$ we can calculate the mean free energy per unit as $\lim_{n\to 0} \frac{d}{dn} E_n$ where we used (2.3). Thus the quenched averaged free energy per unit is:

$$\frac{\langle f \rangle}{T} = \mu - \frac{1}{2}\sigma^2 - 2\gamma + \frac{\sigma^4}{48\gamma} \tag{2.37}$$

where we used (2.32).

Another way to get information about the system is the following. Write $\langle Z^n \rangle = \langle \exp[n \log Z] \rangle$. This is the characteristic function of the random variable $\log Z$. Now make a Taylor-expansion of this quantity:

$$\begin{aligned} \langle Z^n \rangle = \langle \exp[n \log Z] \rangle &\overset{\log Z := Y}{=} \\ \langle \exp nY \rangle \overset{Taylor}{=} \sum_{k=0}^{\infty} \frac{\langle Y^k \rangle n^k}{k!} &:= \exp\left[\sum_{j=1}^{\infty} \frac{n^j}{j!} C_j(Y) \right] \end{aligned} \tag{2.38}$$

Now we try to find expressions for the cumulants $C_j(Y)$:

$$\sum_{k=0}^{\infty} \frac{\langle Y^k \rangle n^k}{k!} = 1 + \sum_{j=1}^{\infty} \frac{n^j}{j!} C_j(Y) + \frac{1}{2}\left(\sum_{j=1}^{\infty} \frac{n^j}{j!} C_j(Y) \right)^2 + \frac{1}{6}\left(\sum_{j=1}^{\infty} \frac{n^j}{j!} C_j(Y) \right)^3 + \dots$$

Matching the same coefficients in n^k gives for the first three cumulants:

$$\begin{aligned} C_1(Y) &= \langle Y \rangle \\ C_2(Y) &= \langle Y^2 \rangle - \langle Y \rangle^2 \\ C_3(Y) &= \langle Y^3 \rangle - 3 \langle Y \rangle \langle Y^2 \rangle + 2 \langle Y \rangle^3 \end{aligned}$$

If we compare the two identities for Z^n, $\exp[-E_n T] = \exp\left[\sum_{j=1}^{\infty} \frac{n^j}{j!} C_j(\log Z) \right]$, and we match the the terms in the exponents with the same n-dependence , see equation (2.36), we see that only the first and the third cumulant of $\log Z$ are non-vanishing. We obtain:

$$\begin{aligned} C_1(\log Z) &\overset{(2.37)}{=} \frac{\langle f \rangle}{T} = \mu - \frac{1}{2}\sigma^2 - 2\gamma + \frac{\sigma^4}{48\gamma} \\ C_3(\log Z) &\overset{(2.36)}{=} 3! \frac{1}{3} \gamma \kappa^2 T = \frac{\sigma^4 T}{8\gamma} \end{aligned}$$

In principle the results of this section are also valid for a step on a cylinder, instead of a step on a strip of infinite width. (If we replace $|x_a - x_b|$ in equation (2.33) by $x_a - x_b \pmod L$ we obtain a periodic function without zero points and we obtain the same conclusions.) But we forget in this reasoning the finite size effect. For instance a unfavorable region of width L can be easily avoided on a strip of infinite width while it is important on a cylinder of width L. Therefore we get a finite size correction, see section 2.7.

2.4 Fluctuations in the free energy

The higher order cumulants are a measure for the typical fluctuations in the step free energy Δf. Because the second cumulant is vanishing, the third cumulant dominates the typical fluctuations. Because $C_3(\log Z) \sim T$, we have that the typical fluctuations are of the form $\Delta f \sim T^{\frac{1}{3}}$ instead of $\Delta f \sim T^{\frac{1}{2}}$ as one would expect naively. One would naively expect a dependence proportional to the square root of the length, because each interface is more or less a straight line, and will therefore encounter T random bonds (see [14]). That this is not the case is due to transverse fluctuations of interfaces to take advantage of energetically favorable bonds. If we assume that the interface is a kind of string, we have that a transverse fluctuation x results in an increase in the energy proportional to $\frac{x^2}{T}$. (This is the increase in the length of the interface). If we combine this result with the typical fluctuations in the free energy we get $x \sim T^{\frac{2}{3}}$. This result was found numerically at zero temperature by Huse and Henley [15].

2.5 vicinal surfaces

Now we try to handle the following more difficult problem. Suppose we have a vicinal surface on a three dimensional crystal. This means that the surface makes a tiny angle α with a facet, a surface which orientation is macroscopically flat. If we look microscopically at the vicinal surface, it looks like a perfect staircase at zero temperature, see Figure 1.1 and it looks like a staircase with less regular steps at higher temperature due to thermal fluctuations, see 1.2. The distance between the steps will depend on the angle that the vicinal surface makes with the facet. The steps can be regarded as interfaces, running roughly parallel, and with a mean distance $\frac{1}{\tan\alpha} \approx \frac{1}{\alpha}$ between them.

Another physical system which has the same mathematical framework is the commensurate-incommensurate transition. Suppose we have a crystal-surface. The surface can be described by a two-dimensional lattice, where the atoms (of type α) of the crystal are represented by the lattice points. Furthermore we assume that another kind of atoms (of type β) are present at the surface of the crystal, because the crystal is placed in an environment with a gas of type β. These β-atoms can be adsorbed on the crystal surface. Let's have a look at the one dimensional model of Frank and Van der Merwe (1949). In this model the surface is represented by a periodic potential. The β-atoms prefer to be at the minima of the potential energy. The β-atoms are too big to occupy to neighboring minima. The β-atoms also are too small to make it energetically favorable to occupy only one third of the minima. Therefore we will find a regular pattern, in which an empty and an occupied minima alternate. A commensurate phase. There are two equivalent commensurate phases possible, one in which the even and one in which the odd minima are occupied.

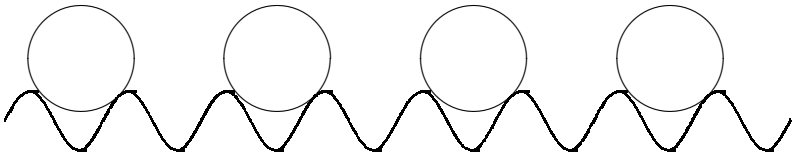

This is the case when the natural distances of β-atoms in a β-lattice coincide with approximately two times the distance between the minima in the α-lattice or the potential-gain of being in the minimum is sufficiently great.

The natural distance of the β-atoms is in general different from the natural distance of the α-atoms in the crystal.(If we have a 2-dimensional system, we assume that the natural distances in the other direction are equal, such uniaxial systems exists). If there is a more than a slight mismatch between the natural distances of the α- and β-atoms, we can get (dependent on the temperature) areas where we have a regular pattern separated by "walls" which separate the two equivalent but different commensurate areas. (see picture)

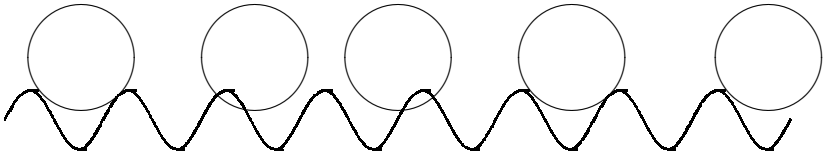

This phase is called an incommensurate phase. So we get also a number of walls walking roughly parallel.

This system of walls, on a vicinal surface or in the incommensurate phase, can be described with the aid of the transfer-matrix-formalism as in one of the former subsections, with the difference that we now have several of them. Furthermore the walls cannot cross each other because we assume that 2 crossing interfaces, and therefore steps of height 2, are energetically highly unfavorable. This last condition can be implemented in the model by regarding the walls as fermionic worldlines of one-dimensional particles.

If we have a system without impurities, it is tempting to consider the motion of a wall as a random walk between it's neighboring walls. But this is not correct. The reason for this is the following. For a random walk, the position of the step is determined forward in time by a stochastic process, while in reality the end position of the step is fixed at the same position as the initial condition.

In the case there are some quenched impurities present, the situation becomes more difficult. We only look at impurities which attract or repel the interfaces. (If the interfaces are walls between regions of particles with spin up and spin down, it is also possible to look at impurities with change the orientation of the spins and therefore couple to the order-parameter. This kind of impurities, which couple to the order-parameter, have been examined by Villain [16]).

Using the transfer-matrix-formalism we get in the continuum limit:
$\mathcal{F}_N(t) = \exp\left[-\mathcal{H}_N(t)\right]$ with

$$\mathcal{H}_N(t) = \int dx \left\{ \left(\mu(x,t) - 2\gamma\right) c^\dagger(x)c(x) - \gamma c^\dagger(x)\frac{\partial^2 c(x)}{\partial x^2} \right\} \tag{2.39}$$

Here $c^\dagger(x)$ and $c(x)$ are fermion fields because the walls are non-crossing. This equation is the field-theoretic analogon of (2.27). Suppose we don't have random impurities, but instead $\mu(x,t)$ is a constant. The free energy of the system in that case can be obtained by finding the ground-state of the Hamiltonian. The ground state is the state where all momenta up to k_F are present. The energy corresponding to momentum k is : $\epsilon(k) = (\mu - 2\gamma) + \gamma k^2$. Therefore we only need to know k_F and $\rho(k)$. Suppose we have a system of width L in the x-direction and length T in the t-direction. For free, one-dimensional, fermions we can follow the standard-derivation of k_F.

$$\left(\mu - 2\gamma - \gamma\frac{\partial^2}{\partial x^2}\right)\Psi(x) = \epsilon\Psi(x)$$

The solutions of these differential equation are:

$$\Psi_k(x) = \frac{1}{\sqrt{L}}e^{ikx} \text{ with } \epsilon_k = \mu - 2\gamma + \gamma k^2$$

From periodic boundaries we obtain the restriction:

$$\Psi(x+L) = \Psi(x) \text{ and therefore } k = \frac{2\pi j}{L} \text{ with } j \in Z \text{ and we obtain } \rho(k) = \frac{L}{2\pi}$$

In the k-volume $[-k_F, k_F]$ there are $\frac{2k_F}{2\pi/L} = \frac{k_F L}{\pi}$ allowed k-values. For a wall-density of $r = N/L$ we obtain: $N = \frac{k_F L}{\pi}$ and thus $k_F = \pi r$. In the continuum limit we have for the free energy that:

$$\frac{f(r)}{LT} = \int_{-k_F}^{k_F}\frac{dk}{2\pi}\epsilon_k = (\mu - 2\gamma)r + \frac{1}{3}\pi^2 r^3 \tag{2.40}$$

When we have quenched impurities, the system becomes more difficult. We have to use the replica-symmetry approach again, but now for fermionic particles. We want to average over the impurities, analogously to the single-step situation in section 2.3. As in section 2.3 we assume $\mu(x,t)$ to be Gaussian distributed with average μ and with mean square displacement σ. When we have averaged over the impurities the Hamiltonian becomes t-independent and can be rewritten as in equation (2.41). To obtain this equation we also looked at the replicated system in the following way: We gave each replicated system a different color. Therefore the Fermi-exclusion principle does not hold for interfaces from different replicas.

$$\mathcal{H}_N^n = \int dx \tag{2.41}$$
$$\left\{\sum_\alpha\left[\left(\mu - \tfrac{1}{2}\sigma^2 - 2\gamma\right)c_\alpha^\dagger(x)c_\alpha(x) - \gamma c_\alpha^\dagger(x)\tfrac{\partial^2 c_\alpha(x)}{\partial x^2}\right] - \sigma^2\sum_{\alpha<\beta}c_\alpha^\dagger(x)c_\alpha(x)c_\beta^\dagger(x)c_\beta(x)\right\}$$

with $c_\alpha^\dagger$ and c_α anticommuting fields for each color. Again we want to find the ground-state-energy of this Hamiltonian. This isn't straightforward and demands some difficult calculations.

We start again with a Bethe-ansatz. We have n species of N one-dimensional particles. (We still see a wall as a fermionic worldline). Therefore we have $(nN)!$ possible different permutations of the particles. We can regard the particles as free, if they are not on the same position. Therefore, for each permutation, we can write the wavefunction of the particles as a product of plane waves.

The ground state solution of this Hamiltonian is hard to find, therefore we dedicated a special section, section 3, to this problem.

From here on we assume that equation 3.32 is known. We continue with the choice of the momenta. In the n-boson-case the momenta were chosen in a n-string, they were equally spaced along the imaginary k-axis. For the $N \times n$-fermion case we assume that for each color the momenta are equally spaced along the imaginary axis, while the real parts of the momentum ($k_j \quad$ with $\quad 1 \leq \alpha \leq N$) for each color are equally spaced along the real axis from $-k_F$ to $+k_F$. This gives as equation for the momenta:

$$k_{\alpha,j} = k_j + i\left(n + 1 - 2\alpha\right)\kappa \quad \text{with} \quad 1 \leq \alpha \leq n \quad \text{and} \quad 1 \leq j \leq N \tag{2.42}$$

If we use the periodic boundary conditions we get as constraint (see chapter (3)):

$$\exp\left[ink_jL\right] = \prod_{\substack{\beta=1 \\ \beta\neq j}}^{N} \prod_{\alpha=1}^{n-1} \frac{ik_\beta - ik_j - 2\alpha\kappa}{ik_\beta - ik_j + 2\alpha\kappa} \tag{2.43}$$

In the appendix in section 5.3 it is shown that in the low-density limit the momentum-density function is equal to:

$$\rho(k) = \frac{\sqrt{k_F^2 - k^2}}{4\pi\kappa} \tag{2.44}$$

The Fermi wave number k_F can now be obtained from:

$$r = \int_{-k_F}^{+k_F} dk\rho(k) = \int_{-k_F}^{+k_F} dk \frac{\sqrt{k_F^2 - k^2}}{4\pi\kappa}$$

Making the substitution $k = k_F \sin\theta$ we obtain:

$$r = \int_{-\frac{1}{2}\pi}^{\frac{1}{2}\pi} d\theta \frac{k_F^2 \cos^2\theta}{4\pi\kappa} = \frac{k_F^2}{8\kappa} \tag{2.45}$$

Therefore the Fermi wave number is given by:

$$k_F = \sqrt{8\kappa r} \tag{2.46}$$

The kinetic energy is given by:

$$E_{kin} = \gamma \int_{-k_F}^{+k_F} dk k^2 \rho(k) = \gamma \int_{-k_F}^{+k_F} dk k^2 \frac{\sqrt{k_F^2 - k^2}}{4\pi\kappa} \tag{2.47}$$

Again using the substitution $k = k_F \sin\theta$ we obtain:

$$E_{kin} = \gamma \int_{-\frac{1}{2}\pi}^{+\frac{1}{2}\pi} d\theta \frac{k_F^4 \left(\frac{1}{2}\sin(2\theta)\right)^2}{4\pi\kappa} = \gamma \frac{k_F^4}{32\kappa} = 2\gamma\kappa r^2 = \frac{\sigma^2 r^2}{2} \tag{2.48}$$

The total free-energy of the system of N interfaces is in the low-density limit:

$$\frac{f}{LT} = \left(\mu - \frac{1}{2}\sigma^2 - 2\gamma + \frac{\sigma^4}{48\gamma}\right) r + \frac{\sigma^2 r^2}{2} \tag{2.49}$$

If we compare this result with the non-random case in (2.40) we see that in the system with quenched impurities we have a term proportional to r^2, which isn't present in the non-random case.

2.6 equilibrium crystal shape

For a vicinal surface of misorientation θ, we can write the surface free energy in one dimension as:

$$f(\theta) = f_0 + f_{step}(\theta)\theta \tag{2.50}$$

The step free energy can be dependent on the angle at higher densities, due to step-step interactions. The step density is here equal to $\theta = \frac{h}{L}$ with h the step height and L the mean distance between two steps. We can make a Taylor-expansion of the step free energy which gives us:

$$f_{step} = f_1 + f_2\theta + f_3\theta^2 + \dots \tag{2.51}$$

f_1 is the step energy of one single step, while f_2 and f_3 correspond tot step interaction energies. Combining equations 2.50 and 2.51, we obtain:

$$f(\theta) = f_0 + f_1\theta + f_2\theta^2 + f_3\theta^3 + \dots \tag{2.52}$$

The equilibrium crystal shape is the shape which minimizes the total surface free energy. This problem can be solved by the Wulff construction, [3] [2]. If we look at a one-dimensional line profile, z(x), across the crystal we obtain for a particle with center at $(0, 0, 0)$ and a facet centered at $(0, 0, z_0)$with borders at $\pm x_f$:

$$z(x, \theta) = f(\theta) - x\theta \quad \text{if } |x| > |x_f| \tag{2.53}$$

$$z(x, \theta) = z_0 = f_0 = f(\theta) \quad \text{if } |x| < |x_f| \tag{2.54}$$

and

$$x(\theta) = \frac{\partial f}{\partial \theta} \tag{2.55}$$

If $|x| > |x_f|$, we obtain the following equation:

$$\frac{\partial z}{\partial x} = -\theta \tag{2.56}$$

If the quadratic term in equation 2.52 is absent, the solution of the differential equation is :

$$z(x) = z_0 - \frac{2}{3^{\frac{3}{2}} f_3^{\frac{1}{2}}} (x - x_f)^{\frac{3}{2}} \quad \text{if } |x| > x_f \tag{2.57}$$

while if the quadratic term is dominant the solution is:

$$z(x) = z_0 - \frac{1}{4f_2} (x - x_f)^2 \quad \text{if } |x| > x_f \tag{2.58}$$

If all the terms in equation 2.52 are relevant, the solution becomes:

$$z(x) = z_0 + \frac{2f_2^3}{27f_3^2} + \frac{f_2}{3f_3}(x - x_f) - \frac{2}{3^{\frac{3}{2}} f_3^{\frac{1}{2}}} \left(x - x_f + \frac{f_2^2}{3f_3} \right)^{\frac{3}{2}} \quad \text{if } |x| > x_f \tag{2.59}$$

We also can approximate the step free energy with a function of the form:

$$f(\theta) = c_0 + c_1 \theta^{c_2} \tag{2.60}$$

This gives as solution:

$$z(x) = z_0 - \left(\frac{1}{c_1 (c_2 + 1)} \right)^{\frac{1}{c_2}} \frac{c_2}{c_2 + 1} (x - x_f)^{1 + \frac{1}{c_2}} \tag{2.61}$$

For a lead crystal at $560K$ Bonzel et al. found an effective exponent of 1.72, see Figure 2.3. This indicates that all terms up to the cubic ones are important.

2.7 Finite size effects for one step on a cylinder

For many simulations we used the model of Kardar (see section 2.3). We let the step start at some point at the cylinder, and with a transfermatrixformalism we calculate the partition function given that the step goes through the point (x, t). In formulas this means:

$$\begin{aligned} &Z(x, 1) = \delta(x, x') \\ &Z(x, t) = e^{-\beta\mu(x,t)} \left\{ Z(x-1, t-1) e^{-\beta K} + Z(x, t-1) + Z(x+1, t-1) e^{-\beta K} \right\} \end{aligned} \tag{2.62}$$

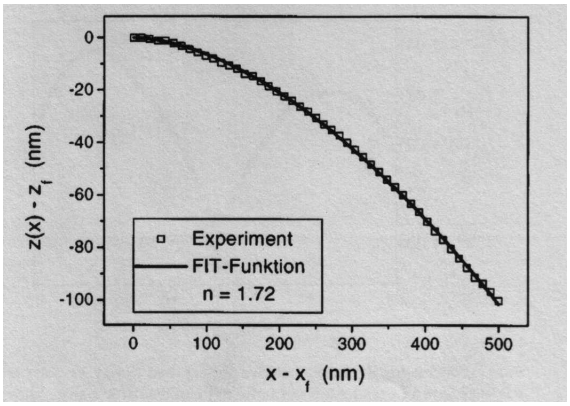

Figure 2.3: Plot of a line profile of the near facet shape, fitted to theoretical expression with effective exponent 1.72. Equilibrium temperature was 560 K.

If we take the logarithm on both sides and if we make the substitution $h(x,t) = \log Z(x,t)$ we obtain :

$$h(x,t) = -\beta\mu(x,t) + \log\left\{\gamma e^{h(x-1,t-1)} + e^{h(x,t-1)} + \gamma e^{h(x+1,t-1)}\right\} = \tag{2.63}$$
$$-\beta\mu(x,t) + h(x,t-1) + \log\left\{\gamma e^{h(x-1,t-1)-h(x,t-1)} + 1 + \gamma e^{h(x+1,t-1)-h(x,t-1)}\right\}$$

with $\gamma = e^{-\beta K}$. If $\gamma \ll 1$ we can expand the logarithm and we obtain:

$$h(x,t) = -\beta\mu(x,t) + h(x,t-1) + \gamma\left(e^{h(x-1,t-1)-h(x,t-1)} + e^{h(x+1,t-1)-h(x,t-1)}\right) + \mathcal{O}\left(\gamma^2\right) \tag{2.64}$$

Expanding the exponentials up to second order gives:

$$\begin{aligned} &h(x,t) = -\beta\mu(x,t) + h(x,t-1) + \\ &\gamma\left(1 + h(x-1,t-1) - h(x,t-1) + \frac{1}{2}\left(h(x-1,t-1) - h(x,t-1)\right)^2\right) + \\ &\gamma\left(1 + h(x+1,t-1) - h(x,t-1) + \frac{1}{2}\left(h(x+1,t-1) - h(x,t-1)\right)^2\right) \end{aligned}$$

Now we replace discrete derivatives by continuous derivatives by using the formulas:

$$h(x-1,t-1) \approx h(x,t-1) - \frac{\partial h(x,t-1)}{\partial x} + \frac{1}{2}\frac{\partial^2 h(x,t-1)}{\partial x^2} \tag{2.65}$$

$$h(x+1,t-1) \approx h(x,t-1) + \frac{\partial h(x,t-1)}{\partial x} + \frac{1}{2}\frac{\partial^2 h(x,t-1)}{\partial x^2} \tag{2.66}$$

This gives:

$$h(x,t) - h(x,t-1) = \tag{2.67}$$
$$-\beta\mu(x,t) + \gamma\left(2 + \frac{\partial^2 h(x,t-1)}{\partial x^2} + \left(\frac{\partial h(x,t-1)}{\partial x}\right)^2 + \frac{1}{4}\left(\frac{\partial^2 h(x,t-1)}{\partial x^2}\right)^2\right)$$

We assume that $h(x,t)$ is a slowly varying function of t and therefore we can replace $h(x,t) - h(x,t-1)$ by $\frac{\partial h(x,t)}{\partial t}$. We obtain:

$$\frac{\partial h(x,t)}{\partial t} = \gamma\nabla^2 h(x,t-1) + \gamma\left(\nabla h(x,t-1)\right)^2 - \beta\mu(x,t) + 2\gamma + \frac{1}{4}\gamma\left(\nabla^2 h(x,t-1)\right)^2 \quad (2.68)$$

The term 2γ can be removed by the substitution $\tilde{h}(x,t) = h(x,t) - 2\gamma t$ while the term $\frac{1}{4}\gamma\left(\nabla^2 h(x,t-1)\right)^2$ is very small because we assume that $h(x,t)$ is also a slowly varying function of x. The term $-\beta\mu(x,t)$ becomes a noise term, $\eta(x,t)$, in the continuum limit. We can replace $h(x,t-1)$ on the right hand side by $h(x,t)$ because we assumed that $h(x,t)$ is a slowly varying function of t. Then we obtain the famous Kardar-Parisi-Zhang (KPZ) equation [17] for the growth of surfaces:

$$\frac{\partial h(x,t)}{\partial t} = \nu\nabla^2 h(x,t) + \frac{\lambda}{2}\left(\nabla h(x,t)\right)^2 + \eta(x,t) \quad (2.69)$$

with $\nu = \gamma$, $\lambda = 2\gamma$ and $\langle\eta(x,t)\eta(x',t')\rangle = D\delta(x-x')\delta(t-t')$. The parameter D can be estimated with the formula: $\langle\mu^2(x,t)\rangle = D$ which gives as result: $D = \mu^2 + \sigma^2$.(μ is usually zero for noise.)

If we want to determine the mean surface growth velocity it is useful to make a Fourier transform. Following Krug [18] we get for the in the x-direction periodic functions $h(x,t)$ and $\eta(x,t)$ with period L:

$$h(x,t) = \sum_q h_q(t)e^{iqx} \quad (2.70)$$

$$\eta(x,t) = \sum_q \eta_q(t)e^{iqx} \quad (2.71)$$

where the sums run over the allowed reciprocal vectors of a lattice of linear size L. In this case the allowed reciprocal vectors are: $q = \frac{2\pi j}{L}$ with j an integer which satisfies $0 \leq j \leq L-1$.For the mean surface growth velocity we obtain:

$$v(t) = \frac{\partial\bar{h}(t)}{\partial t} = \frac{1}{L}\int_0^L dx\left\{\nu\nabla^2 h(x,t) + \frac{\lambda}{2}\left(\nabla h(x,t)\right)^2 + \eta(x,t)\right\} = \quad (2.72)$$

$$\frac{1}{L}\int_0^L dx\left\{\nu\nabla^2\left(\sum_q h_q(t)e^{iqx}\right) + \frac{\lambda}{2}\left(\nabla\left(\sum_q h_q(t)e^{iqx}\right)\right)^2 + \sum_q \eta_q(t)e^{iqx}\right\} =$$

$$\frac{1}{L}\int_0^L dx\left\{\nu\sum_q q^2 h_q(t)e^{iqx} + \frac{\lambda}{2}\left(\sum_q iq h_q(t)e^{iqx}\right)^2 + \sum_q \eta_q(t)e^{iqx}\right\} =$$

$$\frac{1}{L}\int_0^L dx\frac{\lambda}{2}\sum_{q\neq 0} q^2|h_q(t)|^2 + \eta_{q=0}(t) = \frac{\lambda}{2}\sum_{q\neq 0} q^2|h_q(t)|^2 + \eta_{q=0}(t)$$

Because $h(x,t)$ was defined through $h(x,t) = \log Z(x,t)$, the mean surface growth velocity $v(t)$ is proportional to the mean step free energy per unit length and that is a quantity we are interested in. We now want to determine the sum $\frac{\lambda}{2}\sum_{q\neq 0} q^2|h_q(t)|^2 + \eta_{q=0}(t)$. Therefore we look at the differential equations for $h_q(t)$. Inserting the Fourier transforms in the KPZ equation gives:

$$\frac{\partial}{\partial t}\left(\sum_q e^{iqx}h_q\right) = -\nu\sum_q q^2 h_q e^{iqx} + \frac{\lambda}{2}\left(\sum_q iqh_q e^{iqx}\right)^2 + \sum_q \eta_q e^{iqx} \tag{2.73}$$

Collecting terms with the same x-dependence gives as differential equation for the $h_q(t)$'s:

$$\frac{\partial}{\partial t}h_q(t) = -\nu q^2 h_q(t) - \frac{\lambda}{2}\sum_{r=0}^{q} r(q-r)h_r(t)h_{q-r}(t) + \eta_q(t) \tag{2.74}$$

We will first describe the situation with $\lambda = 0$. The general solution of equation (2.74) with $\lambda = 0$ is:

$$h_q(t) = e^{-\nu q^2 t}h_q(0) + \int_0^t d\tau e^{-\nu q^2(t-\tau)}\eta_q(\tau) \tag{2.75}$$

If we assume that the interface is initially flat (in our model this coincides with equal probabilities to start the step at $x = x_1, \ldots, x_L$), we get $h_q(0) = 0$, and $h_q(t)$ becomes:

$$h_q(t) = \int_0^t d\tau e^{-\nu q^2(t-\tau)}\eta_q(\tau) \tag{2.76}$$

If we multiply with $h_{q'}(t)$ and we average over the noise we obtain:

$$\langle h_q(t)h_{q'}(t)\rangle = \int_0^t d\tau \int_0^t d\tau' e^{-\nu q^2(t-\tau)}e^{-\nu q'^2(t-\tau')}\left\langle \eta_q(\tau)\eta'_q(\tau')\right\rangle \tag{2.77}$$

Now we have to calculate $\left\langle \eta_q(\tau)\eta'_q(\tau')\right\rangle$. If we insert the Fourier transform (2.70) in $\langle \eta(x,t)\eta(x',t')\rangle = D\delta(x-x')\delta(t-t')$ we obtain:

$$\left\langle \sum_q \eta_q(t)e^{iqx}\sum_{q'}\eta_{q'}(t)e^{iq'x'}\right\rangle = D\delta(x-x')\delta(t-t') \tag{2.78}$$

The $\delta(x-x')$ on the right hand side demands that $x = x'$ on the left hand side and because there is no x-dependence on the right hand side, there can be no x-dependence on the left hand side. Therefore we obtain:

$$\left\langle \sum_q \eta_q(t)\eta_{-q}(t)\right\rangle = D\delta(t-t') \tag{2.79}$$

This gives:

$$\left\langle \eta_q(\tau)\eta'_q(\tau')\right\rangle = \frac{D}{L}\delta_{q+q'}\delta(\tau-\tau') \tag{2.80}$$

If we insert equation (2.80) in equation (2.77) we obtain:

$$\langle h_q(t)h_{q'}(t)\rangle = \frac{D}{L}\delta_{q+q'}\int_0^t e^{-2\nu q^2(t-\tau)} = \frac{D}{L}\delta_{q+q'}S(q,t) \tag{2.81}$$

with $S(q,t) = \frac{1}{2\nu q^2}\left(1-e^{-2\nu q^2 t}\right)$.

Now it is time to handle the case with $\lambda \neq 0$. Although solving the differential equations (2.74) is not possible for $L > 3$, we can determine $\langle h_q(t)h_{q'}(t)\rangle$. For the case $L = 3$ we get as solutions for $h_q(t)$:

$$\begin{aligned}
h_0(t) &= \int_0^t \eta_0(\tau)d\tau \\
h_{\frac{2\pi}{L}}(t) &= \int_0^t e^{-\frac{4\nu\pi^2(t-\tau)}{L^2}}\eta_1(\tau)d\tau \\
h_{\frac{4\pi}{L}}(t) &= \int_0^t e^{-\frac{16\nu\pi^2(t-\tau)}{L^2}}\eta_2(\tau) - \frac{1}{2}\lambda e^{\frac{8\nu\pi^2\tau-16\nu\pi^2 t}{L^2}}\left(\int_0^\tau e^{\frac{4\nu\pi^2\tilde{\tau}}{L^2}}\eta_1(\tilde{\tau})d\tilde{\tau}\right)^2 d\tau
\end{aligned}$$

If we average over the noise, the last term in $h_{\frac{4\pi}{L}}(t)$ will vanish, because equation (2.80) says that $\left\langle \eta_q(\tau)\eta'_q(\tau')\right\rangle$ will be equal to zero if $q+q' \neq 0 \pmod 3$ and $1+1 \neq 0 \pmod 3$. Therefore we get the same expressions for $h_q(t)$ as in the case with $\lambda = 0$. For $L > 3$ we can use the same reasoning. For $q = \frac{4\pi}{L}$ we can neglect the same term as before, ($1+1 \neq 0 \pmod{j > 3}$, with j an integer). In the differential equation for h_q, see equation (2.74), with $q > \frac{4\pi}{L}$, we can neglect the part proportional to $\sum_{r=1}^{q-1} r(q-r)h_r(t)h_{q-r}(t)$ because after averaging over the noise it will result in terms proportional to $\langle \eta_r(t)\eta_{q-r}(t)\rangle$ which are equal to zero. Therefore we get the same expression for $\langle h_q(t)h_{q'}(t)\rangle$ as in the case $\lambda = 0$ for all q and q'.

Now we are ready to calculate the mean surface growth velocity. From equation (2.72) we obtain by averaging over the noise:

$$\langle v(t)\rangle = \frac{D\lambda}{2L}\sum_{q\neq 0}\frac{1-e^{-2\nu q^2 t}}{2\nu} \tag{2.82}$$

By taking the limit $t \to \infty$ the q-dependence disappears and we obtain:

$$\langle v(\infty)\rangle = \frac{\lambda D(L-1)}{4\nu L} \tag{2.83}$$

This equation shows that there is a finite size correction Δv of:

$$\Delta v = \langle v(L) \rangle - \langle v(\infty) \rangle = -\frac{D\lambda}{4\nu L} \tag{2.84}$$

Because the stationary average surface velocity is proportional to the average step free energy per unit length, we expect that in our simulations an $\frac{1}{L}$-dependence will appear in the step free energy. The $\frac{1}{L}$-dependence should be for our model of the form $-\frac{\sigma^2}{2L}$ if we insert our parameters in equation (2.84), and we assume $\mu = 0$, which can be done because a change in the mean impurity leads only to a shift in the step free energy. This result coincides with the result of Kardar for many steps, see equation (2.49). This method has the advantage that we don't have to use the not-totally justified replica method and the difficult Bethe ansatz solutions.

We indeed find the predicted finite size effect, see chapter 4, if σ is not too large.

2.8 'justification' of the replica method

The scheme of the replica method consists of finding an analytical continuation for Z^n for non-integer n. After that we have to take the limit $n \to 0$. This procedure is not justified for all cases, but there are some arguments why this method is so widely used.

The first argument is that all calculations which could be done on two ways, one using and one avoiding the replica method, gave identical results. Remark the resemblance of equation (2.49) and equation (2.84), although the situation is a bit different. Of course this is no proof for the the validity of the replica method, but it points out that the method makes sense at least in some cases.

The second argument is that in the high temperature region, the free energy is often an analytically function of all the parameters, and therefore the free energy can be written in powers of β. If this is the case, the validity of the replica method can be proven.

The third one is the most important argument. If we have a disordered system, there are many alternatives for the ground state, which are defined by the quenched disorder. These many ground states break the ergodicity. If we now want to calculate the thermodynamics of such a system, we have to take into account all the minima, and therefore we have to sum over all these ground states, and therefore it is reasonable to look at many replicas of the system, see [19].

This last argument can be made more formal in the following way.

Consider a spin system with Hamiltonian $\mathcal{H} = \mathcal{H}_J[S]$, which depends on the spin degrees of freedom and on the spin-spin interactions J_{ij}. (The same reasoning is also valid for many other systems.) If the interactions are quenched, the free energy is given by:

$$\frac{f_{\mathbf{J}}}{N} = -\frac{1}{\beta N} \log Z_J \quad \text{with} \quad Z_{\mathbf{J}} = \left\{ \sum_{\{\mathbf{s}\}} e^{-\beta \mathcal{H}_{\mathbf{J}}[s]} \right\} \tag{2.85}$$

In reality, the interactions (impurities) are not perfectly quenched. They can also change their value, only the typical time in which they change is much larger than the time the spin variables need to reach their thermal equilibrium. Therefore equation (2.85) makes sense.

If we assume that the spin variables, σ, and the spin interactions, J_{ij}, are not in thermal equilibrium we get interesting results. If the interactions have temperature T', and the spins have temperature T, we can write the total partition function of the system as:

$$Z_N = \int d\mathbf{J} P(\mathbf{J}) \exp\left[-\beta' f_{\mathbf{J}}\right] = \int d\mathbf{J} P(\mathbf{J}) \exp\left[\frac{\beta'}{\beta} \log Z_{\mathbf{J}}\right] = \int d\mathbf{J} P(\mathbf{J}) Z_{\mathbf{J}}^n \qquad (2.86)$$

with $n = \frac{T}{T'}$. Therefore the total free energy of the system is:

$$f = -k_B T' \log \langle Z^n \rangle \quad \text{with} \quad \langle Z^n \rangle = \int d\mathbf{J} P(\mathbf{J}) Z_{\mathbf{J}}^n \qquad (2.87)$$

The annealed case now corresponds to $n = 1$ while the quenched case corresponds to the limit $n \to 0$. Therefore we conclude that the replica method is more than just a mathematical trick.

2.9 Replica Symmetry Breaking

When we worked through the Sherrington Kirkpatrick model we found that the entropy became smaller than zero. This problem is not inherent to the model, but it is due to the assumptions we made in our calculations. We assumed that all the replicas were identical, see page 10, and that turns out to be the source of the negative entropy problem. The solution to the problem is called replica symmetry breaking. In contradiction to our assumption in (2.18), it turns out that we cannot take all the Q_{ab}'s equal to q. The technical reason for the problem of the negative entropy is the analytical continuation for all n. In general there are many different analytical continuations. For the S-K model there is a very ingenious continuation of Parisi [20], which breaks the replica symmetry. A very thorough treatment of this solution can be found in the book of Mezard, Parisi and Virasora [8] and in the book of Dotsenko [19]. Happily for short range interactions, for instance only neighboring spins interact with each other in the original model, it can be shown, see [4], that the replica symmetric solution is exact. For the model of Kardar it is not quite clear whether the replica method still works, therefore we performed some simulations to check this, see section 4.3.

Before we start with technical details, let's first try to explain what the replica symmetry breaking means physically.

For the Ising model of a ferromagnet, the concept of spontaneous symmetry breaking is well known. Below a critical temperature T_c, the spins will align spontaneously. Below T_c the expectation value of a spin, $\langle \sigma_i \rangle$, will be $\pm m$ for all spins. This is a bit strange

because the Hamiltonian of the system is symmetric with respect to inversion of all the spins, and therefore in a finite system, all the thermal averages $\langle\sigma_i\rangle$ are all equal to zero. However, if we take the thermodynamic limit, $N \to \infty$, the two states become separated by an infinite barrier and therefore the system will never jump from the state of magnetization $+m$ to the state of magnetization $-m$ or visa versa. The system is therefore not in the Gibbs state (obtained by summing over all the states in the partition function), but in a so called pure state in which there are non-zero site magnetizations.

A pure state can be characterized by the following property: All connected correlation functions are equal to zero at large distances. (For instance:
$\langle\sigma_i\sigma_j\rangle_c \equiv \langle\sigma_i\sigma_j\rangle - \langle\sigma_i\rangle\langle\sigma_j\rangle$=0.) In general replica symmetry breaking means that at low temperature, there are many pure states in the thermodynamic limit.

In a spin glass system we have many spins which interact with each other. Sometimes the interaction is ferromagnetic and sometimes anti-ferromagnetic. In the ferromagnetic case the spins tend to align, while in the anti-ferromagnetic case they tend to be opposite. If we are looking for the ground state, we would like the spins to arrange in such a way that for all pairs of spins, the energy of such a pair is as low as possible. Unfortunately, this is not possible in general. For instance in the 3-particle case. If the spins interact in pairs and all the interactions are anti-ferromagnetic, there is no configuration of the spins which minimizes all the spin interactions simultaneously. This effect is called frustration. For a larger system this effect of opposite forces becomes very important. For such a system, the ground state is often (almost) degenerate, which means that by reversing spins, the gain in energy from some interactions cancels (almost) against the loss of free energy from other interactions. If the number of particles grows, one can expect that, at low temperature, the number of local minima increases very rapidly, where local means that by flipping only one spin, the total energy doesn't decrease. The hypothesis is that at low temperature the free energy landscape contains an exponential number of local minima, which play the role of the pure states in the case of the ferromagnet. The idea is that we have to take all the minima into account if we determine the free energy.

Suppose we have a system of N particles. The free energy is a functional of the temperature and the density $\rho(x)$. This system has according to the hypothesis many minima, which we shall label with α. For each minimum we have a free energy F_α and a corresponding mean free energy per particle $f_\alpha = \frac{F_\alpha}{N}$. At low temperature the system will be in a minimum. Because at sufficiently low temperature, the barrier between two local minima is too high to cross, all the minima (not only the lowest) contribute to the free energy. Therefore we can make the following approximation: (see [21])

$$Z := \exp\left(-\beta N f_S\right) \approx \sum_\alpha \exp\left(-\beta N f_\alpha\right) \tag{2.88}$$

When the system becomes very large, the number of minima becomes also very large and it is convenient to introduce the function $\mathcal{N}(f, T, N)$ which is the density of minima whose free energy is equal to f. We assumed that for large N the number of minima

grows exponentially, and thus we write:

$$\mathcal{N}(f,T,N) \approx \exp(N\Sigma(f,T)) \tag{2.89}$$

In the previous formula $\Sigma(f,T)$ is called the complexity or configurational entropy. It is the entropy which arises from the presence of many local minima. Now we can approximate the partition function as:

$$Z = \int df \exp(-\beta N f)\mathcal{N}(f,T,N) \approx \int df \exp(-N\{\beta f - \Sigma(f,T)\}) \tag{2.90}$$

The integral in (2.90) goes over all the values of f with local minima, and therefore $f_m(T) < f < f_M(T)$ with f_m and f_M the free energy in the local minimum with the lowest respectively the highest free energy.. Moreover the hypothesis of the exponential number of minima is only valid in this region. According to [21], $\Sigma(f_m(T),T) = 0$ in all cases known and $\Sigma(f,T)$ is continuous at f_m. For large systems ($N \to \infty$), the integral in (2.90) can be approximated by it's maximum value. If the maximum value of $\Phi(f) := \beta f - \Sigma(f,T)$ is achieved in f^* we obtain:

$$\beta f_S = \min_f \Phi(f) := \beta f^* - \Sigma(f^*,T) \tag{2.91}$$

Now there are two possibilities:

- $f_m < f^* < f_M$. In this case f^* satisfies the equation $\beta = \frac{\partial\Sigma(f,T)}{\partial f}\Big|_{f=f^*}$. The system will be in one of the local minima. The number of minima that are allowed is $\exp(N\Sigma(f^*,T))$. The total entropy of this system is therefore equal to the typical entropy of an allowed minimum plus the configurational entropy coming from the presence of the other allowed minima.
- f^* lies on the edge of the interval $[f_m, f_M]$. The minimum is obtained in f_m, and we have $\Phi(f^*) = \beta f^*$. In this case there is no contribution to the entropy from the configurational entropy. The free energy is therefore dominated by one minimum. If this is the case, the free energy is dominated by only a few minima, we say that the replica symmetry is broken.

2.9.1 Replica symmetry breaking in the S-K model

In equation (2.17), Q_{ab} was defined as $Q_{ab} := \langle S_a S_b\rangle = q \quad \forall a \neq b$. Parisi's scheme for the Q_{ab}'s is far more ingenious. We regard Q_{ab} as matrix elements of the symmetric matrix Q. In the replica symmetric model the Q_{ab}'s are chosen as:

$$Q_{ab} = q \text{ if } a \neq b$$

Parisi's scheme consists of an infinite series of subdivisions.

$$\begin{pmatrix} Q_2 & Q_1 & Q_1 & Q_0 & Q_0 & Q_0 \\ Q_1 & Q_2 & Q_1 & Q_0 & Q_0 & Q_0 \\ Q_1 & Q_1 & Q_2 & Q_0 & Q_0 & Q_0 \\ Q_0 & Q_0 & Q_0 & Q_2 & Q_1 & Q_1 \\ Q_0 & Q_0 & Q_0 & Q_1 & Q_1 & Q_1 \\ Q_0 & Q_0 & Q_0 & Q_1 & Q_1 & Q_2 \end{pmatrix}$$

Figure 2.4: The elements of the matrix Q_0 are all equal to q_0, the elements of Q_1 are q_1 and the matrix Q_2 will be subdivided further.

- First the $n \times n$-matrix Q is divided into $\left(\frac{n}{m_1}\right)^2$ blocks of size $m_1 \times m_1$. m_1 has to be a divisor of n, but as n becomes very large (as in the case of the exponential number of local minima in the free energy landscape),and we take the limit $n \to \infty$, this restriction isn't a restriction any more. All the elements in the off-diagonal blocks are given the value q_0.
- The $\frac{n}{m_1}$ blocks on the diagonal are divided further. Each $m_1 \times m_1$-block is divided in $\left(\frac{m_1}{m_2}\right)^2$ sub-blocks of size $m_2 \times m_2$. All the elements in the off-diagonal blocks are given the value q_1. The diagonal blocks are matrices, which we call Q_2,which will be subdivided further (if possible) in an analog way.

The matrix after two steps with the proportions $n : m_1 : m_2 = 6 : 3 : 1$ is shown in Figure 2.4. Therefore after one step, we have $\frac{n}{m_1}$ groups of m_1 replicas, each group is again divided in $\frac{m_1}{m_2}$ groups of m_2 replicas, and so on. The fraction of the matrix which takes the value q, (thus the fraction of the pairs (ab) with $\left\langle s_i^a s_i^b \right\rangle = q$), is given by:

$$P(q) = \lim_{n \to 0} \frac{2}{n(n-1)} \sum_{(ab)} \delta \left(Q_{ab} - q \right) \tag{2.92}$$

For instance let us calculate how many times a q_i appears in the matrix Q. There are $\frac{n}{m_i}$ blocks on the diagonal which will be subdivided in sub-blocks, and wherein a q_i will appear. Each diagonal block is subdivided in $\frac{m_i}{m_{i+1}}$ blocks of size $m_{i+1} \times m_{i+1}$ of which $\left(\frac{m_i}{m_{i+1}}\right)^2 - \frac{m_i}{m_{i+1}}$ will contain q_i as elements. Therefore the total amount of q_i in the matrix Q is $\frac{n}{m_i}\left(\left(\frac{m_i}{m_{i+1}}\right)^2 - \frac{m_i}{m_{i+1}}\right)(m_{i+1})^2$. Dividing this number by $n(n-1)$ gives the fraction of the off-diagonal elements which is q_i. This gives: $P\left(q_i\right) = \frac{m_i - m_{i+1}}{n-1}$. Now we have to perform a mathematical tricky operation. We take the limit $n \to 0$, while before we assumed that $n \gg 1$. If we take into account that q_i can be equal to a q_j we

obtain:

$$P(q) = \sum_{i=0}^{k} (m_{i+1} - m_i)\, \delta(q - q_i) \tag{2.93}$$

So far we considered n and m_i as integers and we had $n \geq m_1 \geq m_2 \geq \ldots \geq 1$, but because we have taken the $n \to 0$ limit this cannot be the case anymore. (2.93) is a positive definite measure, only if $0 \leq m_i \leq m_{i+1} \leq 1$. Now we introduce the function $q(x)$, defined as:

$$q(x) = q_i \quad \text{if} \quad m_i < x < m_{i+1} \tag{2.94}$$

From numerical studies of the saddle-point-equations, see [8], it follows that $q(x)$ is an increasing function. We now want to find the extrema of the free energy as a function of the q_i's and m_i's. It is convenient to introduce the following function:

$$x(q) = \int_{-1}^{q} dq' P(q') \tag{2.95}$$

With this definition we can write the probability $P(q)$ as:

$$P(q) = \frac{dx}{dq} \tag{2.96}$$

If we have an infinite number of subdivisions of the matrix Q, the function $q(x)$ becomes an arbitrary function, because every function with a countable number of discontinuities, can be approximated by piecewise constant functions, see [22].

It turns out that a matrix element can be interpreted as the overlap between two states. For two replicas in different local minima we have that:

$$Q_{ab} = \frac{1}{N} \sum_{i=1}^{N} m_i^a m_i^b \tag{2.97}$$

where the magnetization $m_i^a = \langle S^i \rangle_a$. We are so interested in the overlap between two configurations, because the overlaps control many physical properties. For instance the magnetic susceptibility can be calculated with the aid of the formula, see [23]:

$$\chi = \beta \left(1 - \overline{\langle q \rangle}\right) \tag{2.98}$$

where $\overline{\langle q \rangle}$ is the average over the impurities of the equilibrium expectation of the overlap between two states.

Another way to obtain information about the system is to look at the characteristic function $g(y)$:

$$g(y) = \int dq P(q) e^{yq} = \frac{1}{n(n-1)} \sum_{(ab)} e^{yQ_{ab}} \overset{n \to 0}{\longrightarrow} \int_0^1 dx e^{yq(x)} \tag{2.99}$$

For two replicas a similar expression can be written down for the probability to have overlaps q_1 and q_2:

$$g\left(y_1,y_2\right)=\int dq_1dq_2e^{y_1q_1+y_2q_2}P\left(q_1,q_2\right)=\frac{1}{n(n-1)(n-2)(n-3)}\sum_{\substack{a,b,c,d\\a\neq b\neq c\neq d\\b\neq d\neq a\neq c}}e^{y_1Q_{ab}+y_2Q_{cd}} \tag{2.100}$$

We have that

$$\sum_{\substack{a,b,c,d\\a\neq b\neq c\neq d\\b\neq d\neq a\neq c}}e^{y_1Q_{ab}+y_2Q_{cd}}=\sum_{\substack{a,b\\a\neq b}}\sum_{\substack{c,d\\c\neq d}}e^{y_1Q_{ab}+y_2Q_{cd}}-4\sum_{\substack{a,b\\a\neq b}}e^{y_1Q_{ab}}\sum_{\substack{d\\d\neq a}}e^{y_2Q_{ad}}+2\sum_{\substack{a,b\\a\neq b}}e^{(y_1+y_2)Q_{ab}}=$$
$$n(n-1)g\left(y_1\right)n(n-1)g\left(y_2\right)-4n(n-1)g(y_1)(n-1)g(y_2)+2g(y_1+y_2)n(n-1)=$$
$$\left(n^4-6n^3+9n^2-4n\right)g\left(y_1\right)g\left(y_2\right)+\left(2n^2-2n\right)g\left(y_1+y_2\right)$$

Therefore in the limit $n\rightarrow 0$ we can write $g\left(y_1,y_2\right)$ as:

$$g\left(y_1,y_2\right)=\frac{2}{3}g\left(y_1\right)g\left(y_2\right)+\frac{1}{3}g\left(y_1+y_2\right) \tag{2.101}$$

If we compare this result with the first part of equation (2.100) we get:

$$P\left(q_1,q_2\right)=\frac{1}{3}P\left(q_1\right)\delta\left(q_1-q_2\right)+\frac{2}{3}P\left(q_1\right)P\left(q_2\right) \tag{2.102}$$

This result is very remarkable because for four different replicas one obviously has:

$$P_J\left(q_{12},q_{34}\right)=P_J\left(q_{12}\right)P_J\left(q_{34}\right) \tag{2.103}$$

Averaging over the impurities gives thus a non-trivial result, and therefore $P_J(q)$ has to fluctuate with J_{ij} in a non-trivial way. (See also the next section.)

2.10 Ultrametricity

The same calculation can be done to derive the joint probability distribution for three replicas and their mutual overlap: This gives as result (with the aid of a characteristic function):

$$\begin{aligned}P\left(q_{12},q_{13},q_{23}\right)=&\tfrac{1}{2}P\left(q_{12}\right)x\left(q_{12}\right)\delta\left(q_{12}-q_{13}\right)\delta\left(q_{12}-q_{23}\right)+\\&\tfrac{1}{2}P\left(q_{12}\right)P\left(q_{13}\right)\theta\left(q_{12}-q_{13}\right)\delta\left(q_{13}-q_{23}\right)+\\&\tfrac{1}{2}P\left(q_{13}\right)P\left(q_{23}\right)\theta\left(q_{13}-q_{23}\right)\delta\left(q_{23}-q_{12}\right)+\\&\tfrac{1}{2}P\left(q_{23}\right)P\left(q_{12}\right)\theta\left(q_{23}-q_{12}\right)\delta\left(q_{12}-q_{13}\right)\end{aligned} \tag{2.104}$$

where $x(q)$ is defined in (2.95). Equation (2.104) is interesting, because it contains a special characteristic of the system. The probability is only non zero if at least two of the overlaps are equal and the third one is bigger or equal to the other two overlaps.

The same result can also be derived by looking at the matrix Q; it can be easily checked that $P(q_{12}, q_{13}, q_{23}) = 0$ unless two of the overlaps are equal and the third one is bigger or equal to the other two overlaps. If we also use the invariance of the Hamiltonian under the exchange of the replicas we get as general formula for $P(q_{12}, q_{13}, q_{23})$, see [24]:

$$\begin{aligned} P(q_{12}, q_{13}, q_{23}) &= A(q_{12})\,\delta(q_{12} - q_{13})\,\delta(q_{12} - q_{23}) + B(q_{12}, q_{13})\,\theta(q_{12} - q_{12})\,\delta(q_{13} - q_{23}) \\ &+ B(q_{13}, q_{23})\,\theta(q_{13} - q_{23})\,\delta(q_{23} - q_{12}) + B(q_{23}, q_{12})\,\theta(q_{23} - q_{12})\,\delta(q_{12} - q_{13}) \end{aligned} \tag{2.105}$$

$A(q)$ and $B(q)$ are properly normalized and the function $B(q, q')$ is symmetric in the way that $B(q, q') = B(q', q)$. We can now integrate over q_{23} and we obtain:

$$P_2(q_{12}, q_{13}) = \left[A(q_{12}) + \int_q^\infty dq_{23} B(q_{13}, q_{23}) \right] \delta(q_{12}, q_{13}) + B(q_{12}, q_{13}) \tag{2.106}$$

By integrating again we find the probability for the overlap between 2 replicas. By using the equivalence of the replicas we obtain:

$$P_1(q_{12}) = A(q_{12}) + \int_q^\infty dq_{13} B(q_{12}, q_{13}) + \int_{-\infty}^\infty dq_{13} B(q_{12}, q_{13}) \tag{2.107}$$

In [25], Guerra demonstrated that:

$$\left\langle q_{12}^2 q_{23}^2 \right\rangle = \frac{1}{2} \left\langle q_{12}^4 \right\rangle + \frac{1}{2} \left\langle q_{12}^2 \right\rangle^2 \tag{2.108}$$

where

$$\langle q^n \rangle = \int_{-\infty}^{+\infty} dq P_1(q) q^n$$

The derivation of this equality is not difficult and very general, but to long to show here. If we look separately at the terms with q^4 and $q^2 q'^2$ we get as solution for equation (2.108):

$$A(q) = \int_{-\infty}^q dq' B(q, q') \tag{2.109}$$

$$B(q, q') = 2 \left(\int_{-\infty}^{+\infty} dq'' B(q, q'') \right) \left(\int_{-\infty}^{+\infty} dq'' B(q', q'') \right) \tag{2.110}$$

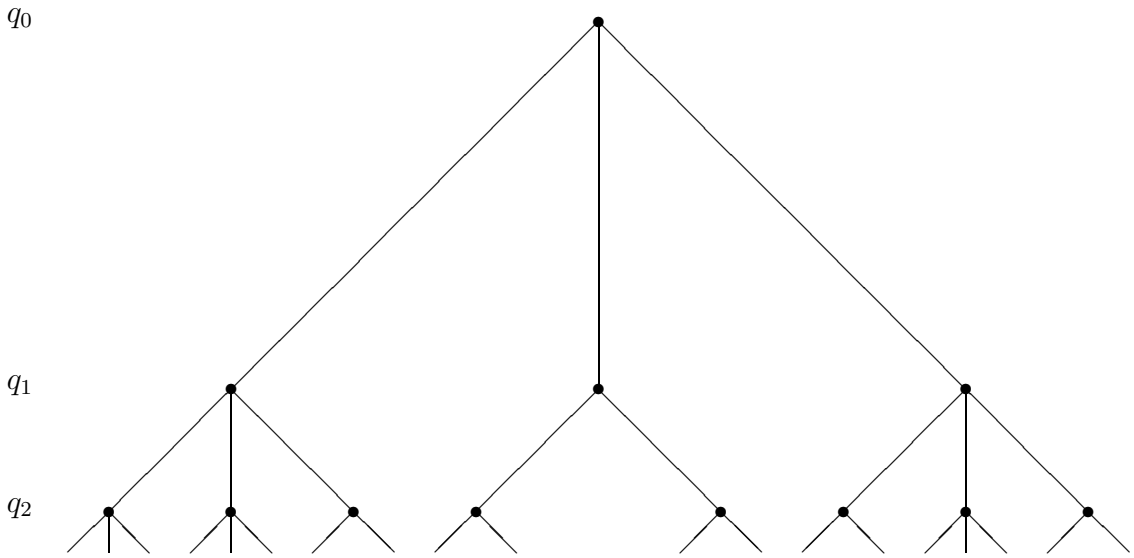

Figure 2.5: An ultrametric tree with 4 levels

Using equations (2.107) and (2.109) we obtain:

$$P_1(q) = 2 \int_{-\infty}^{+\infty} dq' B\left(q, q'\right) \tag{2.111}$$

and therefore we have that:

$$B\left(q, q'\right) = \frac{1}{2} P_1(q) P_1\left(q'\right) \tag{2.112}$$

which gives for $A(q)$:

$$A(q) = \frac{1}{2} x(q) P_1(q) \tag{2.113}$$

The ultrametricity can be represented by a tree, in which all the different configurations are present, see Figure 2.5 This figure should be interpreted as follows: If one goes from one configuration to another configuration via the shortest path over the tree, the overlap between the configurations is associated with the value q_i belonging to the highest vertex of the path. Instead of trying to calculate $\overline{P_J\left(q_1\right) P_J\left(q_2\right)}$, it turns out to be easier to calculate

$$\overline{Y_J(q)^k} = \int_q^{q_{max}} dq_1 \ldots \int_q^{q_{max}} dq_k \overline{P_J\left(q_1\right) \ldots P_J\left(q_k\right)} \tag{2.114}$$

If we introduce the definition, see (2.95):

$$y(q) = 1 - x(q) = \int_q^1 dq' P(q') \tag{2.115}$$

$\overline{Y_J(q)^2}$ can be written as:

$$\overline{Y_J(q)^2} = \frac{1}{3}y(q) + \frac{2}{3}y(q)^2 \tag{2.116}$$

where we used equation (2.102) The results of $\overline{Y_J(q)^k}$ for $k = 2 \ldots 7$, including a derivation can be found in [26]. We know that we only have given a very small part of the available techniques to deal with replica symmetry breaking in the S-K model. The interested reader can find much more details in [27], [8],[28],[29] and [30].

Chapter 3

Bethe-ansatz for 1-dimensional particles

A very thorough treatment of the Bethe-ansatz can be found in Thacker [31]. Before we go to the problem we want to solve, we describe the easier case of a system of N non-relativistic bosons. The derivation is mainly the same, but the technical details are easier.

3.0.1 Bethe-ansatz for N bosons

Let's start with the Hamiltonian for bosonic particles with an δ-function potential [32].

$$\mathcal{H} = \int \left(\partial_x \phi^*(x) \partial_x \phi(x) + c\phi^*(x)\phi^*(x)\phi(x)\phi(x)\right) dx \tag{3.1}$$

where $\phi(x)$ and $\phi^*(x)$ are boson-fields with the standard commutation-relation (at equal time):

$$[\phi(x), \phi^*(y)] = \delta(x - y) \tag{3.2}$$

Because the particle-number-operator $\int dx \phi^* \phi$ commutes with the Hamiltonian, we can hold the particle-number fixed at N. So the Hamiltonian describes a system of N bosons with a two body delta-function potential (the last term in the Hamiltonian).

To enlighten the Bethe-ansatz for this system, we try to solve the system with time-independent perturbation-theory first. Therefore we look at the Lippmann-Schwinger equation, see Sakurai [33]. We write

$$\mathcal{H} = \mathcal{H}_0 + V \text{ with } \mathcal{H}_0 = \int \partial_x \phi^* \partial_x \phi dx \text{ and } V = \int c\phi^* \phi^* \phi \phi dx \tag{3.3}$$

We want to find the solutions of:

$$\mathcal{H} |\psi\rangle = E |\psi\rangle \Rightarrow (E - \mathcal{H}_0) |\psi\rangle = V |\psi\rangle \tag{3.4}$$

The general solution of this equation is:

$$\left|\psi^{+}\right\rangle = |\phi\rangle + G_0^{+}\left(E_0\right) V \left|\psi^{+}\right\rangle \tag{3.5}$$

where $|\phi\rangle$ is an eigenstate of $\mathcal{H}_0$ and thus a product of plain waves, and G_0^+ is Green's function $\frac{1}{E_0-\mathcal{H}_0+i\epsilon}$. We took the Green's function G_0^+ instead of $G_0^- = \frac{1}{E_0-\mathcal{H}_0-i\epsilon}$ because in the G_0^+ case we have no incoming spherical wave, see Sakurai [33]. That (3.5) is a solution of (3.4) can be checked by applying $E_0 - \mathcal{H}_0$ to (3.5). For the state with N particles with momenta $k_1, k_2, \ldots, k_N$ we write $|\phi\rangle = |k_1, k_2, \ldots, k_N\rangle$. This state can be constructed by applying creation-operators N times to the vacuum, where a creation-operator for a particle with momentum k is given by $a_k^\dagger = \int dx e^{ikx}\phi^*(x)$. The energy of this state is $E_0 = \sum_{i=1}^{N} k_i^2$. If we iterate (3.5) we obtain:

$$\left|\psi^{+}\right\rangle = |\phi\rangle + G_0\left(E_0\right) V |\phi\rangle + \left(G_0\left(E_0\right) V\right)^2 |\psi\rangle = \ldots = \sum_{j=0}^{\infty} \left(G_0\left(E_0\right) V\right)^j |\phi\rangle \tag{3.6}$$

The zero-order term of (3.6) is the free state. The first and higher-order terms have to be calculated. For N=2 equation (3.6) can be represented by the following Feynman-diagrams.

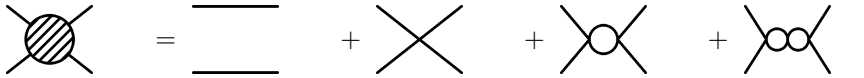

The first order term is given by: see for instance [34] (we have δ-function interactions):

$$\int \frac{dp_1}{2\pi}\frac{dp_2}{2\pi}\frac{1}{k_1^2+k_2^2-p_1^2-p_2^2+i\epsilon}(4c)(2\pi)\delta\left(k_1+k_2-p_1-p_2\right) a_{p_1}^\dagger a_{p_2}^\dagger |0\rangle \tag{3.7}$$

where $|0\rangle$ is the vacuum state, which contains no particles. Suppose we take $k_2 > k_1$. Then we only get a contribution if $x_1 > x_2$. We know from Cauchy's-theorem that if $k_1 < k_2$ (by taking as integration-contour the lower part of the circle with origin 0 and radius R and the real-axis from -R to R and taking the limit $R \to \infty$):

$$\lim_{\epsilon \downarrow 0} \int dp \frac{e^{ipx_2} e^{i(k1+k2-p)x_1}}{k_1^2+k_2^2-p^2-\left(k_1+k_2-p\right)^2+i\epsilon} = \frac{\pi i}{k_1-k_2} e^{i(k_1x_1+k_2x_2)} \tag{3.8}$$

We get an extra minus sign from the non-standard orientation of the integration contour. If we interchange the role of x_1 and x_2 we can write the first order term as:

$$\left(\frac{2ic}{k_1-k_2}\right)\int dx_1 dx_2 \theta(x_1-x_2) e^{i(k_1x_2+k_2x_1)} \phi^*\left(x_1\right)\phi^*\left(x_2\right)|0\rangle \tag{3.9}$$

The second order term Feynman-diagram contains one loop. Such a loop gives as contribution the factor:

$$2c\int \frac{\frac{dp}{2\pi}}{k_1^2+k_2^2-p^2-\left(k_1+k_2-p\right)^2+i\epsilon} = \frac{ic}{k_2-k_1}$$

Therefore we can write the wave function as:

$$\left|\psi^{+}\right\rangle = \int dx_1 dx_2 \left(1 + \sum_{j=1}^{\infty} 2 \left(\frac{ic}{k_1 - k_2}\right)^{j} \theta(x_2 - x_1)\right) e^{i(k_1 x_1 + k_2 x_2)} \phi^{*}(x_1)\, \phi^{*}(x_2) \left|0\right\rangle \tag{3.10}$$

Writing 1 as $\theta(x_2 - x_1) + \theta(x_1 - x_2)$ and using the geometrical serie we get:

$$\left|\psi^{+}(k_1, k_2)\right\rangle = \int dx_1 dx_2 \left(\theta(x_1 - x_2) + \theta(x_2 - x_1) \tfrac{k_1 - k_2 + ic}{k_1 - k_2 - ic}\right) e^{i(k_1 x_1 + k_2 x_2)} \phi^{*}(x_1)\, \phi^{*}(x_2) \left|0\right\rangle \tag{3.11}$$

If we do not pay attention to the normalization, we can multiply the wave-function with the constant $1 + \frac{ic}{k_2 - k_1}$ to obtain the more convenient formula for the wave-function:

$$\left|\psi^{+}(k_1, k_2)\right\rangle = \int dx_1 dx_2 \left(1 - \frac{ic}{k_1 - k_2} \epsilon(x_1 - x_2)\right) e^{i(k_1 x_1 + k_2 x_2)} \phi^{*}(x_1)\, \phi^{*}(x_2) \left|0\right\rangle \tag{3.12}$$

where we used the step-function

$$\epsilon(x) = \begin{cases} -1 & \text{if } x < 0 \\ 1 & \text{if } x > 0 \end{cases}$$

$\left|\psi^{+}(k_1, k_2)\right\rangle$ obeys the following eigenvalue equation:

$$\mathcal{H} \left|\psi^{+}(k_1, k_2)\right\rangle = \left(k_1^2 + k_2^2\right) \left|\psi^{+}(k_1, k_2)\right\rangle \tag{3.13}$$

This can be shown directly by applying (3.1) to (3.12). Performing integration by parts for the free part gives the desired contribution plus a δ-function contribution from the step-function, which cancels against the potential-term in the Hamiltonian.

If $c < 0$, that means that the δ-function-potential is attractive, we need to look closer to the wave function. We want that the system is in a bounded state, and therefore we want the wave-function to fall off if $|x_1 - x_2|$ becomes large. Therefore we have to allow the momenta to become complex-valued. Otherwise the exponential-function in (3.12) would never fall off. We have to impose some other restriction, because if the exponential in (3.12) falls off for one configuration of x_1 and x_2, the exponential would blow up for the configuration $x_1 \to -x_1$ and $x_2 \to -x_2$. Therefore we demand that $\left(1 - \frac{ic}{k_1 - k_2} \epsilon(x_1 - x_2)\right)$ vanishes for one branch of the step-function. This gives the restriction: $k_1 - k_2 = -ic$. Furthermore we want that the total momentum remains real, thus we can write: $k_1 + k_2 = K$. With these assumptions (3.12) can be written as:

$$\left|\psi^{+}(k_1, k_2)\right\rangle = 2 \int dx_1 dx_2 \theta(x_2 - x_1)\, e^{\frac{1}{2} c (x_1 - x_2)} e^{\frac{1}{2} i K (x_1 + x_2)} \phi^{*}(x_1)\, \phi^{*}(x_2) \left|0\right\rangle \tag{3.14}$$

This equation contains as internal the wave-function the standard Bethe-ansatz for two particles, which is used on page 15:

$$\psi(x_1, x_2) = e^{\frac{1}{2}c|x_1 - x_2|} \tag{3.15}$$

The absolute value in the exponent comes from symmetry arguments. This is a bounded state with energy $E = k_1^2 + k_2^2 = \frac{1}{2}(K^2 - c^2)$, so the binding energy is equal to $\frac{1}{2}c^2$.

If we are working on a cylinder (a periodic box), all states are bounded states, and therefore we cannot use the previous reasoning and we have to use equation (3.12). For the internal wave function

$$\psi(x_1, x_2) = \left(1 - \frac{ic}{k_1 - k_2}\epsilon(x_1 - x_2)\right) e^{i(k_1 x_1 + k_2 x_2)} \tag{3.16}$$

we obtain as boundary conditions:

$$\begin{aligned} \psi(0, x_2) = \psi(L, x_2) &\Leftrightarrow \left(1 + \frac{ic}{k_1 - k_2}\right) = e^{ik_1 L}\left(1 - \frac{ic}{k_1 - k_2}\right) \\ \psi(x_1, 0) = \psi(x_1, L) &\Leftrightarrow \left(1 + \frac{ic}{k_2 - k_1}\right) = e^{ik_2 L}\left(1 - \frac{ic}{k_2 - k_1}\right) \end{aligned} \tag{3.17}$$

Now we have reached the point where we can use the Bethe-ansatz for N bosons. Bethe's idea [13] was that the wave-function for N particles would be a generalization of the two-body case. For this system, the Bethe-ansatz can be written as:

$$\begin{aligned} &|\psi(k_1, \ldots, k_N)\rangle = \\ &\int \left(\prod_{j=1}^{N} e^{ik_j x_j} dx_j\right) \prod_{1 \le i < j \le N} \left(1 - \tfrac{ic}{k_i - k_j}\epsilon(x_i - x_j)\right) \phi^*(x_1) \ldots \phi^*(x_N) |0\rangle \end{aligned} \tag{3.18}$$

This state is also an eigenfunction of $\mathcal{H}_N$ with eigenvalue $\sum_{i=1}^{N} k_i^2$. (Again this can be proven by performing partial integration, where the δ-functions cancel against each other.) If we have an attractive potential, $c < 0$, then we look again for bounded states. As for the two-particle state we keep the total momentum $K = \sum_{i=1}^{N} k_i$ real and we have to choose the k_i complex to let the exponentials in (3.18) fall off. Furthermore for all but one ordening ($x_1 < x_2 < \ldots < x_N$), we want that $\prod_{1 \le i < j \le N} \left(1 - \frac{ic}{k_i - k_j}\epsilon(x_i - x_j)\right)$ becomes zero, to prevent the wave-function to blow up. This gives for the momenta:

$$k_i = \frac{K}{N} + \frac{1}{2}(N - (2i - 1))\, ic \qquad 1 \le i \le N \tag{3.19}$$

Such a configuration of momenta is called a 'N-string'. With these assumptions the wave-function becomes:

$$\begin{aligned} &|\psi(k_1, \ldots, k_N)\rangle = \\ &\int \left(\prod_{j=1}^{N} dx_j\right) e^{i\frac{K}{N}\sum_{j=1}^{N} x_j} e^{\frac{1}{2}c\sum_{i<j}|x_j - x_i|} \prod_{1 \le i < j \le N} \theta(x_j - x_i)\, \phi^*(x_1) \ldots \phi^*(x_N) |0\rangle \end{aligned} \tag{3.20}$$

After symmetrization we get as wave-function in the rest-frame ($\sum_{j=1}^{N} x_j = 0$):

$$\psi(x_1, x_2, \ldots, x_N) = e^{\frac{1}{2}c\sum_{i<j}|x_j - x_i|} \tag{3.21}$$

which is used in (2.33). The energy of this state is

$$E = \sum_{j=1}^{N} k_j^2 = \sum_{j=1}^{N} \left(\frac{K}{N} + \frac{1}{2}(N - (2j-1))\, ic \right)^2 = \frac{K^2}{N} - \frac{c^2}{12}\left(N^3 - N\right)$$

where we used (2.35).

Suppose that the N bosons are in a box of size L with periodic boundary-condition. Equivalent to equation (3.17) we get boundary conditions like:

$$\psi(0, x_2, \ldots, x_N) = \psi(L, x_2, \ldots, x_N)$$

With the aid of the internal wave function in (3.18), this is equivalent to:

$$\prod_{j\neq i}\left(1 + \frac{ic}{k_i - k_j}\right) = e^{ik_iL}\prod_{j\neq i}\left(1 - \frac{ic}{k_i - k_j}\right) \tag{3.22}$$

This can be written as:

$$e^{ik_iL} = \prod_{j\neq i}\frac{k_i - k_j + ic}{k_i - k_j - ic} \tag{3.23}$$

There is no general solution (for all N) for the k_i. Therefore we can not give a closed expression for $E(N, L)$.

3.0.2 Bethe-ansatz for n replicas of N identical fermions

Let's have a look now at the Hamiltonian for n replicas of N identical fermions which interact via a δ-function potential.

$$\mathcal{H} = \int dx \left(\sum_a \partial_x \phi_a^* \partial_x \phi_a + c \sum_{a,b} \phi_a^* \phi_b^* \phi_a \phi_b \right) \tag{3.24}$$

where we sum over the different colors. This problem was solved by Yang in 1967 [35]. Again we look first at the two-particle system. If we assume that the colors of the particles are w_1 and w_2, we can write the eigenstate as:

$$|k_1, k_2\rangle = \int dx_1 dx_2 \psi(x_1, x_2)\, \phi_{w_1}^* \phi_{w_2}^* |0\rangle \tag{3.25}$$

where the wave-function $\psi(x_1, x_2)$ is a generalization of the bosonic case, see the previous subsection. The Bethe-ansatz for this case can be written as:

$$\psi(x_1, x_2) = \sum_{P,Q} [Q, P] \theta(x_{Q_1} < x_{Q_2}) \, e^{i\left(k_{P_1} x_{Q_1} + k_{P_2} x_{Q_2}\right)} \tag{3.26}$$

with Q and P are permutations of {1,2}. For $N = 2$ there are only two different permutations; the identity, and the permutation which maps $1 \to 2$ and $2 \to 1$, which we denote by 12 and 21 for later convenience. $[Q, P]$ are coefficients. If we write out (3.26) we obtain:

$$\begin{aligned}\psi(x_1, x_2) = \theta(x_1 < x_2)\,[12, 12] e^{i(k_1 x_1 + k_2 x_2)} + \theta(x_1 < x_2)\,[12, 21] e^{i(k_2 x_1 + k_1 x_2)} + \\ \theta(x_2 < x_1)\,[21, 12] e^{i(k_1 x_2 + k_2 x_1)} + \theta(x_2 < x_1)\,[21, 21] e^{i(k_2 x_2 + k_1 x_1)}\end{aligned} \tag{3.27}$$

We demand that the wave-function is continuous at $x_1 = x_2$, that restricts the coefficients $[Q, P]$ by the formula:

$$[12, 12] + [12, 21] = [21, 12] + [21, 21] \tag{3.28}$$

The state $|k_1, k_2\rangle$ can only be an eigenstate of (3.24) if the δ-functions from the kinetic part of the Hamiltonian cancel against the potential term. (If this happens, the eigenvalue is $k_1^2 + k_2^2$). This restricts the coefficients $[Q, P]$ even further. When we demand the δ-functions to cancel we obtain as equation:

$$\begin{aligned}[12, 12] - [12, 21] + [21, 12] - [21, 21] = \\ \tfrac{ic}{k_1 - k_2} \left([12, 12] + [12, 21] + [21, 12] + [21, 21]\right)\end{aligned} \tag{3.29}$$

Combining this equation with (3.28) we can write these equations in a form which is useful for the many-particle case, using the notation $\lambda_{12} = \frac{ic}{k_1 - k_2}$ we obtain:

$$\begin{pmatrix} [12, 21] \\ [21, 21] \end{pmatrix} = \frac{-\lambda_{12}}{1 + \lambda_{12}} \begin{pmatrix} [12, 12] \\ [21, 12] \end{pmatrix} + \frac{1}{1 + \lambda_{12}} \begin{pmatrix} [21, 12] \\ [12, 12] \end{pmatrix} \tag{3.30}$$

We can rewrite (3.30) in the following way: The coefficient $[Q, P]$ form a 2×2-matrix, and the columns of this matrix are denoted by ξ_P.

$$\xi_{21} = \Upsilon \xi_{12} \quad \text{with} \quad \Upsilon = \frac{-\lambda_{12}}{1 + \lambda_{12}} + \frac{1}{1 + \lambda_{12}} \mathcal{P}_{12} \tag{3.31}$$

and $\mathcal{P}_{12}$ permutates the two components of the wave-vector. Let's look closer to (3.30). We can see it as a scattering-process of two one-dimensional particles on a line. We can interpret the permutations Q and P as follows. A permutation Q changes the ordening of the color-labels and a permutation P does the same for the momenta. Therefore the coefficient $[Q, P]$ can be regarded as the amplitude for finding a specific ordening of the momenta and colors. ($[12, 21]$ is the amplitude for finding particle one with color w_1

and momentum k_2.) Suppose $k_1 > k_2$. If the two particles scatter they might exchange their color or momentum. (The first and second term on the righthandside of (3.30).) With this interpretation we can generalize the equations to the N-particle system. We obtain as state:

$$|k_1, k_2, \ldots, k_N\rangle = \int dx_1 dx_2 \ldots dx_N \psi(x_1, x_2, \ldots x_N)\, \phi^*_{w_1}(x_1)\, \phi^*_{w_2}(x_2) \ldots \phi^*_{w_N}(x_N) \tag{3.32}$$

with as N-body wave-function:

$$\psi(x_1, x_2 \ldots, x_N) = \sum_{P,Q} [Q, P]\, \theta(x_{Q_1} < x_{Q_2}, \ldots, x_{Q_N})\, e^{i\left(\sum_j k_{P_j} x_{Q_j}\right)} \tag{3.33}$$

For this system we would like to do the same as for the two-particle case. Unfortunately the N-body case requires a lot of algebra. We now return to the approach in the article of Kardar, in which he gives a short-handwaving argument to obtain the restrictions due to the periodic-boundary conditions. The interested reader can find some more information in the review-article on the Bethe-ansatz by Thacker [31], and in the article of Yang [35]

We demand that the wave-function is continuous, and we also demand that $|k_1, k_2, \ldots, k_N\rangle$ is an eigenstate of the Hamiltonian in (3.24), which means that the δ-functions cancel against each other. This gives restrictions on the coefficients $[Q, P]$ analogue to the two-particle case. If we interchange to fermions of the same color, we demand that the wave-function is antisymmetric. If we interchange two fermions of different color, we demand that the wave-function is symmetric. Finally the periodic boundary conditions relate the amplitude for finding a particle with the same color and momentum at the other end of the box.

Because we want that the wave-function doesn't blow up, we have to take the momenta complex-valued. The precise form of the momenta depends on the number of fermions of each color.

Chapter 4

simulations

4.1 A square lattice

4.1.1 introduction

For many of our simulations we used the model of Kardar (see theory). We have a finite square (two-dimensional) lattice and we made the lattice cylindrical by identifying two ends of the lattice. On this cylindrical lattice we forced a step, or an interface. We have assumed the following (see Figure 4.1) If the step goes through a transversal bond the energy cost is equal to the constant K and if the step runs over a parallel bond, the energy cost is $\mu(x,t)$, a random distributed quantity. Furthermore we assumed that transversal kinks are rare, and that transversal kinks which are larger than one are even more rare. Therefore we restrict the transversal displacements, for simplicity, to at most one lattice spacing per time unit. For this system we calculated the partition function of the interface with the aid of the transfer matrix formalism.

$$Z = \sum_{\{\mathbf{s}\}} e^{-\beta H_J[s]} \tag{4.1}$$

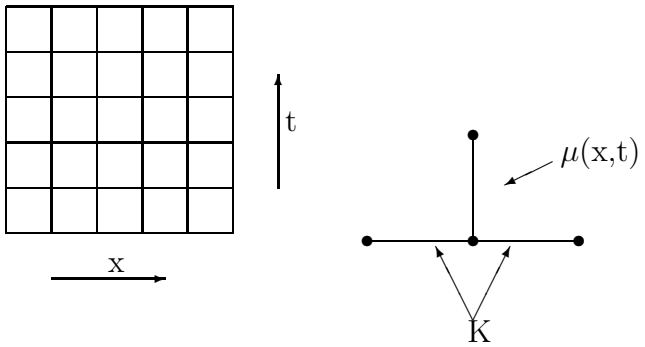

Figure 4.1:

where s is a possible configuration of the step. The Hamiltonian is dependent on the actual configuration of the $\mu(x,t)$'s. The transfer matrix formalism works as follows in this particular situation. We let the interface start at a certain point x' at the bottom of the cylinder. Now we assign a value Z(x,t) to each lattice point on the cylinder, with the following equations:

$$\begin{aligned} Z(x,1) &= \delta(x,x') \\ Z(x,t) &= e^{-\beta\mu(x,t)}\left\{Z(x-1,t-1)e^{-\beta K} + Z(x,t-1) + Z(x+1,t-1)e^{-\beta K}\right\} \end{aligned} \tag{4.2}$$

In this way we can calculate the partition function to start at $(x',1)$ and to end at (x,t) for each lattice point. (If we take $\mu(x,t)$ equal to infinity with probability p and zero with probability $(1-p)$, the problem is just the problem of directed percolation, which has not been solved analytically yet, see [36].) In our computer model we kept the terms in equation (4.2) in an acceptable range by determining for all t the largest term $Z(x,t)$. If the largest term was too large (bigger than 1000) or too small (smaller than 1/1000), we divided respectively multiplied $Z(x,t)$ for all x by a factor 1000. By counting the number of times we did this, we can get the correct result without the problem of too large terms.

4.1.2 optimization of the length of the system

We expect that the average free energy per unit length for $t \to \infty$ will hardly fluctuate anymore because the system will be much larger than the correlation length. We also expect that for large t the free energy per unit length will not depend any more on the starting point of the interface. Numerical simulations, which were intended to choose a suitable length of the cylinder for the rest of the simulations, confirm this. On the one hand one wants to take the length of the system as large as possible to obtain a very accurate result. On the other hand you want to choose the system as small as possible to obtain the results very fast. We performed some numerical simulations on this system for diffent lengths and widths of the cylinder. In these simulations we kept the energy of a transversal bond K equal to 1, and we chose the energy of the parallel bond in the following way: $\mu(x,t) = 0$ with probability $\frac{9}{10}$ and $\mu(x,t) = 1$ with probability $\frac{1}{10}$. Here and in the rest of our simulations we obtained the estimates for the errors in our results by performing the same simulations several (N) times. We took as measure for the error the following quantity:

$$\begin{aligned} \text{mean value} := m &= \frac{1}{N}\sum_{j=1}^{N} x_j \\ s &= \sqrt{\sum_{j=1}^{N} \frac{(x_j - m)^2}{N-1}} \end{aligned} \tag{4.3}$$

The results of these simulations are plotted in figure 4.2: (For clarity the points for a fixed width are plotted around the value for the width , which is an integer) We see that

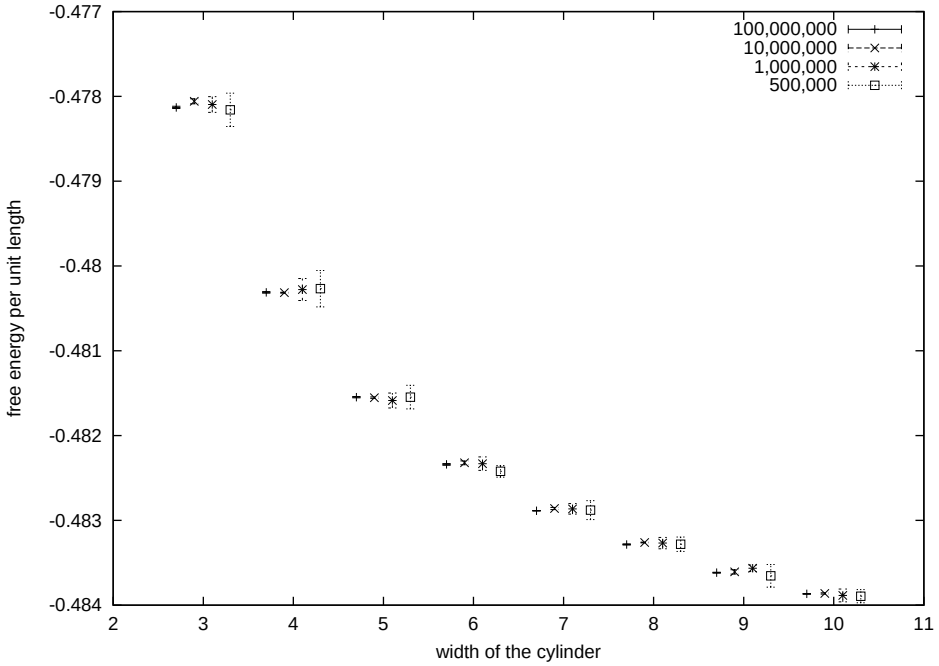

Figure 4.2: $K = 1$, fraction impurities=0.1,$\mu(x,t) = 1$, $\sigma = 0$

the results indeed become more accurate by increasing the length of the system. *For the rest of our simulations we use a system length of 10,000,000* unless stated differently, because the error in the results doesn't become much smaller by increasing the system length and the computer can perform the simulations in an acceptable time.
Note: Our initial conditions $Z(x,1) = \delta(x,x')$ are far from the best we can choose with respect to the rapidness of convergence of the free energy to the actual value. Therefore the length we have chosen is an upper bound for which our simulations are reliable.

4.1.3 different kinds of impurities

We also looked at different kinds of impurities. For instance we performed two simulations in which K was equal to 5. In simulation 1, the impurities ($\mu(x,t)$) where Gaussian distributed with mean 0.1 and mean square error 0.3. In simulation 2, the impurities were distributed according to: $\mu(x,t)$=0 with probability $\frac{9}{10}$ and $\mu(x,t)$=1 with probability $\frac{1}{10}$. Simulation 2 has the advantage that the simulation time is a bit shorter. For both simulations we have that $\sigma = 0.3$ and $\mu = 0.1$. The results of these are shown in Figure 4.3. If we subtract the value for the free energy for the width $\to \infty$ we obtain the results in Figure 4.4. If we fitted the numerical results in Figure 4.4 we obtained the following results, see Table 4.1; we did the same for the parameter set with $K = 1$. The results do not alter qualitatively and they can be found in Table 4.2.
Remark: The coefficients of the fit are of course dependent on the fitting range. Be-

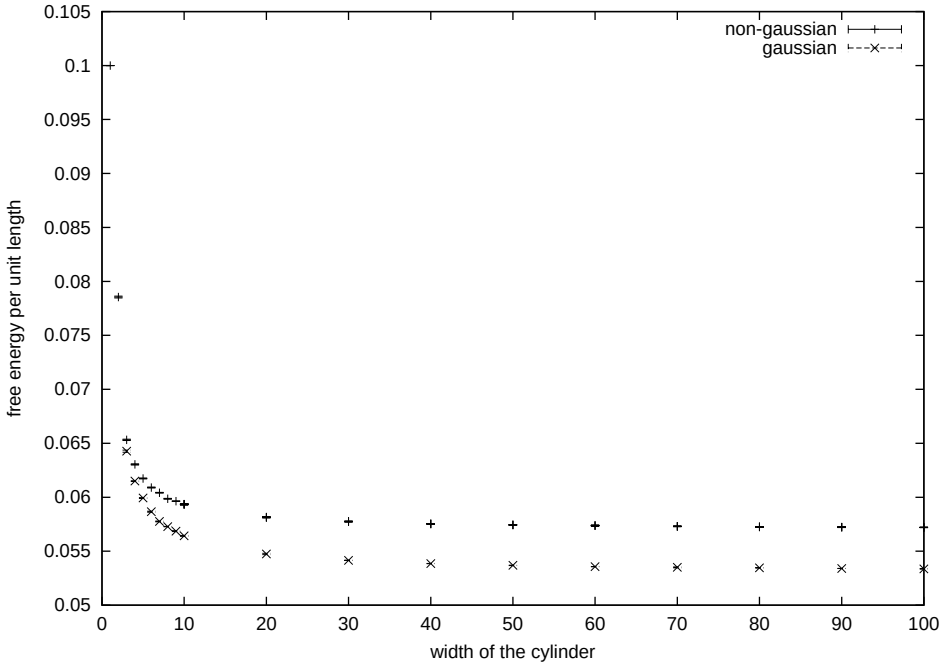

Figure 4.3: numerical results of the Gaussian and the non-Gaussian case with $K = 5$, $\mu = 0.1$ and $\sigma = 0.3$

cause we are interested in the results for large L, we checked up to which small L, the coefficients remained similar. (We also like to have as many points as possible.) We found that if we omitted the results for L-values smaller than 4, the results are reliable and these results are shown in the tables.

We see that the absolute values for the free energy in these two cases are close to each other for all lengths of the cylinder. However the qualitative behavior is different as follows from Table 4.3. In the non-Gaussian case there is also a $\frac{1}{L^2}$-dependence present. Because an other possible origin of the $\frac{1}{L^2}$-dependence is an interaction between diffent steps (see sections 4.1.5 and 4.1.6), we decided to use Gaussian impurities in our simulations on a square lattice, although simulations with Gaussian impurities are a bit

Table 4.1: results of the fit of the numerical results in Figure 4.3 against $a_0 + \frac{a_1}{L} + \frac{a_2}{L^2}$ with $K = 5$,$\mu = 0.1$ and $\sigma = 0.3$

	non-Gaussian	Gaussian
a_0	0.056956 ± 5e-06	0.05304 ± 2-05
a_1	0.0239 ± 0.0002	0.0341± 0.0006
a_2	0.0005 ± 0.002	-0.002± 0.003

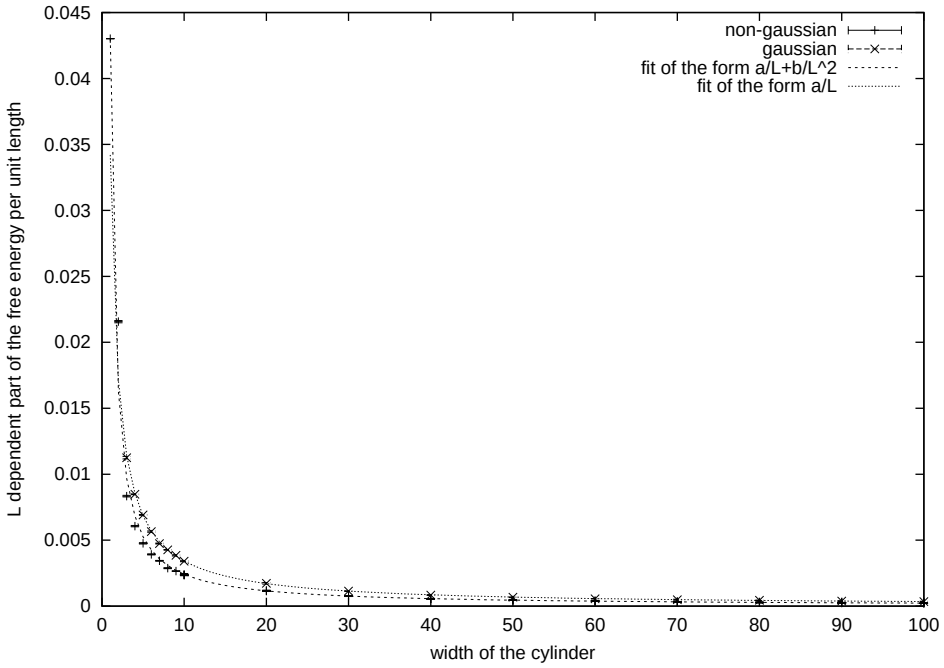

Figure 4.4: The L-dependent part of the step free energy for the Gaussian and the non-Gaussian case, including fits against $\frac{a}{L} + \frac{b}{L^2}$. $K = 5$, $\mu = 0.1$ and $\sigma = 0.3$

Table 4.2: results of the fit of the numerical results in Figure 4.3 against $a_0 + \frac{a_1}{L} + \frac{a_2}{L^2}$ with $K = 1$,$\mu = 0.1$ and $\sigma = 0.3$

	non-Gaussian	Gaussian
a_0	-0.485985 ± 5e-06	-0.495673 ± 2e-06
a_1	0.02034 ± 0.00013	0.0443± 0.0004
a_2	0.0094 ± 0.0006	-0.0001± 0.004

Table 4.3: coefficients of the fit of Figure 4.5 against $a_0 + \frac{a_1}{L}$ and against $c_0 + c_1 L^{c_2}$, $\mu = 0.1$, $\sigma = 0.3$, $K = 1$.

a_0	-0.495673 ± 2e-06
a_1	0.04481 ± 0.00013
c_0	-0.495675 ± 2e-06
c_1	0.0371 ± 0.0004
c_2	-0.992 ± 0.004

slower. (The $\frac{1}{L}$-term is a finite size effect, see section 2.7.)

4.1.4 One step on a cylinder

For a step on a strip (cylinder) of infinite width, the free energy per unit length is given by equation (2.37). For a finite cylinder we get a correction of the form $-\frac{\sigma^2}{2L}$, see equation (2.84). This gives for the average free energy per unit length on a cylinder:

$$\frac{\langle f \rangle}{T} = \mu - \frac{1}{2}\sigma^2 - 2\gamma + \frac{\sigma^4}{48\gamma} + \frac{\sigma^2}{2L} \tag{4.4}$$

(This result is identical to equation (2.49), but there we work with an infinite system with average distance between the steps of L.) We performed some simulations to check this theoretical result. We are especially interested in the range of parameters in which this theoretical result is accurate. We do not expect it to be valid for every set of parameters because we made some approximations to obtain this result.

We performed an accurate simulation for parameters for which the approximations should be valid. The impurities were (Gaussian) distributed with mean 0.1, a rms of 0.3 and a transversal bond energy of 1. (Unless explicitly stated, we chose $\beta = \frac{1}{k_B T}$ equal to 1.) For each width of the cylinder, from 3 to 210, we performed the simulation 5 times to get a qualitative measurement for the variance in the results. The results of this simulation are plotted in Figure 4.5. Around the width of 25 we found a very small irregularity, which we found again if we repeated the simulations for that width. Probably this is an indication for an imperfection in the program that generates the Gaussian impurities, but we couldn't find it.

We tried to fit these results. We fitted against functions of the form $\sum_{i=0}^{p} \frac{a_i}{L^i}$, with $p \in \{1, 2, 3, 4\}$. We obtained that only for $i = 0$ and $i = 1$ the coefficients a_i were significantly different from 0. Therefore we only give the results for $p = 1$, see Table 4.3.

We also tried to fit the results against a function of the form $c_0 + c_1 L^{c_2}$ The results, see Table 4.3, also indicate that a fit against the theoretical predictions, $a_0 + \frac{a_1}{L}$

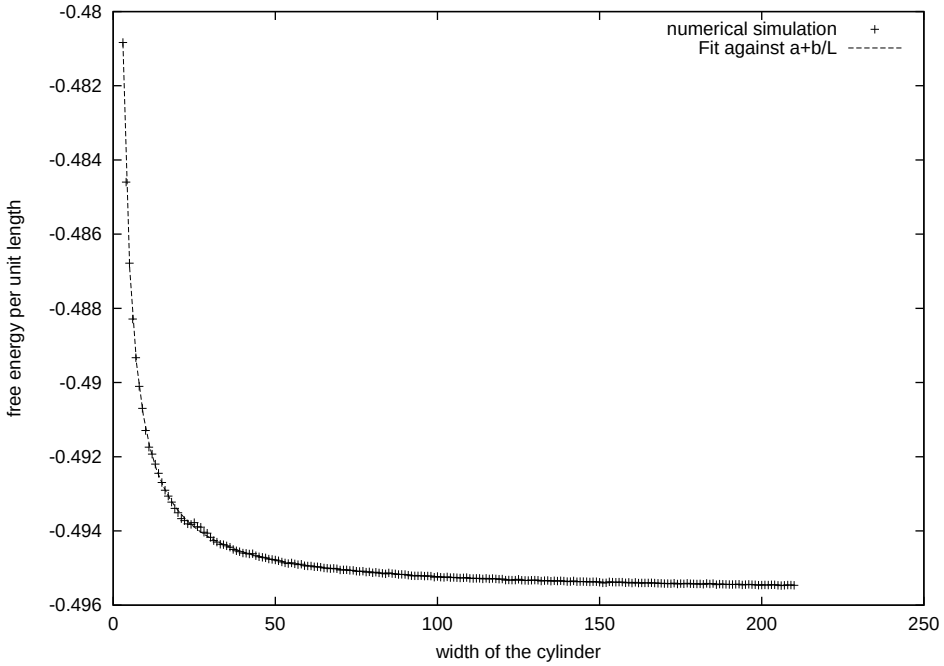

Figure 4.5: $K = 1$, mean impurity energy = 0.1, rms = 0.3

gives the best fit.The coefficient a_1 coincides with the theoretical prediction of 0.045, while the prediction for a_0 differs significantly from Kardar's theoretical prediction -0.68. This might be a consequence of short range corrections. For small K and no restriction on the kink size, the results should be better. If there are no impurities, we can calculate the step free energy also analytically without approximations. This gives $f_{step} = -\beta \log\left(e^{-\mu} + 2e^{-\mu-K}\right)$ which is equal to -0.451 for these parameters. This coincides perfectly with the simulations. The reason for this discrepancy between the results of Kardar and the simulations lies in the fact that $k_B T = 1$ in these simulations. This is of the same order as the energy of a kink. Therefore kinks will occur rather often, and in the model of Kardar we assumed that kinks were rare.

Different rms in the impurity energy

We did the same sort of simulations for different values of the parameters, but we performed only simulations for a relatively small set of widths to obtain the results faster. For a transversal bond energy, $K = 1$, and a mean impurity energy of 0.1 we performed simulations for several values of the rms in the impurity energy, σ. (The impurities have a Gaussian distribution.) When we tried to fit these numerical results a fit against $a_0 + \frac{a_1}{L}$ always gave good results, although for large σ, the results became a bit worse, see Table 4.4. The results of all the simulations for different σ, and the results of the fits against $a_0 + \frac{a_1}{L}$ are shown in Figure 4.6 and Table 4.5. We see that up

Table 4.4: coefficients of the fit of numerical results against $a_0 + \frac{a_1}{L}$, $b_0 + \frac{b_1}{L} + \frac{b_2}{L^2}$ and against $c_0 + c_1 L^{c_2}$, $\mu = 0.1$ and $K = 1$

	σ=1.5	$\sigma = 3.0$
a_0	-1.29854 ± 0.00013	-2.842 ± 0.006
a_1	0.8344 ± 0.0017	2.73 ± 0.08
b_0	-1.29815 ± 9e-05	-2.809 ± 0.02
b_1	0.819 ± 0.002	1.77 ± 0.05
b_2	0.063 ± 0.009	2.42 ± 0.12
c_0	-1.29779 ± 0.00013	-2.798 ± 0.003
c_1	0.853 ± 0.003	3.52 ± 0.08
c_2	-1.016 ± 0.002	-1.27 ± 0.03

Table 4.5: results of the fit of the L-independent part of the free energy against the function $a_0 + a_2\sigma^2 + a_4\sigma^4$, and of the $\frac{1}{L}$-dependent part against $b_2\sigma^2$. For both fits we used the results up to $\sigma = 1.5$. mean impurity energy is 0.1, $\sigma = 0.3$, $K = 1.0$, ($\beta = 1.0$)

	theory, see (4.4)	numerical value
a_0	-0.635759	-0.451446 ± 1.601e-05
a_2	-0.5	-0.494676± 0.003211
a_4	0.05663	0.0564892± 0.004239
b_2	0.5	0.453436 ± 0.01788

to $\sigma = 1.5$ the theoretical predictions are confirmed rather well, while for larger σ the results deviate from the theoretical results rather strongly. This is expected, because we restricted our model to transversal displacements of at most one per time step. In the continuum model every transversal displacement is allowed. For large σ transversal displacement are frequently larger than 1 and therefore the continuum model will no longer be a good description of the lattice model with restrictions for the allowed paths. If we allow in our numerical model transversal displacements up to 2 per time step, we would expect that the models give similar results up to larger σ, see also subsection 4.1.4.

Simulations for different transversal bond energies

We also performed simulations in which we kept the mean impurity energy fixed at $\mu = 0.1$ and the rms in the impurity energy fixed at $\sigma = 0.3$, but varied the transversal bond energy K. For small K, transversal steps are hardly repressed. If σ is large,

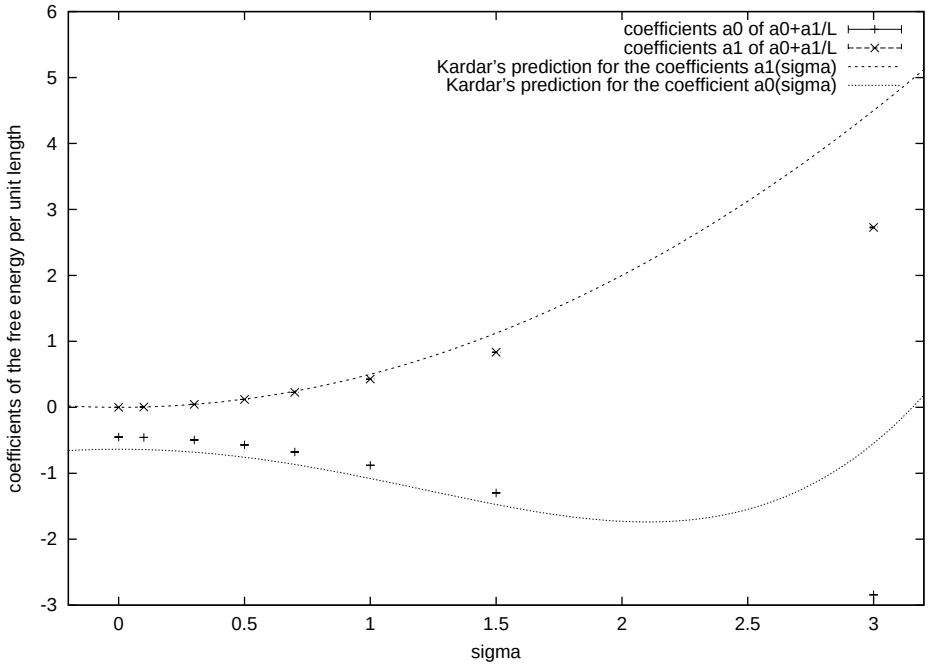

Figure 4.6: $K = 1$, mean impurity energy = 0.1

we expect that in this case the results should be similar to the results for large σ in the previous subsection. We plotted some results of our simulations in Figure 4.7: For all values for K, from 0 to 10, fits against $b_0 + \frac{b_1}{L} + \frac{b_2}{L^2}$ and against $c_0 + c_1 L^{c_2}$ gave almost the same results as against $a_0 + \frac{a_1}{L}$. Therefore we only pay attention to the results of the fit against $a_0 + \frac{a_1}{L}$. These results are plotted in Figure 4.8 For large K, the theory predicts a fast increase in the free energy, because there is a term proportional to $\frac{1}{\gamma} = e^K$. This is a strange artifact of the theory. We would expect that if $K \to \infty$, the interfaces will become straight lines, and therefore the free energy of an interface converges to the mean value of the energy $\mu(x,t)$ of a parallel bond, instead of blowing up. The reason for this strange behavior is the continuum-approximation. For very stiff interfaces the continuum-limit allows small transverse fluctuations, while in the lattice model transverse fluctuations become very rare. But it remains strange that in the continuum limit the free energy blows up for very stiff interfaces.

On the other hand, for small K the model doesn't correspond anymore to Kardar's continuum limit. For small K transversal steps larger than unity will occur, and therefore the explicit disallowance of such large transversal steps isn't realistic anymore.

The term proportional to $\frac{1}{L}$ also gives a problem. For small K the numerical results for this term are in good agreement with the theoretical predictions, but for $K \gg \sigma$ the results become rapidly worse. The model of Kardar predicts that in the low density limit,this term doesn't depend on K anymore. Our simulations indicate the contrary. There seems to be a strong correlation between the value of K and the value of the

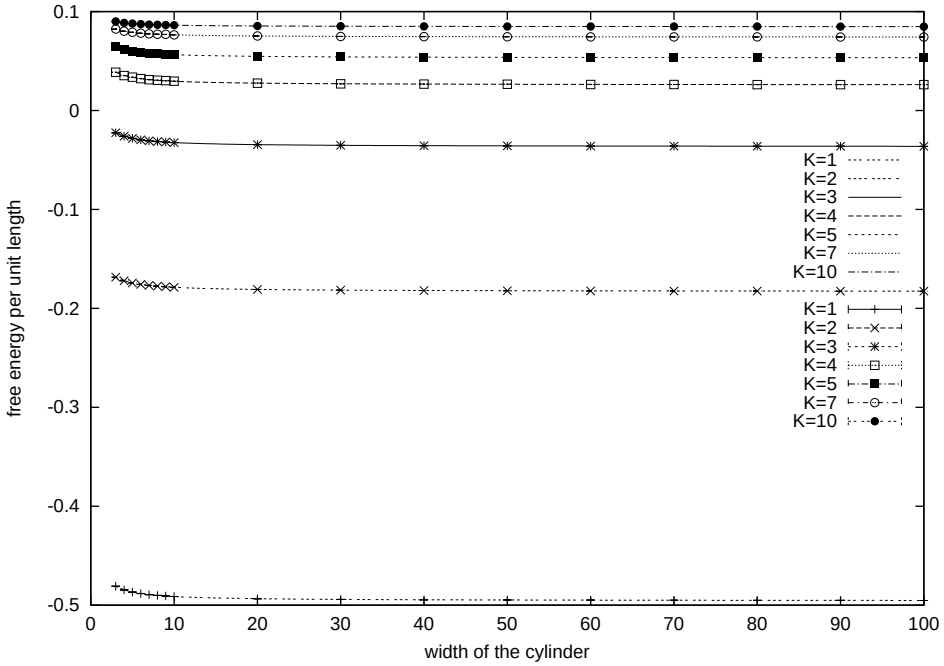

Figure 4.7: mean impurity energy = 0.1, $\sigma = 0.3$. The lines are fits against $a_0 + \frac{a_1}{L}$.

term proportional to $\frac{1}{L}$.

For small K we expect that the deviation from the theoretical results are due to the fact that relatively large transversal displacements will take place in the continuum model, while in our lattice model only transversal displacements of at most 1 lattice unit are allowed. Therefore we performed some simulations in which we also allowed transversal displacements of two lattice units. In these simulations we gave a transversal displacement of two lattice units twice the energy costs of a single transverse displacement. Again we only pay attention to a fit of the results against $a_0 + \frac{a_1}{L}$, because the fits against the functions $b_0 + \frac{b_1}{L} + \frac{b_2}{L^2}$ and $c_0 + c_1 L^{c_2}$ gave the same results. ($b_2 \approx 0$ and $c_2 \approx -1$.) The results of these simulations are shown in Figure 4.8. We conclude that, especially for the L-independent part of the free energy, the results coincide better for small K with the theoretical predictions in the continuum limit. We expect that simulations in which all transversal displacements are allowed will give even better results. The value of the coefficient proportional to $\frac{1}{L}$ does not change much.

4.1.5 One step on a strip

We performed some simulations in which we didn't work on a cylinder but on a strip. If the step is at the edge of the strip, the possible configurations of the steps are decreased. Therefore the step free energy on a strip should be larger than on a cylinder, while the difference between these two cases should vanish in the limit $L \to \infty$. We indeed find

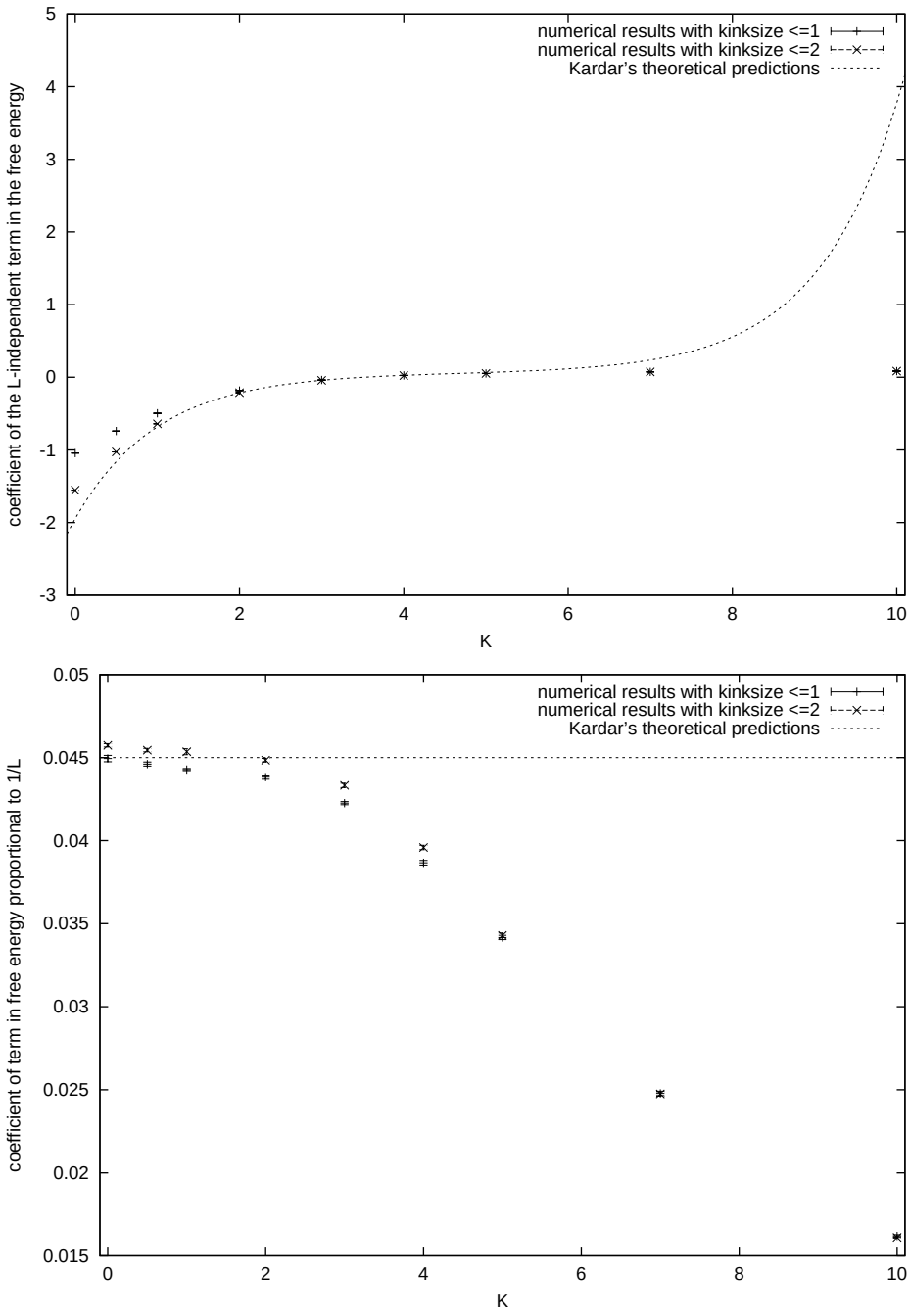

Figure 4.8: results of the fit of the free energy per unit length of simulations against $a + \frac{b}{L}$ with $\mu = 0.1$, $\sigma = 0.3$. In the first simulation only transversal displacements of size 1 are allowed. In the second simulation transversal displacements of size 1 and 2 are allowed, where the energy of a transversal displacement of size 2 is twice the energy of a displacement of size 1

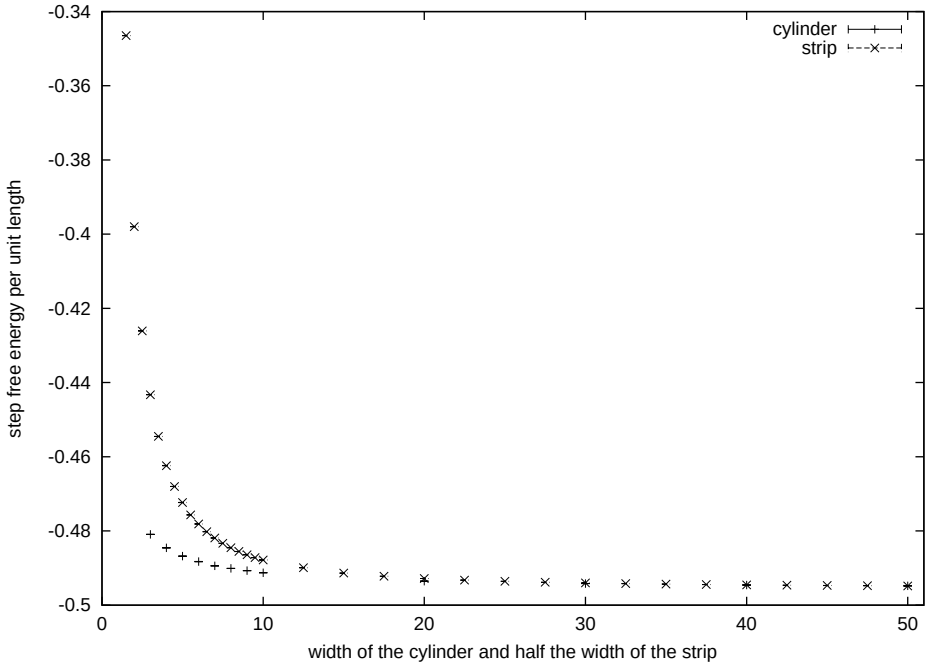

Figure 4.9: The step free energy on a cylinder and on a strip. mean impurity energy = 0.1, $\sigma = 0.3$, $K = 1$

this behavior, see Figure 4.9. We are interested in this case because it is a simplified model for the case of N steps on a cylinder of width $\frac{NL}{2}$. (We regard the neighboring steps to be straight lines). This simplified model should be quite realistic in the case of stiff steps. We are especially interested in the L-dependence due to the restricted number of configurations. Therefore we will subtract many times the finite size effects we found on a cylinder of width $\frac{L}{2}$.

no impurities

In the case without impurities we can calculate the step free energy analytically on the cylinder and on the strip for small L. If we assume that $\mu = 0$, we get that the step free energy on the cylinder is L-independent (if $L > 1$) while the free energy on a strip does depend on L. For some small values of L we give some exact results in Table 4.6. If L becomes larger we have to find the roots of a polynomial of order 5 and higher, which cannot be solved analytically. Therefore we also use another analytical method to find the step free energy on a strip.

In the limit that the length of the strip goes to infinity, we have that

$$\begin{aligned} Z(0,t) &= 0 \\ Z(L+1,t) &= 0 \\ Z(x,t) &\propto \sin\left(\tfrac{x\pi}{L+1}\right) \end{aligned} \tag{4.5}$$

It follows from the previous equation that:

$$f_{step} = -\log\left(1 + 2\cos\left(\frac{\pi}{L+1}\right)e^{-K}\right) \tag{4.6}$$

which corresponds with the results in Table 4.6. For large L, we obtain:

$$f_{step} = -\log\left(1 + 2e^{-K}\right) + \frac{\pi^2 e^{-K}}{1 + 2e^{-K}}\frac{1}{L^2} \tag{4.7}$$

If $K = 1$, we get for large L: $f_{step} \approx -0.55 + \frac{2.09}{L^2}$

We also performed simulations in the impurity free case to check the validity of the fitting range. The results on the strip for $K = 1$ and $\mu = 0$ are plotted in Figure 4.11. When we tried to fit these results against a function of the form $\sum_{i=0}^{p} \frac{a_i}{L^i}$, we found that p should be 3 or larger to obtain a good fit in the full range. If we omitted the the values for small L a fit against $a_0 + \frac{a_1}{L} + \frac{a_2}{L^2}$ gave also very good results. If we omitted the values for $L = 1, 2, 3$ we found as parameters $a_0 = -0.5526 \pm 0.0002$, $a_1 = 0.076 \pm 0.005$, $a_2 = 1.09 \pm 0.02$. We also fitted against the function $c_0 + c_1 L^{c_2}$. If we omitted the values for $L = 1, 2, 3$ we found: $c_0 = -0.55183 \pm 8e-05$, $c_1 = 0.920 \pm 0.013$ and $c_2 = -1.714 \pm 0.009$. We did the same again, but now we omitted all the widths smaller than 50, so we are looking at the low density region. We found as parameters: $a_0 = -0.551453 \pm 1.2e-06$, $a_1 = 0.00201 \pm 0.00016$, $a_2 = 1.932 \pm 0.005$, $c_0 = -0.551446 \pm 7e-07$, $c_1 = 1.76 \pm 0.02$ and $c_2 = -1.966 \pm 0.003$. Because the results differ so much for these two fitting ranges, we examined the fitting range more accurate, see Figure 4.10

We conclude that the fit is apparent dependent on the fitting range. Only if the fitting range is in the low density region, we obtain the exact results of equation 4.7. In that case, the L-dependence is quadratic for large widths according to Gruber and Mullins, [37].

The parameters a_0 and c_0 we found in the fits, differ 5 times their error from the actual value. This is an indication that the errors we find in the parameters of a fit are too small.

different rms in the impurity energy

In these simulations we kept the transversal bond energy constant at $K = 1$ and we kept the mean impurity energy constant at $\mu = 0.1$. (This only increases the step free energy per unit length by the constant 0.1.) For several values for the rms in the parallel bond energy we performed simulations on a strip. We will compare the results with the results on a cylinder, see subsection 4.1.4. The results for $\sigma = 0.3$ are shown in Figure 4.9. If we subtract the results for the case of a cylinder , see Figure 4.12, we obtain the L-dependence due to the decrease in the allowed paths, and not due to the universal finite size correction, see chapter 2.7. (We obtain the new errors by the

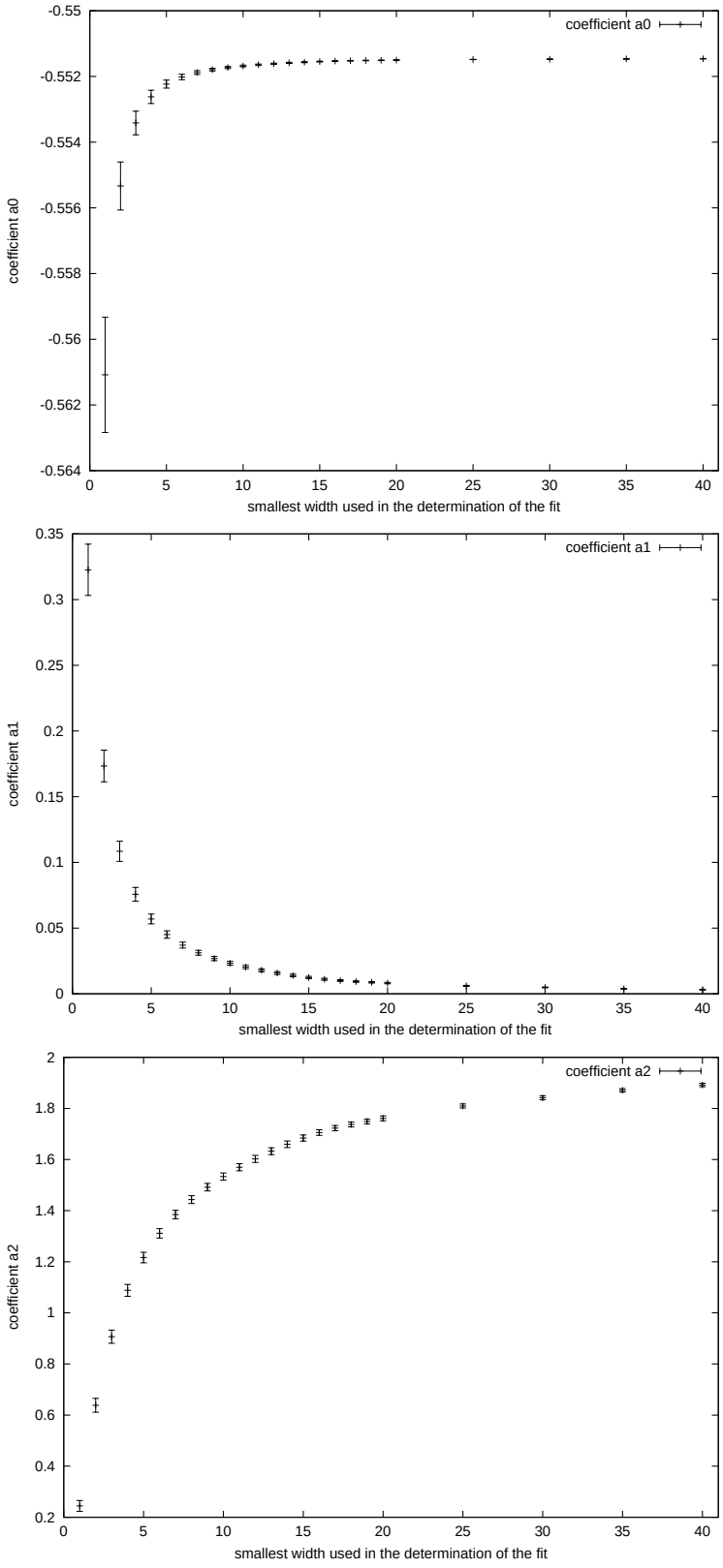

Figure 4.10: The coefficients of step free energy on a strip without impurities if we fit against $a_0 + \frac{a_1}{L} + \frac{a_2}{L^2}$. The fitting range starts at the point at the horizontal axis. mean impurity energy $= 0.1$, $K = 1$.

Table 4.6: step free energy on a strip and on a cylinder without impurities. $\mu = 0$ For instance for $L = 6$ we have to solve an third order polynomial which has an exact solution, but the solution is a rather long expression.

	strip	cylinder
1	0	0
2	$-\log\left(1+e^{-\beta K}\right)$	$-\log\left(1+2e^{-\beta K}\right)$
3	$-\log\left(1+\sqrt{2}e^{-\beta K}\right)$	$-\log\left(1+2e^{-\beta K}\right)$
4	$-\log\left(1+\left(\frac{1}{2}+\frac{1}{2}\sqrt{5}\right)e^{-\beta K}\right)$	$-\log\left(1+2e^{-\beta K}\right)$
5	$-\log\left(1+\sqrt{3}e^{-\beta K}\right)$	$-\log\left(1+2e^{-\beta K}\right)$
7	$-\log\left(1+\sqrt{2+\sqrt{2}}e^{-\beta K}\right)$	$-\log\left(1+2e^{-\beta K}\right)$
9	$-\log\left(1+\sqrt{\frac{1}{2}\left(5+\sqrt{5}\right)}e^{-\beta K}\right)$	$-\log\left(1+2e^{-\beta K}\right)$
∞	$-\log\left(1+2e^{-\beta K}\right)$	$-\log\left(1+2e^{-\beta K}\right)$

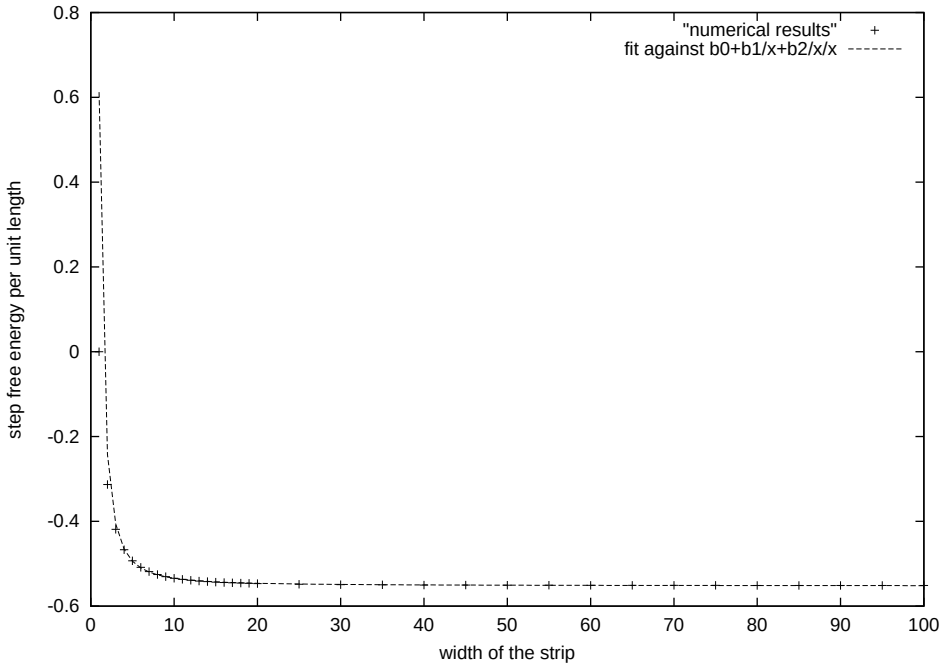

Figure 4.11: The step free energy on a strip without impurities.$\mu = 0$, $K = 1$. We omitted the points $L = 1, 2, 3$ in the determination of the fit.

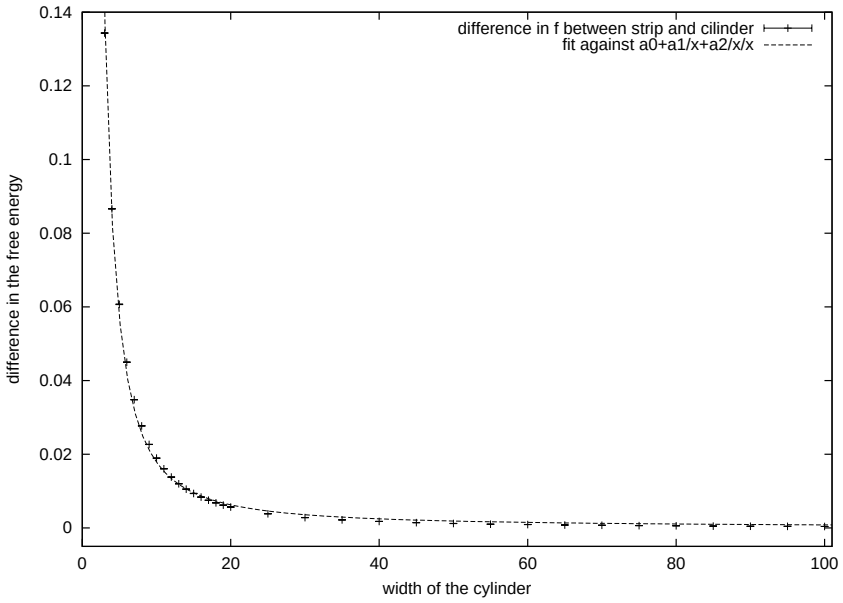

Figure 4.12: Difference between the step free energy on a strip and on a cylinder. $K = 1$, $\sigma = 0.3$.

Table 4.7: coefficients of the fit of the difference in step free energy between a strip and a cylinder against $\frac{a_1}{L} + \frac{a_2}{L^2}$ and against $c_1 L^{c_2}$, $\mu = 0.1$ and $K = 1$, $\sigma = 0.3$

a_1	0.073 ± 0.005
a_2	1.06 ± 0.03
c_1	0.842 ± 0.011
c_2	-1.652 ± 0.007

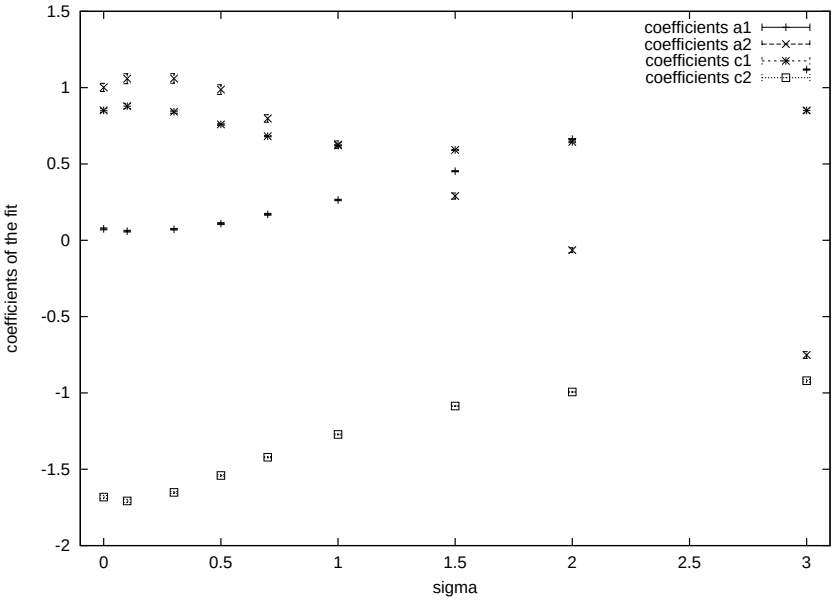

Figure 4.13: Fit of the difference between the step free energy on a strip and a cylinder against $\frac{a_1}{L} + \frac{a_2}{L^2}$ and against $c_1 L^{c_2}$. $K = 1$. For small σ the root mean square of the residuals is about 2 times as high for the fit against $\frac{a_1}{L} + \frac{a_2}{L^2}$ as for the fit against $c_1 x^{c_2}$, while for large σ, both fits have approximately the same rms of residuals. Therefore the fit with a non-integer power law is the best fit. But we should stress that also the fit against $\frac{a_1}{L} + \frac{a_2}{L^2}$ gives very good results

formula $error = \sqrt{error_{strip}^2 + error_{cylinder}^2}$.) The parameters of a fit of the difference against $\frac{a_1}{L} + \frac{a_2}{L^2}$ and against $c_1 L^{c_2}$ are shown in Table 4.7. We performed the same fits for other values of σ. The results are plotted in Figure 4.13: We see that the effective exponent c_2 is about -1.7 for small σ while it tends to -1 if σ becomes large.

4.1.6 Two and three steps on a cylinder

In section 2.5 we obtained the prediction for the mean step free energy per unit length if there are infinitely many steps on a cylinder of infinite width, with average distance L between the steps. The results was:

$$\frac{f}{T} = \mu - \frac{1}{2}\sigma^2 - 2\gamma + \frac{\sigma^4}{48\gamma} + \frac{\sigma^2}{2L} \tag{4.8}$$

To check this theoretical prediction, we performed simulations with two and three steps on a cylinder. In principal we could also perform simulations with N steps on a cylinder, but then we face the problem that our computer program isn't suited for that case. Our computer program, which performs the transfer matrix formalism, is based on an exact

model. (The results we obtain are of course not exact due to the fact that for a computer, each number consists of a finite number of digits.) Because our program is based on an exact model, it has its limitations because the running time increases very fast: For two interfaces, with L as width of the cylinder, the first cylinder can be on L places, while the second one has L-1 possible positions. Therefore for each extra interface the running time of the program increases roughly with the width of the cylinder. (To be precise the running time increases for $n > 1$ with $\frac{L(L-1)...(L-n+1)}{(n-1)!}$) and because we are working in the low-density limit, the width cannot be very small. We will compare the results with the results of one step on a strip and on a cylinder. The results for $K = 1$, $\mu = 0.1$ are plotted in Figure 4.14 for $\sigma = 0.3$ and for $\sigma = 0.05$. We see that a step on a cylinder has the lowest free energy, while the free energy per step is maximal for three steps on a cylinder. The free energy of 3 steps on a cylinder is a bit larger than the free energy of 2 steps on a cylinder, but the difference is rather small, especially if the mean distance between two steps is large, and therefore we expect that the results of two steps on a cylinder are a good indication for the results of N steps on a cylinder. Furthermore for $L \to \infty$ the results for these 4 cases indeed converge to the same limit, but the limit value is not the same as the theoretical prediction, see subsection 4.1.4. When we try to fit the results for 3 steps on a cylinder, we face the problem that we only have data for small L, but our theoretical results are only valid in the low density limit. Therefore we cannot expect to obtain reliable results. For the case of two steps on a cylinder the results should be quite accurate. The results of the fits against $a(L) = a_0 + \frac{a_1}{L} + \frac{a_2}{L^2}$ and against $c(L) = c_0 + c_1 L^{c_2}$ are shown in Table 4.8. (with L respectively 1, $\frac{1}{2}$, $\frac{1}{3}$ times the width of the cylinder if we have 1, 2 and 3 steps on the cylinder and L is $\frac{1}{2}$ times the width of the strip) We should stress that the fit depends rather strongly on the fitting range. If we fit for instance the results for the free energy of two steps on a cylinder to $a(L)$, we find that the coefficient a_1 becomes almost twice as large if we also include the simulations for average widths between the steps smaller than 10. Because our theoretical results are valid in the low density limit, we omitted in our fits the results of the simulations with high density. If we look at the coefficient a_1 in the case of two steps on a cylinder, we see that the deviation from the theoretically predicted value 0.045 is rather small.

4.2 A triangular lattice

Let's have a look at the physical situation of a lead crystal. A lead crystal has the closed packed structure of an fcc-crystal. If we regard the atoms as hard spheres, we can visualize the structure, see Figure 4.15. If we look at one layer of spheres, for instance the white spheres in Figure 4.15, we conclude that the crystal has a triangular structure. If we now create a step, by placing a row of atoms above an existing layer of atoms, we see that this can be done in two different ways. The two kind of steps, A-steps and B-steps, differ in the position of the upper layer with respect to the lower layer at the step, see Figure 4.15.

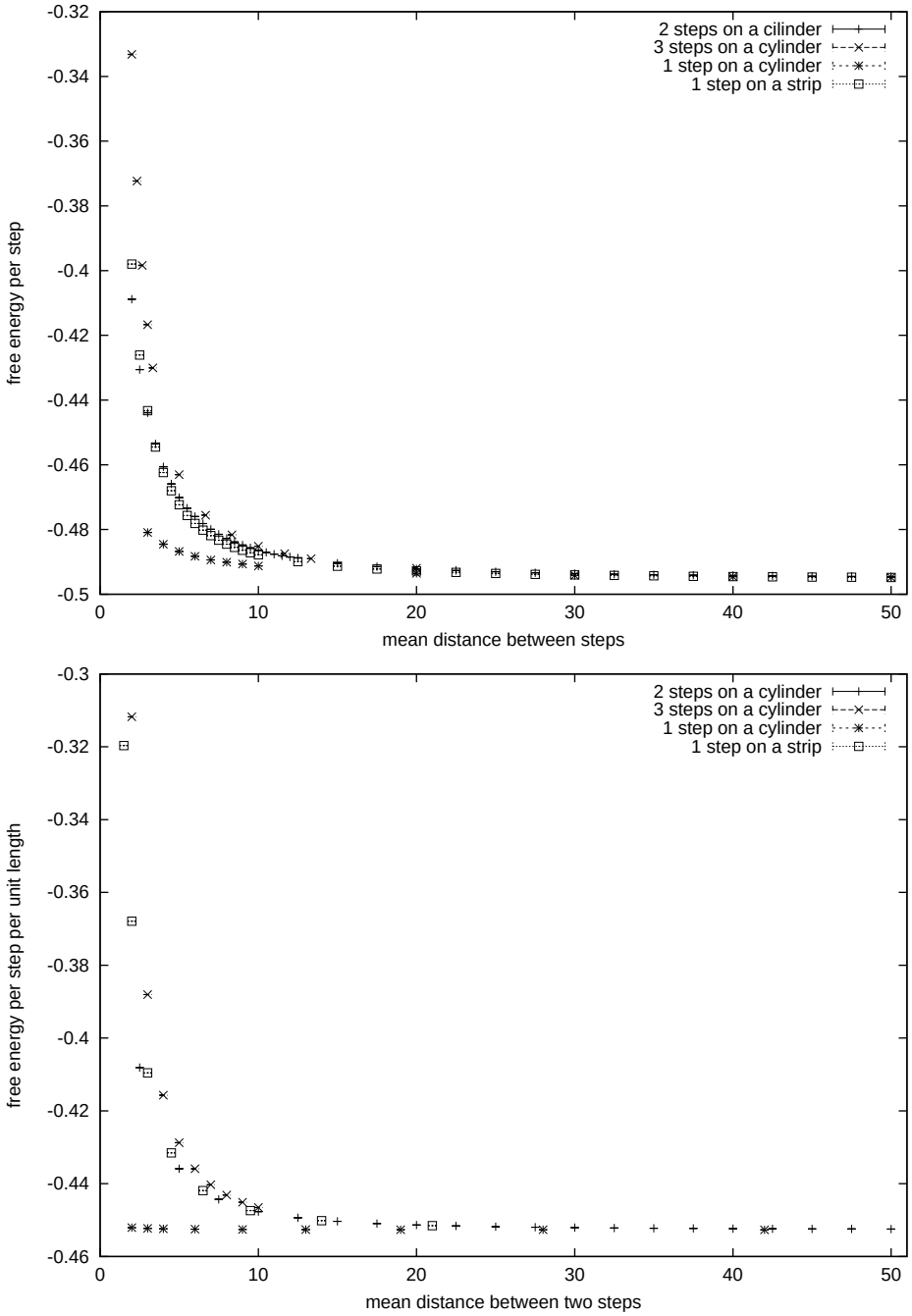

Figure 4.14: Free energy per step per unit length $K = 1$, $\mu = 0.1$.Upper part: $\sigma = 0.3$. Lower part: $\sigma = 0.05$.

Table 4.8: coefficients of the fit of the step free energy against $\frac{a_1}{L} + \frac{a_2}{L^2}$ and against $c_1 L^{c_2}$, $\mu = 0.1$ and $K = 1$, $\sigma = 0.3$

	1 step on a cylinder	2 steps on a cylinder	3 steps on a cylinder	1 step on a strip
a_0	$-0.495682 \pm 7e-06$	$-0.495697 \pm 1.8e-05$	-0.49580 ± 0.00011	$-0.49584 \pm 3e-05$
a_1	0.0444 ± 0.0003	0.0470 ± 0.0008	0.0478 ± 0.002	0.042 ± 0.001
a_2	-0.0003 ± 0.0008	0.470 ± 0.010	0.580 ± 0.011	0.39 ± 0.01
c_0	$-0.49568 \pm 2e-05$	$-0.495515 \pm 1.2e-05$	$-0.49487 \pm 2e-05$	$-0.49533 \pm 2e-05$
c_1	0.0443 ± 0.0002	0.243 ± 0.006	0.506 ± 0.003	0.306 ± 0.005
c_2	-1.00 ± 0.004	-1.427 ± 0.010	-1.719 ± 0.003	-1.607 ± 0.007

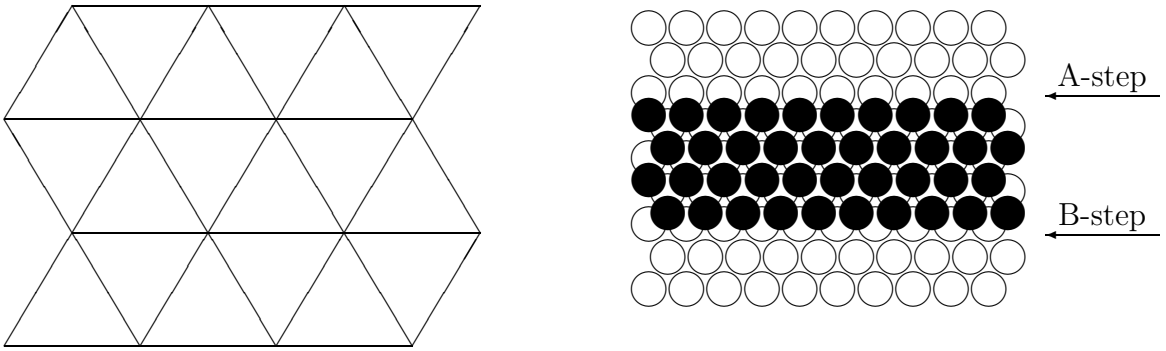

Figure 4.15: If we identify the left points on the lattice in the left figure with the right points on the lattice, we get a cylinder of width 3, with a triangular lattice structure. This triangular structure arises naturally by regarding the atoms as hard spheres.

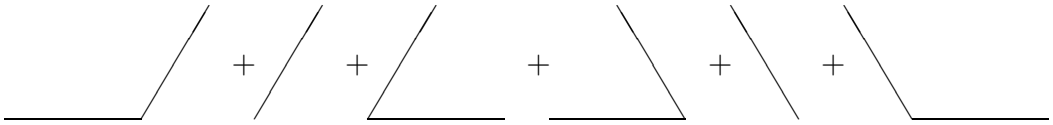

Figure 4.16: The 6 allowed paths in our model

A number of experiments have been done on lead crystals by Bonzel et al, [38], [1], [39], [40].We have done some numerical work to determine whether we can reproduce their results.

First we have done simulations for the triangular lattice in Figure 4.15. We made the lattice cylindrical by identifying the left and the right points of the lattice in Figure 4.15. For the moment we neglect the differences between A- and B-steps. We regard the situation of two steps on a cylinder where the steps go on average in a direction just between two symmetry directions of the lattice. We used again a transfer matrix formalism in which we allowed transversal displacements of at most 1 per transfer matrix step and we excluded displacements in the negative t-direction. As length of our cylinder we choose $T = 10,000$ which is relatively short (but fast). For such a short cylinder the initial conditions become important and therefore we ran our simulations first for a cylinder of length $1,000$. The results of these simulations were used as initial conditions for our final simulations. (If we did the same, but now for a system length of 100,000 we found very similar result, only with smaller errors.)

In our simulations we used as ratio between the energy μ to cross a bond and k_BT the value $\frac{1,000}{440}$. We used this ratio because they coincide with the ratio at the experiments of Bonzel. For simplicity we take $\mu = 1000,0$ and $k_BT = 440$ until we take the differences between A-steps and B-steps into account. Therefore the units are arbitrary.

If there are no impurities, the step free energy becomes $f = -\frac{1}{\beta}\log\left(2e^{-\beta\mu} + 4e^{-2\beta\mu}\right)$ and therefore $f = 613$ for these parameters. (The six paths which contributes are shown in Figure 4.16.)

Bonzel has seen no impurities in his crystals (other atoms than lead atoms) [41], but of course there can be lattice imperfections. Only we do not know the concentration and strength of these lattice imperfections.

First we did simulations in which the concentration of lattice imperfections (impurities) was 0.01. This means that if the step goes through one of these bonds (also a choice), the energy cost will be different from $\mu = 1,000$. For several strengths of the impurities, we performed the simulations for different width of the cylinder. We fitted the results against the functions $b_0 + \frac{b_1}{L} + \frac{b_2}{L^2}$ and $c_0 + c_1 L^{c_2}$ we obtained the following results, see Figures 4.17 and 4.18. We see that for very unfavorable impurities (μ'=5000) the L-dependence is quadratic. This is not so strange. Because only one percent of the bonds is unfavorable, it is rather easy for the step to avoid them. Therefore the influence of unfavorable bonds will be small, and the step free energy is close to the step free energy in the case without impurities, which has a $\frac{1}{L^2}$-dependence,see equation 2.40

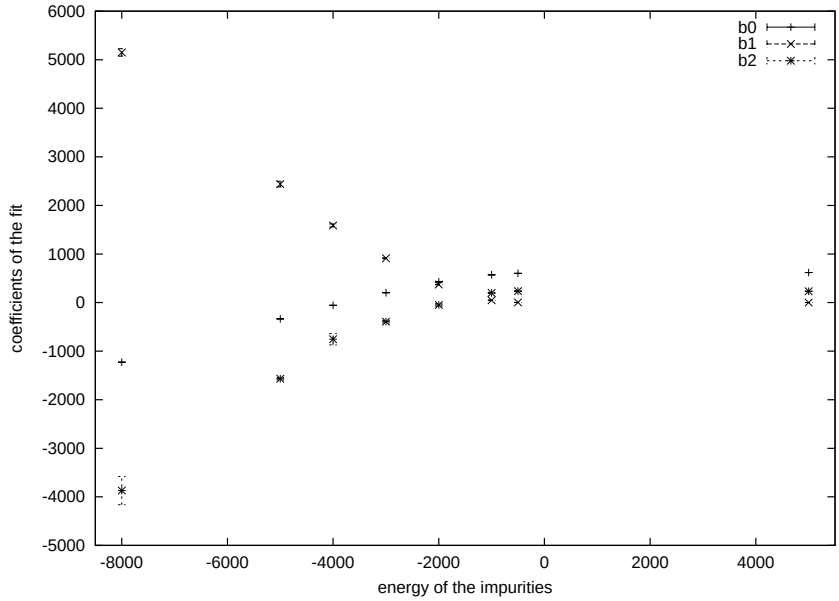

Figure 4.17: Coefficients of the fit of the free energy per step. There are two steps on a cylinder and the lattice is triangular. Fraction impurities = 0.01, Energy of a bond without impurity = 1000, else 1000 plus the value in the Figure, $\beta = 0.002273$. For the units see page 65.

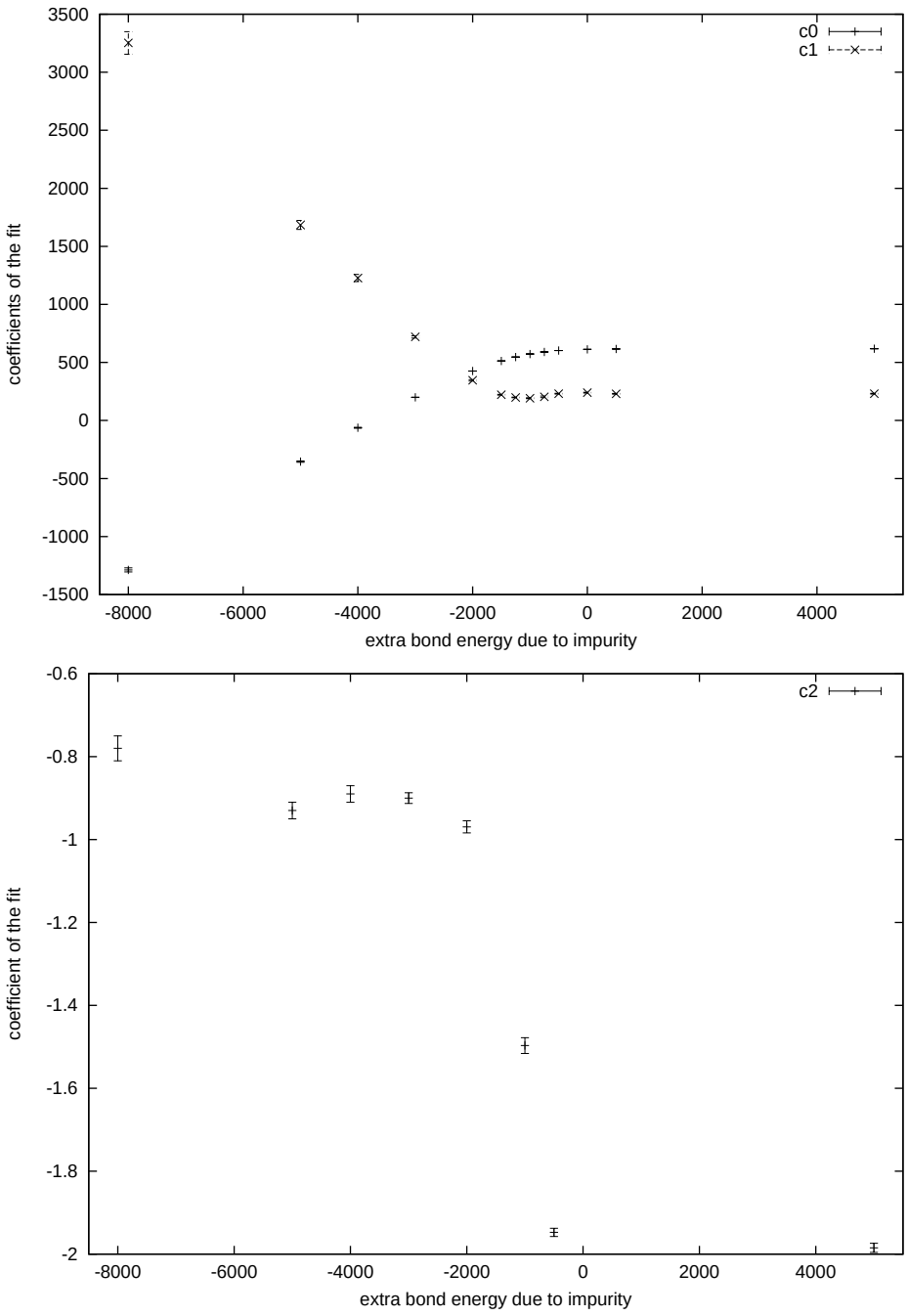

Figure 4.18: coefficients c_0 and c_1 of the fit against $c_0 + c_1 L^{c_2}$ There are two steps on a cylinder and the lattice is triangular. Fraction impurities = 0.01, Energy of a bond without impurity = 1000, else 1000 plus the value in the Figure, $\beta = 0.002273$. For the units see page 65.

(we expect that the results for a square lattice and this triangular lattice belong to the same equivalence class). If we make some bonds favorable due to impurities, the step, at $T = 0$, wants to go through as many favorable bonds as possible, but also wants to minimize its transversal displacements. At higher temperature also entropic effects will play an important role. The result of the competition of these effects is not easy to predict.

We performed the same simulations for a fraction of the bond with impurities of 0.01, 0.02 and 0.1. The results of this these simulations are plotted in Figure 4.19. We see that the L-dependence for all fractions looks similar, although the influence of a larger fraction impurities becomes visible at lower strengths of the impurities.

We performed also simulations for temperatures of 110 K and 220 K. We used a system length of $T = 100000$. By doing simulations for different temperature we can investigate the difference between two processes. First, if k_BT becomes of the order of the energy of a bond, also transversal displacements will take place regularly. Secondly, if the energy gain of going through an impurity becomes of the order of the bond energy of a regular bond, a transversal displacement is no longer energetically unfavorable, if it allows the step to go through an extra impurity. In Figures 4.20 and 4.21 we see that the L-dependence for the three temperatures is similar. If k_BT, becomes as large as the energy the step wins by going through an impurity, the free energy looses its $\frac{1}{L^2}$-dependence because the effect of the impurities becomes significant. On the other side, the step free energy has an $\frac{1}{L}$-dependence if the strength of the impurities becomes approximately $5k_BT$. The fact that the L-dependence is the same for the three temperatures, indicates that kinks transverse to the direction of the step, occur rarely because without these transversal bonds, the situation for the three temperatures is identical. This confirms our assumption that we only allow transversal displacements of at most 1.

Now let us include the differences between A- and B-steps.

A-steps are less favorable than B-steps, see [42]. Now suppose that we have a small mono adatomic island, a region with an extra layer of atoms. If we have a B-step at a side of the island, we have an A-step on the opposite site, as can be seen in Figure 4.15. On the other hand, if we have a train of steps as in the case of a vicinal surface, all the steps have to of the same type. Otherwise the structure of the lead crystal would be no longer of the fcc-structure. Therefore, in the ECS, we have a more or less hexagonal facet. At three edges of the facet, the near facet shape will be created by A-steps, while at the opposite edges of the facet, the near facet shape will be created by B-steps.

In principle we would like to calculate the step free energy for all directions of the step. Unfortunately this is not easy to calculate with a transfer matrix formalism. If the direction of the step is just between two symmetry directions of the lattice, see Figure 4.15, we have to calculate the partition function for all $0 < x < L$ for each integer t. If the direction of the step is different, we cannot use this model anymore because the direction in which we perform the transfer matrix formalism is not equal to the direction of the step. For a step in a direction of a symmetry axis of the lattice, we have to use the following model, see Figure 4.22. Now we also have to calculate

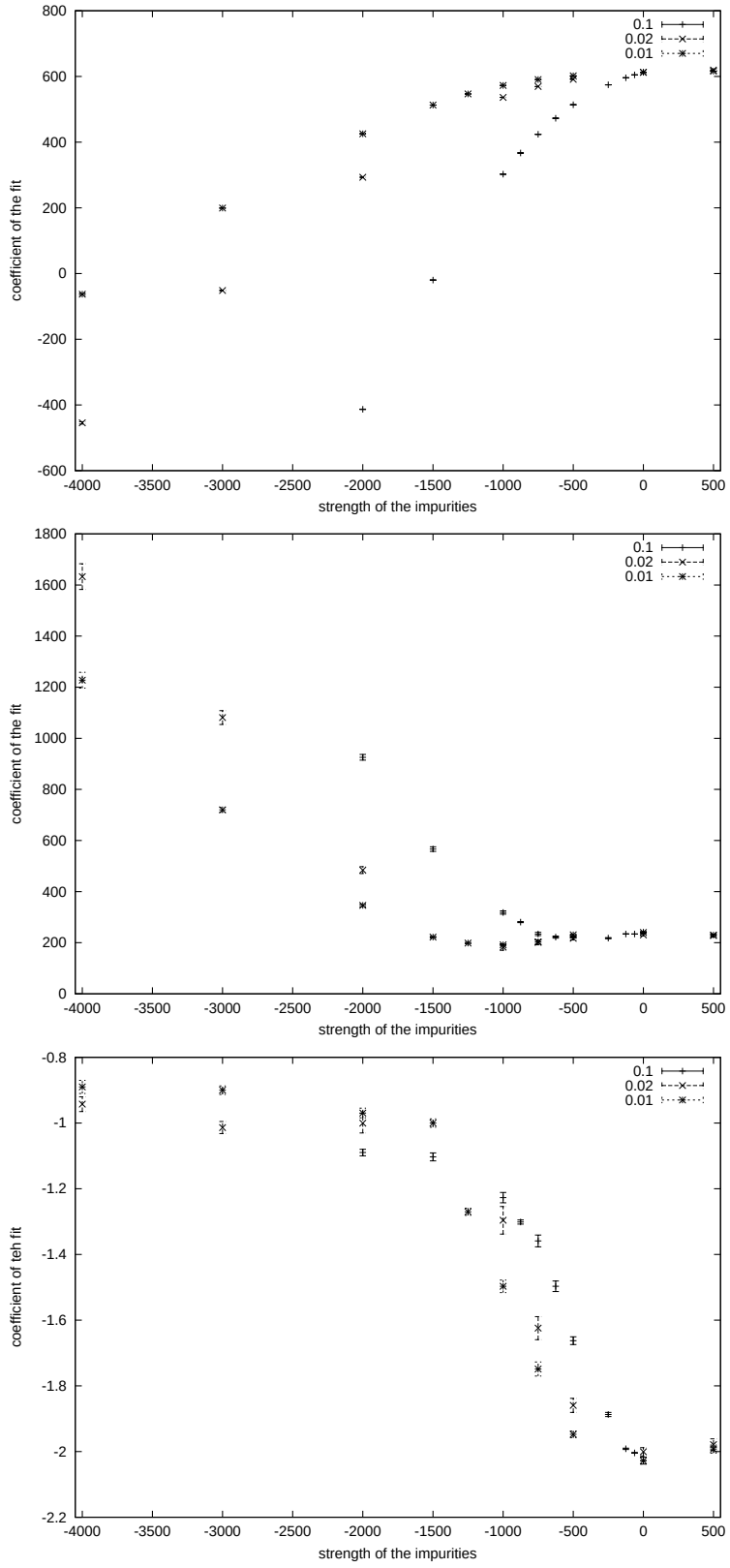

Figure 4.19: coefficients c_0 and c_1 of the fit against $c_0 + c_1 L^{c_2}$ There are two steps on a cylinder and the lattice is triangular. Fraction impurities = 0.01, 0.02 and 0.1 Energy of a bond without impurity = 1000, else 1000 plus the value in the Figure, $\beta = 0.002273$. For the units see page 65.

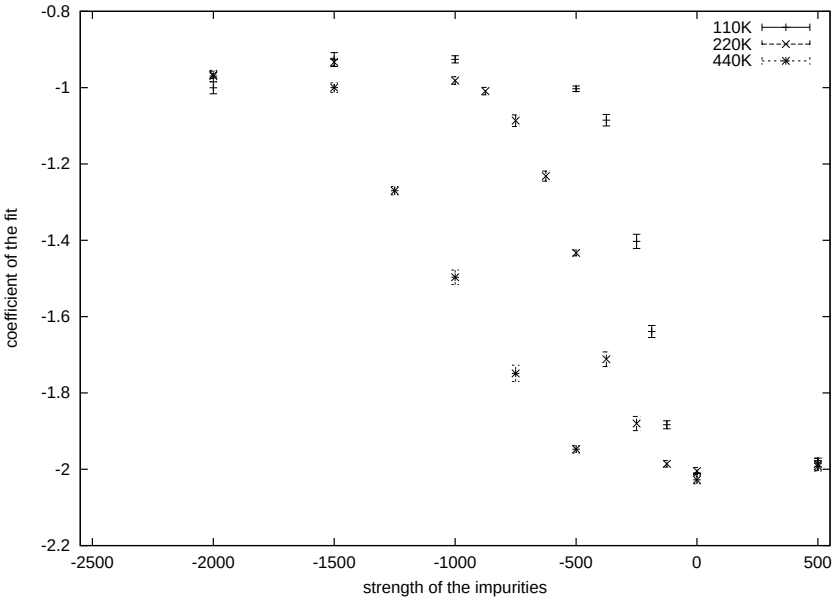

Figure 4.20: coefficient c_2 of the fit against $c_0 + c_1 L^{c_2}$ There are two steps on a cylinder and the lattice is triangular. Fraction impurities = 0.01 , Energy of a bond without impurity = 1000, else 1000 plus the value in the Figure,$k_B T = 110K$, $k_B T = 220K$ and $k_B T = 440K$.

the partition function for t of the form $\frac{2k+1}{2}$. For other directions we have to adjust our model again and therefore we restrict ourself to A- and B-steps and the direction just between two symmetry directions of the lattice. If the direction of the step is not parallel to one of the symmetry directions of the lattice, we expect that the step free energy will be larger than the step free energy of a B-step, but whether it is larger than an A-step is difficult to predict and depends on the exact value of parameters like the kink energy of A- and B-steps, the fraction lattice imperfections and so on.

Experiments have been done with a scanning tunneling microscope (STM), to determine the exact shape of a mono atomic island in a lead crystal. Bonzel e.a., [1], found as result the picture in Figure 4.23. The shape of an adatom island on a lead crystal is, according to Figure 4.23, more or less hexagonal, where opposite sides have different lengths due to the A- and B-steps. Figure 4.24 is an idealized representation of Figure 4.23.

We can determine the lengths of the sides in the hexagonal in the experiments of Bonzel (neglecting the rounded edges due to roughening at non-zero temperature). With these lengths we can estimate the ratio of the free energy of an A-step and a B-step using a Lagrange multiplier. If we call the length of the short sides of the hexagonal (A-steps) a, and the length of the long sides b, we can write the area of the hexagonal

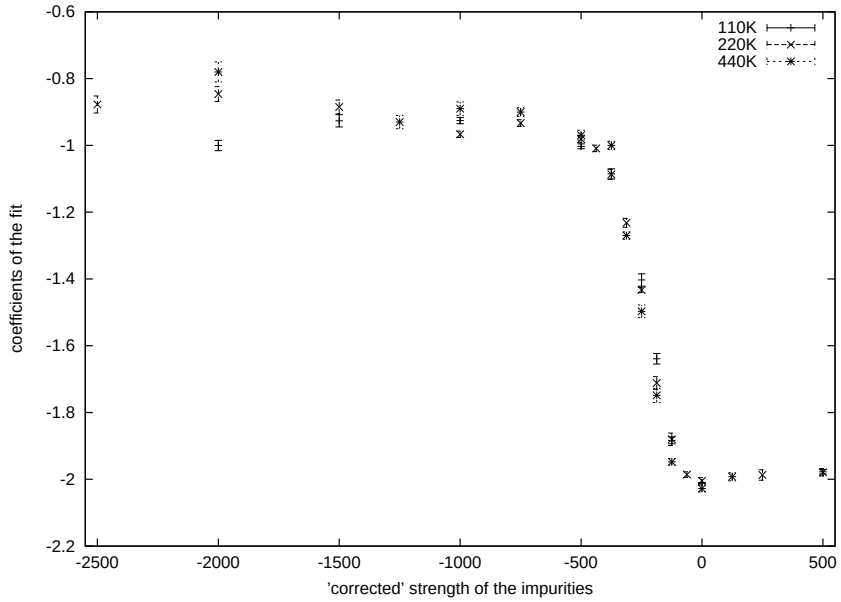

Figure 4.21: coefficient c_2 of the fit against $c_0 + c_1 L^{c_2}$. The values at the x-axis are correct for $T = 110K$, while the values on the x-axis are a factor 2 and 4 too small for $T = 220K$ and $T = 440K$ respectively. There are two steps on a cylinder and the lattice is triangular. Fraction impurities = 0.01 , Energy of a bond without impurity = 1000, else 1000 plus the value in the Figure,$k_B T = 110K$, $k_B T = 220K$ and $k_B T = 440K$. For the units on the x-axis, see page 65.

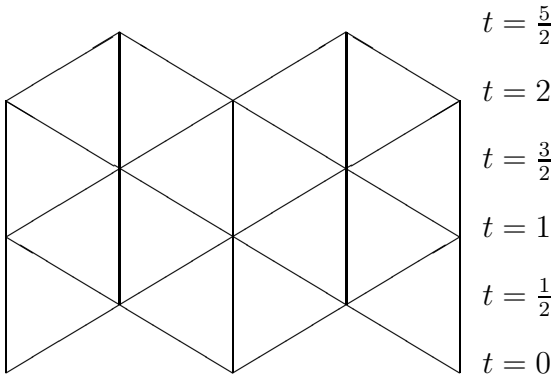

Figure 4.22: model for a step in a symmetry direction of the lattice

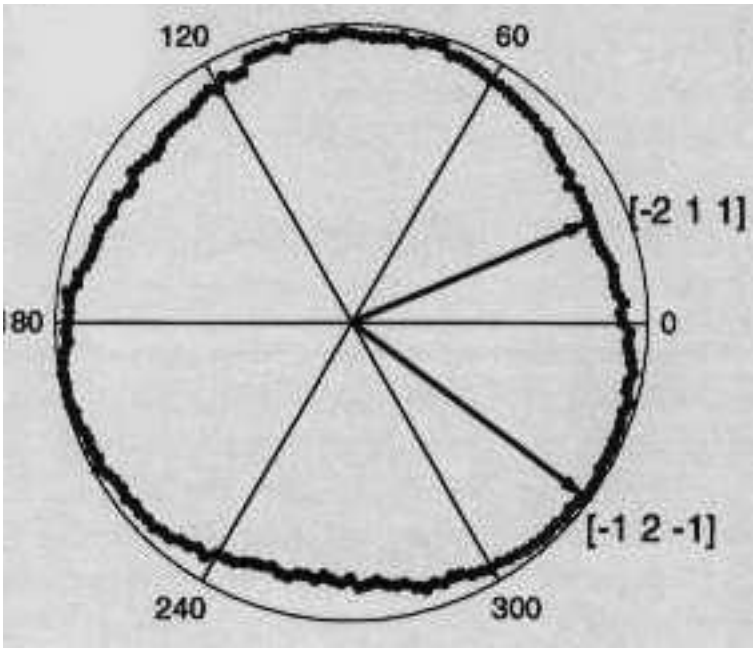

Figure 4.23: the shape of an lead adatom island found experimentally by Bonzel e.a.

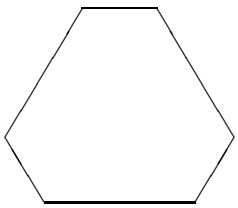

Figure 4.24: shape of an adatom island

as:

$$A = \frac{1}{4}\sqrt{3}\,(b+2a)^2 - \frac{3}{4}\sqrt{3}a^2 \tag{4.9}$$

The total step free energy of the adatom island is:

$$f_{step} = 3af_a + 3bf_b \tag{4.10}$$

with f_a the step free energy of an A-step and f_b the step free energy of a B-step. We now want to minimize the step free energy under the constraint that the total area of the adatom island remains constant. Using the Lagrange multiplier formalism, this gives: (with $r = \frac{b}{a}$)

$$\frac{f_b}{f_a} = \frac{r+2}{1+2r} \tag{4.11}$$

From the Wulff construction, [3] [2], it also follows that the step free energy is proportional to the distance to the centre of the facet. From Bonzel's experiments we find the estimation $r = 1.57 \pm 0.08$, and therefore we get as estimation for the ratio of the step free energies: $\frac{f_b}{f_a} = 0.87 \pm 0.03$. We performed simulations to check if we could find this ratio. Particularly, we are interested if we need imperfections in the lattice to obtain this ratio. Because the experiments in this case were performed on an adatomic island of one atomic height, we put one step on a cylinder in our simulations. In our first simulations on the lattice of Figure 4.22, we gave vertical bonds the energy of an A-step (B-step) and the diagonal bonds the energy of a B-step (A-step). The step energy according to Bonzel et al. is 90.7 meV for an A-step and 81.9 meV for a B-step, while the temperature at which they performed their experiments was 440 K, which corresponds to 37.92 meV. If there are no impurities in the system, we found: $\frac{f_b}{f_a} = 0.89$. If we add impurities to the system, the ratio becomes closer to 1. Therefore we expect that the impurities play an unimportant role. Unfortunately they neglected the corner energy in their derivation of the step energy. We follow Feibelman's article, [42].

Suppose that the step makes a kink of length n_k, see Figure 4.25. The energy to create a kink of length 1 in an A-step is:

$$E_K(A,1) = E_{step}(B) - \frac{1}{2}E_{step}(A) + E_C(A) \tag{4.12}$$

with E_{step} the energy per atom to create a step and E_C is the energy to create the two corners. The energies for kinks of length n_k are:

$$E_K\,(A,n_k) \;= n_k\left[E_{step}(B) - \tfrac{E_{step}(A)}{2}\right] + E_C\,(A,n_k) \tag{4.13}$$

$$E_K\,(B,n_k) \;= n_k\left[E_{step}(A) - \tfrac{E_{step}(B)}{2}\right] + E_C\,(B,n_k) \tag{4.14}$$

If n_k becomes large, the corner energy will approach a constant. The two corners of the kink are far apart and therefore they will not interact anymore. If we look closer,

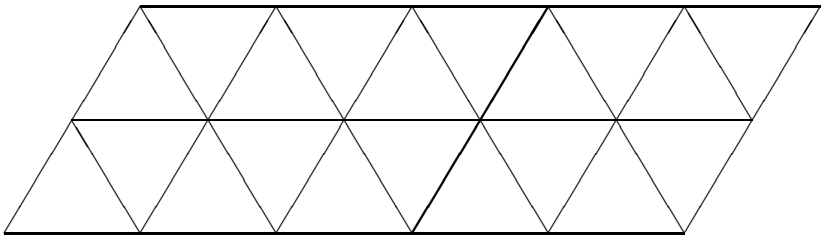

Figure 4.25: Kink of length 2 in a step

we see that for large n_k, $E_{corner}(A, n_k)$ and $E_{corner}(B, n_k)$ are equal. Therefore we can write:

$$\lim_{n_k \to \infty} E_C(A, n_k) = \lim_{n_k \to \infty} E_C(B, n_k) = E_C \tag{4.15}$$

The question is from which n_k we may assume that the corner energy has reached a constant value. If it is already allowed for $n_k = 1$ Feibelman has shown that $E_C = 7$ meV, while if it allowed from $n_k = 2$, $E_C = 10$ meV. Bonzel et al. neglected the corner energy in their calculations to obtain E_K. Furthermore, equations 5 and 6 in [38], are derived for a square lattice, which is not the case for a lead crystal. Therefore we use the results of Feibelman, [42], in our numerical simulations.

Suppose we have no impurities. In that case we can calculate the free energy for an A-step and a B-step analytically. If we have a very long cylinder we get the following equations for an A-step: (We suppress the x-dependence in the notation, because $Z(x,t) = Z(x',t) \quad \forall \quad x, x'$ if $t \gg 1$.)

$$Z\left(t+\frac{3}{2}\right) = 2\exp\left[-\beta\left(E_{step}(B)+E_C(A)\right)\right]Z\left(t+1\right) + \exp\left[-\beta E_{step}(A)\right]Z\left(t+\frac{1}{2}\right)$$

$$Z\left(t\right) = 2\exp\left[-\beta\left(E_{step}(B)+E_C(A)\right)\right]Z\left(t+\frac{1}{2}\right) + \exp\left[-\beta E_{step}(A)\right]Z\left(t\right)$$

$$\frac{Z\left(t+\frac{3}{2}\right)}{Z\left(t+\frac{1}{2}\right)} = \frac{Z\left(t+1\right)}{Z\left(t\right)}$$

Table 4.9: Experimental data

	A-step	B-step
f_{step}	75.6 $\frac{\text{meV}}{\text{atom}}$	68.3 $\frac{\text{meV}}{\text{atom}}$

For a B-step we obtain:

$$Z\left(t+\frac{3}{2}\right) = 2\exp\left[-\beta\left(E_{step}(A)+E_C(B)\right)\right]Z\left(t+1\right) + \exp\left[-\beta E_{step}(B)\right]Z\left(t+\frac{1}{2}\right)$$

$$Z\left(t\right) = 2\exp\left[-\beta\left(E_{step}(A)+E_C(B)\right)\right]Z\left(t+\frac{1}{2}\right) + \exp\left[-\beta E_{step}(B)\right]Z\left(t\right)$$

$$\frac{Z\left(t+\frac{3}{2}\right)}{Z\left(t+\frac{1}{2}\right)} = \frac{Z\left(t+1\right)}{Z\left(t\right)}$$

This gives as step free energies:

$$f_{step} = -\frac{1}{\beta}\log\left\{\epsilon_1 + \epsilon_2^2 + 2\epsilon_2\sqrt{(}\epsilon_1+\epsilon_2^2)\right\}$$
$$\text{with } \epsilon_1 = \exp\left[-\beta E_{step}(A)\right] \text{ and } \epsilon_2 = \exp\left[-\beta\left(E_{step}(B)+E_C(A)\right)\right] \text{ for an A} - \text{step}$$
$$\text{and } \epsilon_1 = \exp\left[-\beta E_{step}(B)\right] \text{ and } \epsilon_2 = \exp\left[-\beta\left(E_{step}(A)+E_C(B)\right)\right] \text{ for an B} - \text{step} \tag{4.16}$$

Bonzel et al.experimental results for the step free energy can be found in Table 4.9. We are interested if we can reproduce Bonzel's results numerically. Feibelman found as kink energies the values 42 and 69 meV/atom for respectively an A-step and a B-step. For an B-step this value is remarkable bigger than $k_BT = 37.92$ meV. Therefore we expect that most kinks will have length 1, for an A-step it is questionable but for simplicity we assume it here too. If we combine these results with the calculations of Feibelman, which give for for the step energy 95 and 78 meV/atom for respectively an A-step and a B-step, we find for the corner energies 11.5 and 13 meV. These values are close together. Therefore we assume that the corner energy is independent of the type of step. If we use a corner energy of 13 meV, we find in the impurity free case as step free energies 71.3 and 65.8 meV/atom for respectively an A-step and a B-step. These results are rather close to the experimental values of 75.6 and 68.3 meV/atom, but they are a bit too small. According to our simulations on a square lattice, impurities can not be the reason for this difference, because a low fraction of impurities which repel the step, has hardly any influence, while impurities which attract the step only make the free energy lower. Therefore either the step energy or the corner energy has to be larger. This is not so strange because we assumed that all kinks are of length one and Feibelman

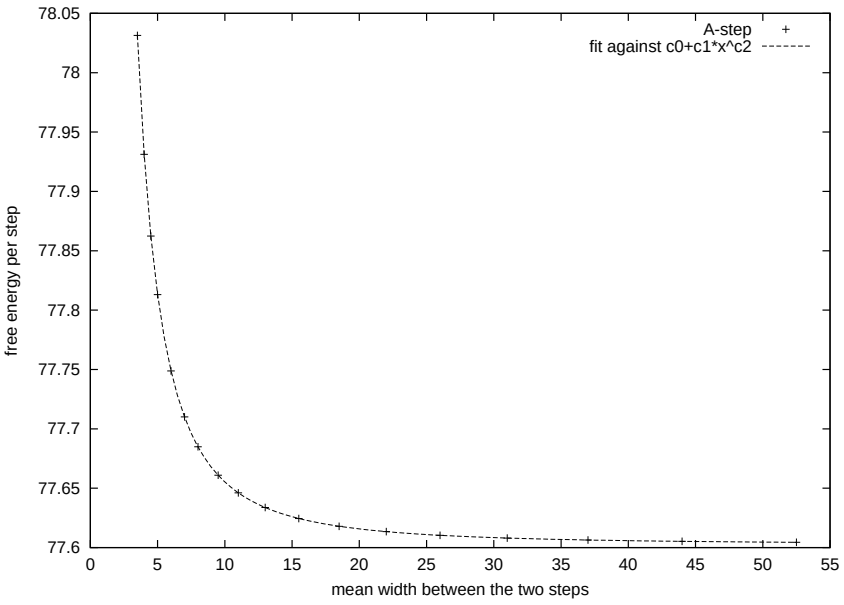

Figure 4.26: Width dependence of the step free energy on a triangular lattice. We used the model of Figure 4.22 with two steps on a cylinder. The temperature is 37.92 meV, the energy of a vertical bond is 95 meV and the energy of a diagonal bond is 103 meV. There a no impurities

calculations depend rather strongly on the details of the calculation. For instance, if we use a corner energy of 21 meV, we obtain as step free energies 75.7 and 68.1 meV/atom respectively for an A-step and a B-step which are very close to the experimentally found values. In the rest of our simulations we use the following parameters:

$$\begin{aligned} E_{step}(A) &= 95meV \\ E_{step}(B) &= 78meV \\ E_C(A) = E_C(B) &= 25meV \end{aligned}$$

For steps in other directions, we expect that the step free energy will be larger than for a B-step, because the step has to make many kinks to stay in the right direction and these kinks are unfavorable, although at sufficient high temperature, the entropic influence will dominate the energetic one.

Now let us examine the width dependence of the A-steps and B-steps. For an both A-steps and B-steps on a lattice without impurities, we find a $\frac{1}{L^2}$-dependence as in the case that we neglected the differences between A and B-steps, see Figure 4.26 and 4.27 and Table 4.10. This is not so strange because we expect the two models to be in the same equivalence class and the entropic step repulsion will determine the behavior.

For the lattice with impurities, the situation becomes more complicated. Nevertheless we expect the same kind of behavior as in the case that we neglected the difference

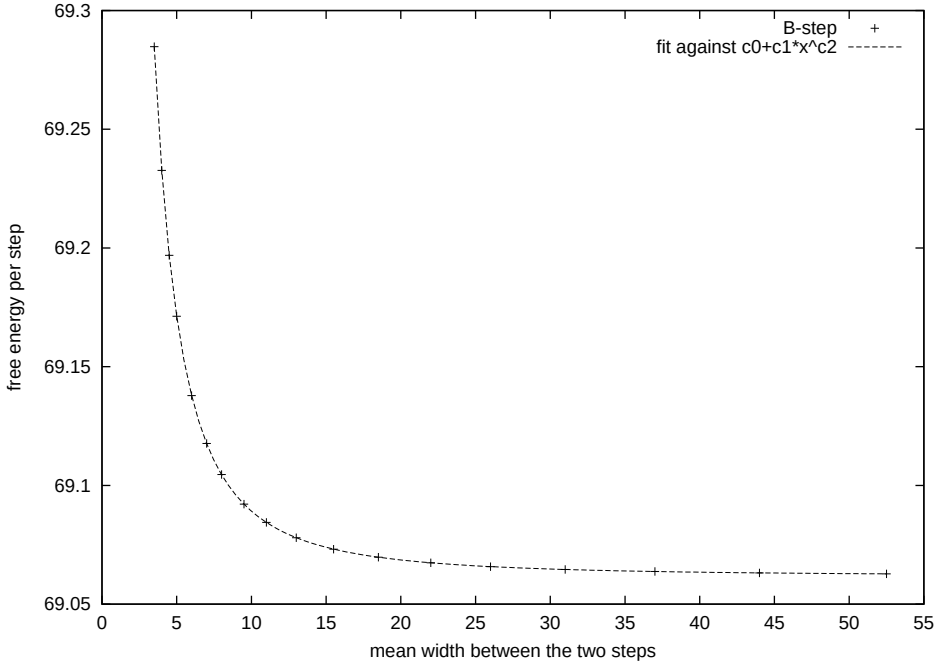

Figure 4.27: Width dependence of the step free energy on a triangular lattice. energy of a vertical bond is 78 meV and the energy of a diagonal bond is 120 meV. There are no impurities.

Table 4.10: fit of Figure 4.26 and 4.27 against $c(L) = c_0 + c_1 L^{c_2}$

	A-step	B-step
c_0	$77.6025 \pm 1.7e-05$	$69.0617 \pm 9e-06$
c_1	5.227 ± 0.002	2.7165 ± 0.0014
c_2	-1.996 ± 0.0003	-1.9950 ± 0.0004

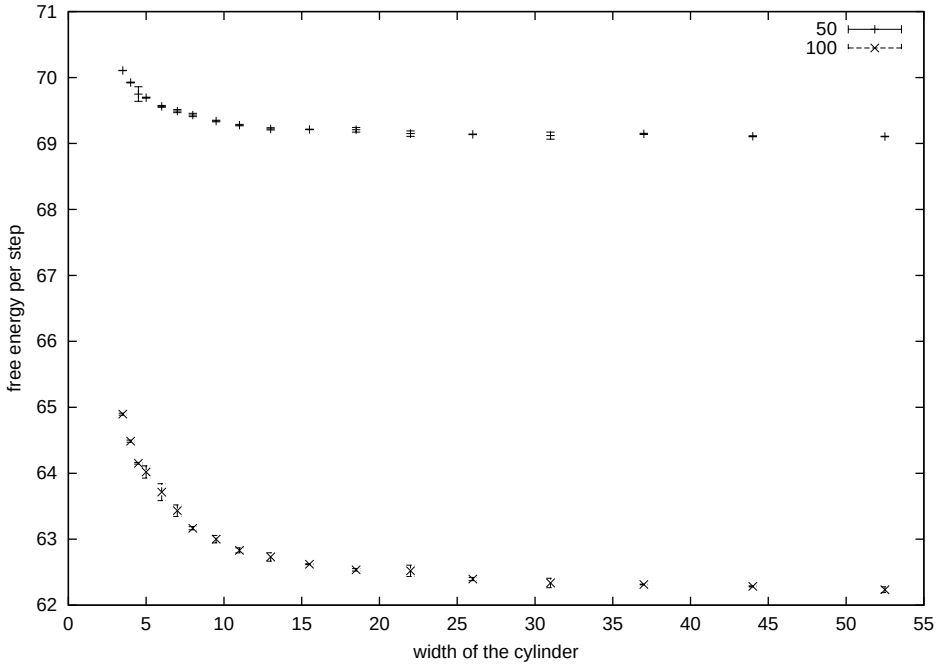

Figure 4.28: Width dependence of an A-step free energy on a triangular lattice. energy of a vertical bond is 95 meV and the energy of a diagonal bond is 103 meV. In one simulation the fraction impurities was 0.0074416 and the strength of an impurity 50 meV, in the other simulation the fraction was 0.0364 and the strength of the impurities 100 meV

between A-steps and B-steps, that means a transition from a $\frac{1}{L^2}$-dependence to $\frac{1}{L}$-dependence if we add impurities. There are two different ways in our simulations to increase the influence of the impurities in our system. We can add more impurities to the system, and we can increase the strength of the impurities. That these two methods do not produce the same results becomes clear from Figure 4.28. In Figure 4.28 we plotted the L-dependence of the step free energy. In one simulation the strength of the impurities is twice as large but they occur also half of the time. It follows from Figure 4.28 that a few strong impurities decrease the step free energy more. We fitted the results in Figure 4.28 against $c_0 + c_1 L^{c_2}$. The results can be found in Table 4.11. We did the same sort of simulations for many other fractions and strengths of the impurities, for both A-steps and B-steps. The results of the fits against $c(L) = c_0 + c_1 L^{c_2}$ can be found in Figure 4.29 and 4.30. The advantage of fitting against this function is the fact that it is rather easy to find an effective exponent for the near-facet shape of an crystal in equilibrium, see section 2.6.

We see that the results for an A-step and a B-step are qualitatively the same. We see that for small fractions of the impurities, the step free energy of an isolated step, the coefficient c_0, is a straight line. The slope of the line depends of course on the strength

Table 4.11: fit of Figure 4.28 against $c(L) = c_0 + c_1 L^{c_2}$.

fraction impurities	0.0364	0.074416
strength of the impurities	-100meV	-50 meV
c_0	69.084 ± 0.004	62.151 ± 0.009
c_1	6.04 ± 0.18	12.1 ± 0.2
c_2	-1.42 ± 0.03	-1.190 ± 0.016

of the impurities, and is for an A-step larger than for a B-step. This is not strange because kinks in an A-step are less suppressed. Therefore an A-step can benefit more from the impurities, because the step is less stiff. For larger fractions impurities, the slope decreases and tends to a straight line if the fraction impurities goes to 1. This corresponds to the situation of a small fraction impurities which repel the step. Because it is rather easy to avoid a small fraction of the bonds, the influence of small fraction repelling impurities is small and therefore the slope of the line is rather small.

If we look at the L-dependent part of the step free energy, we see that if the strength of the impurities is rather high (much larger than $k_B T$), a very small fraction attractive impurities can change the L-dependence drastically. For both an A-step and a B-step, the L-dependence changes from a $\frac{1}{L^2}$-dependence if there are no impurities to an $\frac{1}{L}$-dependence if the fraction impurities is about $\frac{1}{1000}$. Increasing the fraction impurities further, doesn't change the behavior until the fraction becomes about 0.2. From that point the L-dependence goes very slowly to a $\frac{1}{L^2}$-dependence which is reached if the fraction attractive impurities becomes 1. For such large amount of favorable impurities, it might be illuminating to consider the bounds with impurities as normal bounds and the bonds without impurities as bonds with impurities which repel the steps.

If we look at the dependence of the step free energy on the strength of the impurities, see Figure 4.31, we see that the influence of impurities with energy smaller than $k_B T$, is rather small. They do not change the L-dependence much, even for large amounts of impurities.

4.2.1 The equilibrium crystal shape

With these data and the theoretical results of section 2.6, we can determine the near-facet shape of a crystal in equilibrium. Using equation 2.61, we can determine the effective exponent and the pre-factor. The results are plotted in Figure 4.32. According to section 2.6, we expect a power of $\frac{3}{2}$, if there are no impurities, because the quadratic term in the step free energy will be dominant according to 2.40. With impurities, if we have a dominant $\frac{1}{L}$-term in the step free energy, we expect an exponent of 2. We indeed find this behavior. A very small fraction favorable impurities is sufficient to change the near facet shape drastically. Unfavorable impurities hardly have any influence.

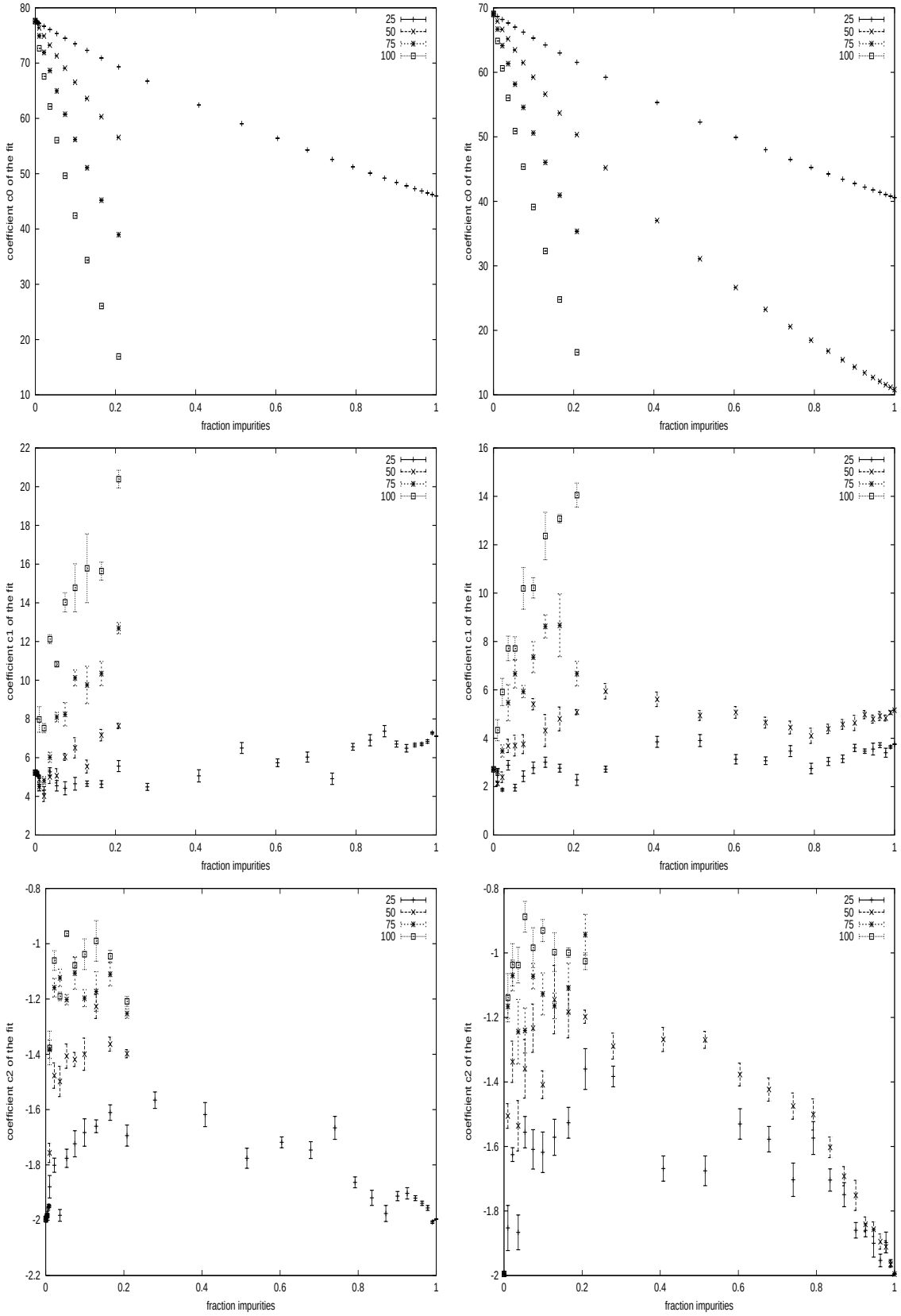

Figure 4.29: The left figures are the result of the fit against $c_0 + c_1 L^{c2}$ for an A-step. The right ones for a B-step.

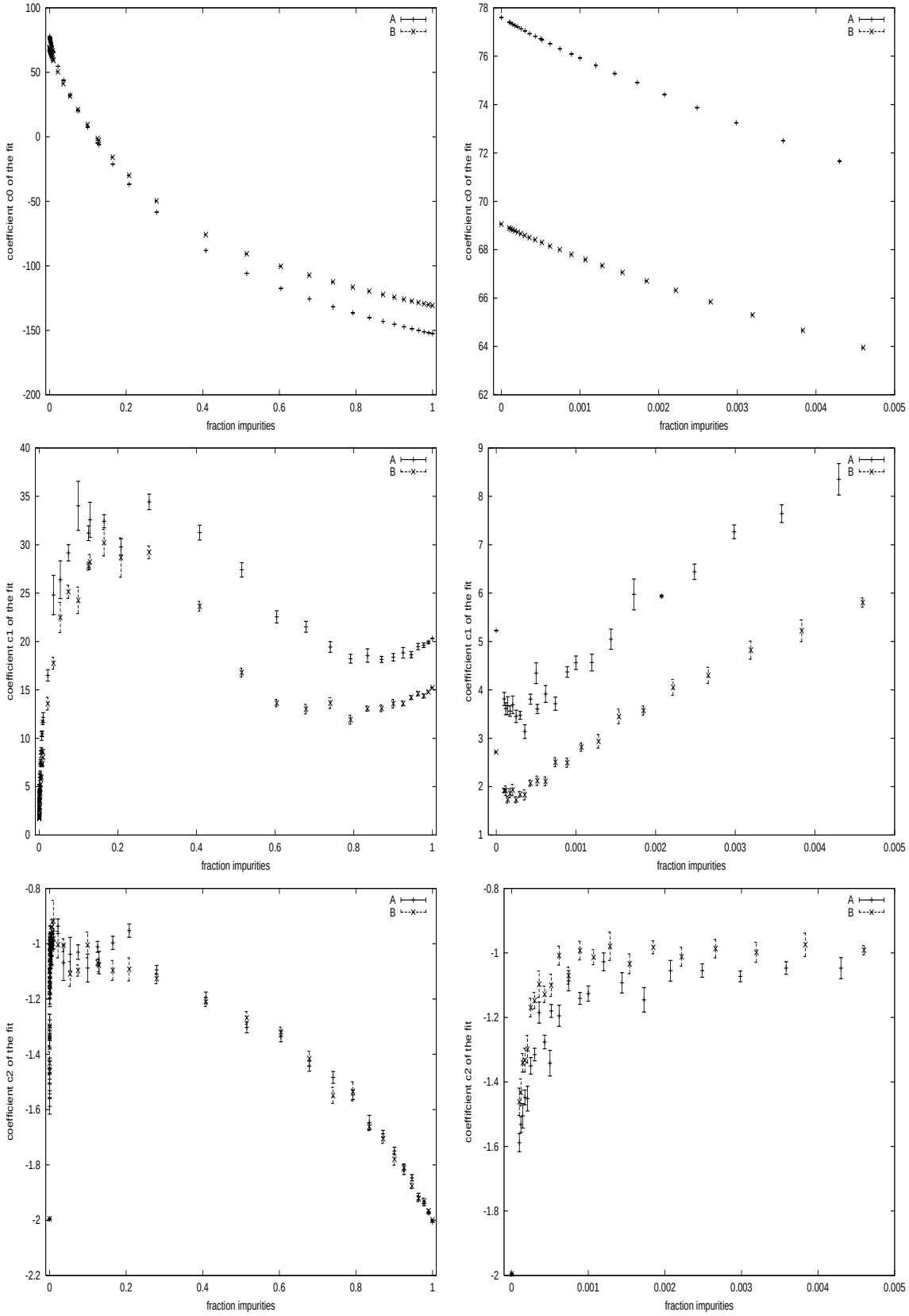

Figure 4.30: The result of the fit against $c_0 + c_1 L^{c2}$. Strength of the impurities is 150 meV

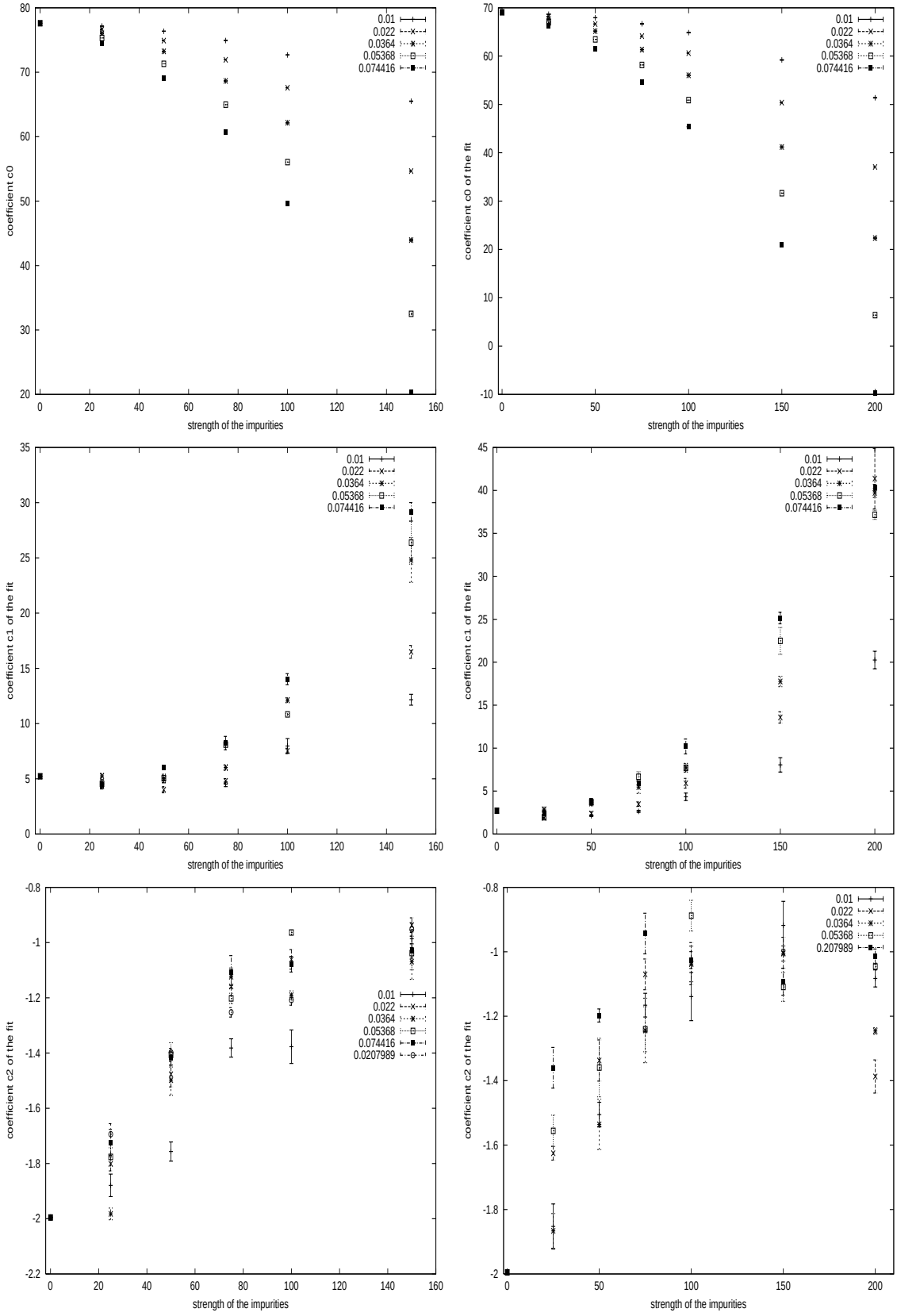

Figure 4.31: The left figures are the result of the fit against $c_0 + c_1 L^{c2}$ for an A-step. The right ones for a B-step.

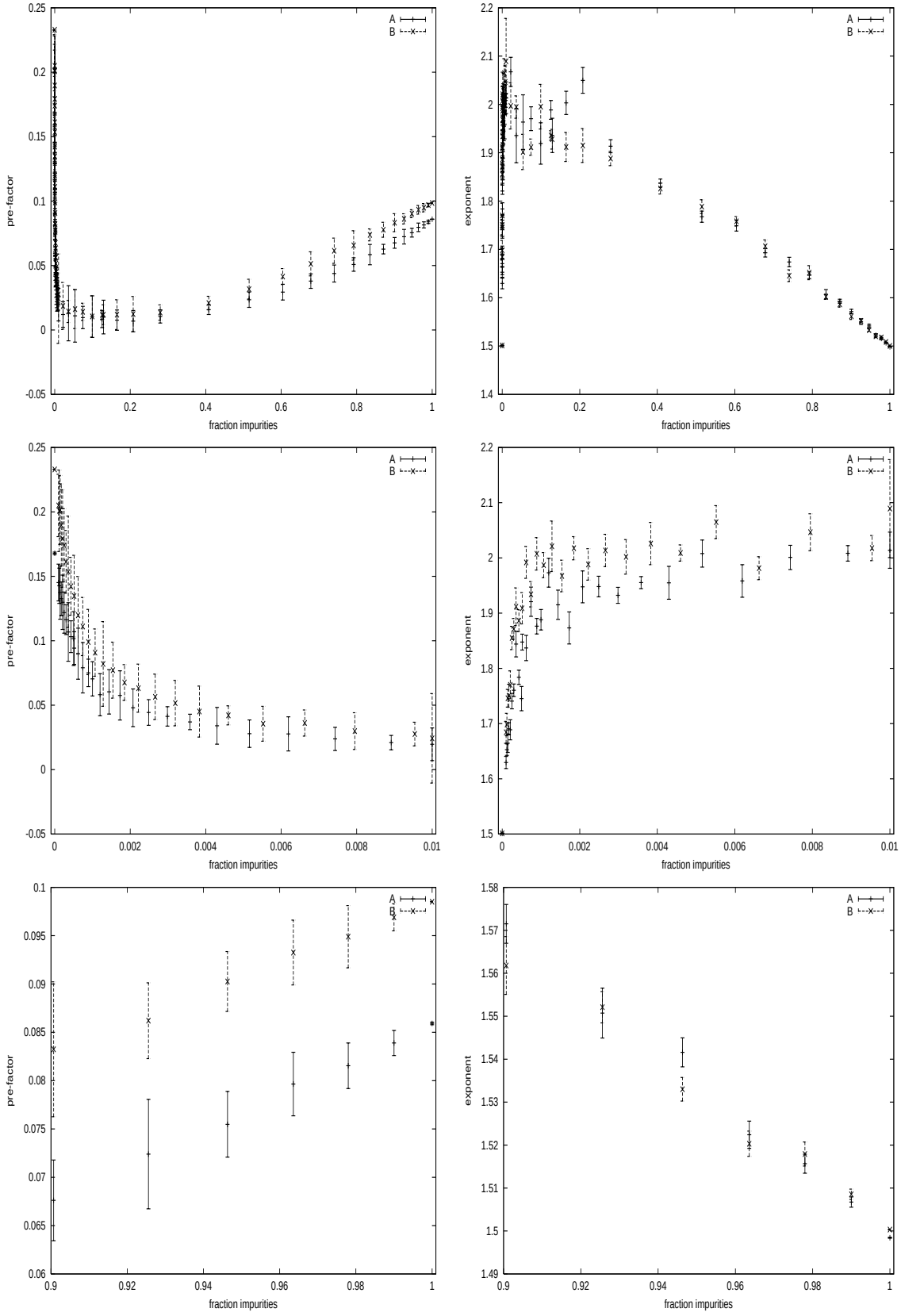

Figure 4.32: The pre-factor and the effective exponent of a near-facet shape, for a crystal in equilibrium for both A-steps and B-steps. The strength of the impurities is -150 meV.

We also tried to fit the step free energy against the function $f(L) = f_0 + \frac{f_1}{L} + \frac{f_2}{L^2} + \frac{f_3}{L^3}$. If we do this, we face the problem that our width can only take values of the form $\frac{k}{2}$ with $k \in \mathbb{N}$. For small L, we have therefore only a few points. This makes the determination of the $\frac{1}{L^3}$-term rather difficult. If we have determined $f(L)$ we can use equations 2.53 and 2.55 to determine the equilibrium crystal shape. We tried to fit this shape against a function of the form $k_0 - k_1 (x - x_f)^{k_2}$.

4.2.2 conclusions

We can reproduce the results from the experiments of Bonzel rather well, if we assume that there are no impurities in the crystal, but we have to give the corner energy a rather high value. On the other hand Bonzel et al. find for a lead crystal at $440K$ an sinus like effective exponent between 1.4 and 1.7, depending on the azimuth, for the line profile of the near facet shape. Their pre-factor is also sinus-like, but is in anti-phase with the shape of the sinus of the effective exponent. We do not find this anti-phase. However to obtain an effective exponent larger than 1.5 for the near-facet shape, as found in the experiments, we need impurities.

Remark: Our simulations to determine the difference between A-steps and B-steps are not very reliable. Because of lack of time, the length of our lattice was rather short and furthermore we only had results for rather small widths of the lattice, see 4.10 for the consequences of this.

4.3 test for replica symmetry breaking

We also performed some simulations to check whether the replica symmetry is broken in the model for our simulations. For that purpose, we performed two simulations for the same configuration of the impurities. The only difference between these two simulations was the starting point. By a width of the cylinder of L, one simulations started at $x = 1$ while the other started at $x = \frac{L}{2}$. If the replica symmetry is broken in the model of Kardar, one would expect that only a few minima would determine the properties of the system, see section 2.9. Therefore one can expect that if the starting points are different, the interfaces arrive at different minima, and remain there rather long because the energy to jump to another minimum is relatively large. If we do not have impurities, we have a diffusive process, and therefore it is expected that the probability to end at a position x after a length of order L^2, doesn't depend anymore on the starting point. A strong indication for replica symmetry breaking is therefore a stronger starting point dependence in the probability to end at a position x after a length of order L^2, than at the impurity free case. We calculated in our numerical simulations the following

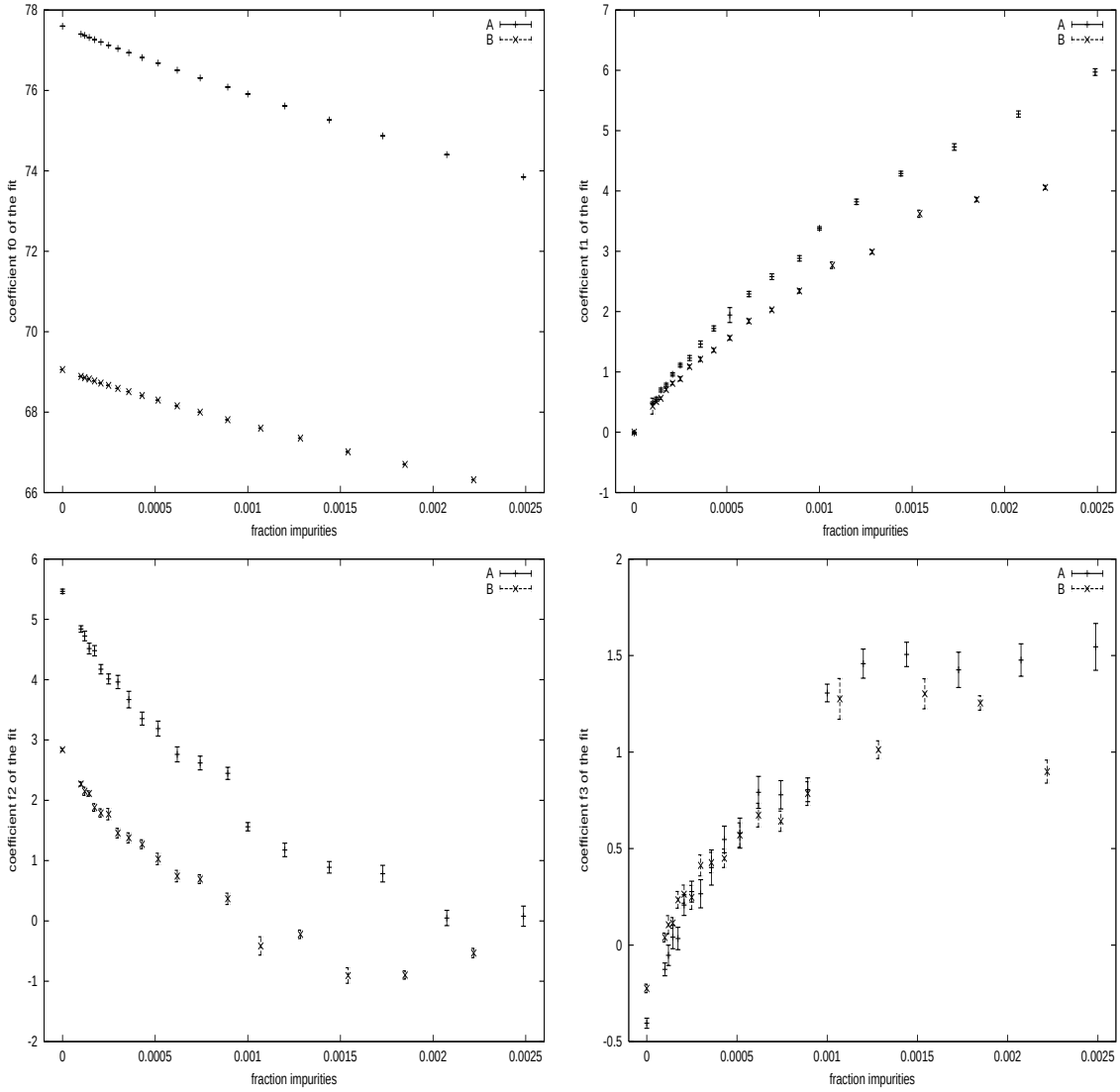

Figure 4.33: results of the fit against $f(L) = f_0 + \frac{f_1}{L} + \frac{f_2}{L^2} + \frac{f_3}{L^3}$

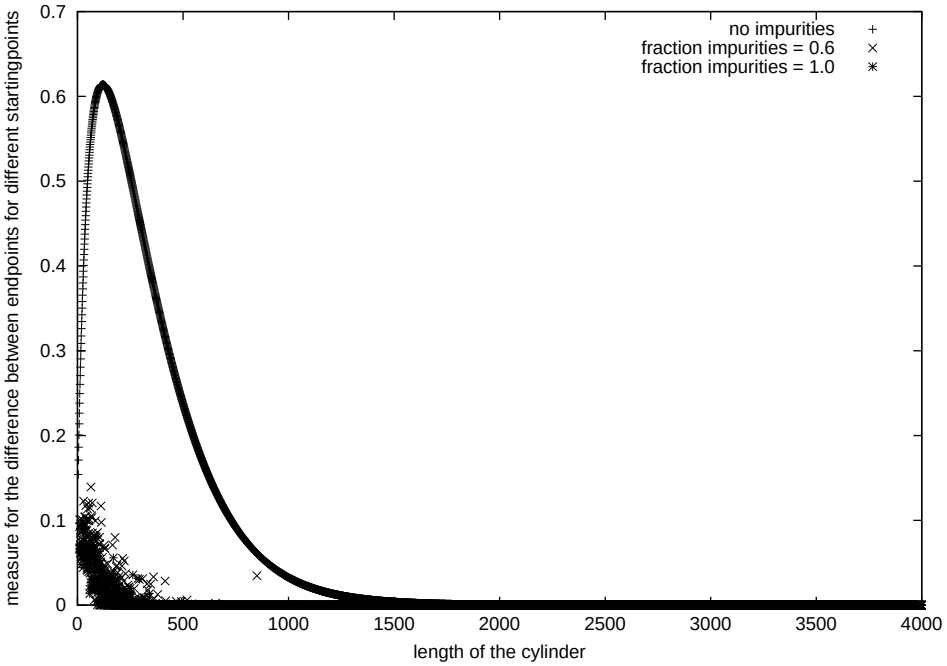

Figure 4.34: $K = 1.0$, mean impurity energy $= 0.1$, $\sigma = 0.3$, width of the cylinder $= 50$

quantity

$$\frac{1}{L}\sum_{x}|Z(x,t) - Z'(x,t)| \tag{4.17}$$

where Z stands for the partition function which started at $x = 1$ and Z' stands for the partition function which started at $x = \frac{L}{2}$. We didn't find any indications for replica symmetry breaking in our numerical simulations. See Figure 4.3 for a typical example of the results of our simulations. We performed this simulations for different kinds of parameters.For instance we performed the same simulation, but now for a different width of the cylinder, see Figure 4.3 We also performed simulations in which we changed the parameters. These simulations gave qualitative the same results. In all cases $\frac{1}{L}\sum_{x}|Z(x,t) - Z'(x,t)|$ converged fast to zero and therefore we didn't find any indication for replica symmetry breaking.

4.4 renormalization

We would like to find out which sets of parameters (μ, σ, K) give the same step free energy. Therefore we tried to perform some real space renormalization. For the model we are working with this means that we are coarse-graining in the length direction of the cylinder. We consider two unit lengths in the model as one unit length in the

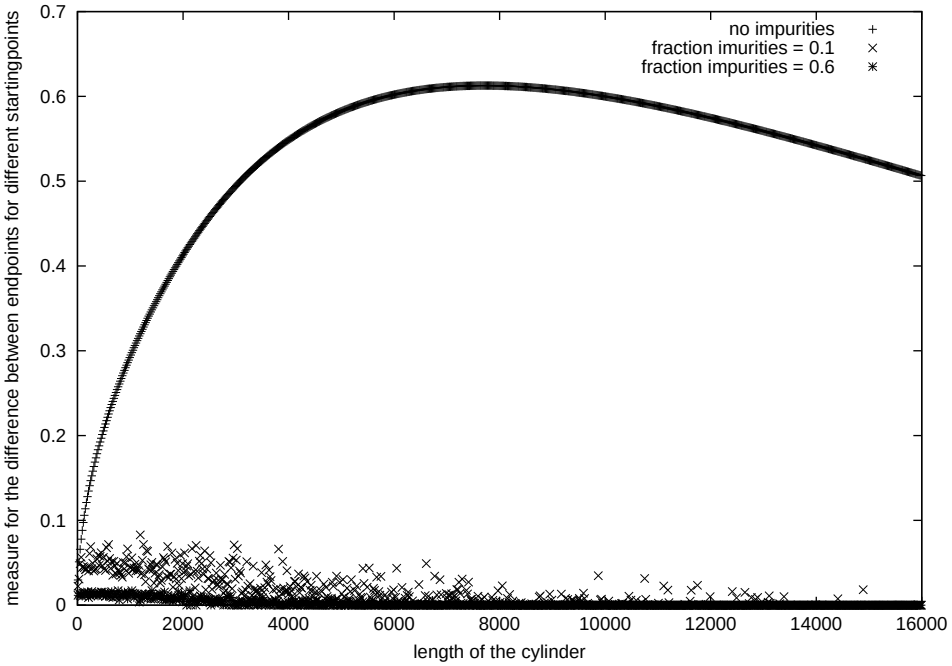

Figure 4.35: $K = 1.0$, mean impurity energy $= 0.1$, $\sigma = 0.3$, width of the cylinder $= 400$

renormalized model. If we apply equation (4.2) twice we get (still in the unrenormalized model):

$$\begin{aligned} Z(x,t) = \; & e^{-\beta\mu(x,t)}\left\{Z(x-1,t-1)e^{-\beta K} + Z(x,t-1) + Z(x+1,t-1)e^{-\beta K}\right\} = \\ & e^{-\beta\mu(x,t)}\{ \\ & Z(x-2,t-2)e^{-2\beta K}e^{-\beta\mu(x-1,t-1)} + \\ & Z(x-1,t-2)\left(e^{-\beta K}e^{-\beta\mu(x-1,t-1)} + e^{-\beta K}e^{-\beta\mu(x,t-1)}\right) + \\ & Z(x,t-2)\left(e^{-2\beta K}e^{-\beta\mu(x-1,t-1)} + e^{-\beta\mu(x,t-1)} + e^{-2\beta K}e^{-\beta\mu(x+1,t-1)}\right) + \\ & Z(x+1,t-2)\left(e^{-\beta K}e^{-\beta\mu(x,t-1)} + e^{-\beta K}e^{-\beta\mu(x+1,t-1)}\right) + \\ & Z(x+2,t-2)e^{-2\beta K}e^{-\beta\mu(x+1,t-1)}\} \end{aligned}$$

If we assume that $K \gg 1$ terms proportional to $e^{-2\beta K}$ become small, and therefore we neglect them. That gives:

$$\begin{aligned} Z(x,t) = \; & e^{-\beta\mu(x,t)}\{ \\ & Z(x-1,t-2)\left(e^{-\beta K}e^{-\beta\mu(x-1,t-1)} + e^{-\beta K}e^{-\beta\mu(x,t-1)}\right) + \\ & Z(x,t-2)e^{-\beta\mu(x,t-1)} \\ & Z(x+1,t-2)\left(e^{-\beta K}e^{-\beta\mu(x,t-1)} + e^{-\beta K}e^{-\beta\mu(x+1,t-1)}\right)\} \end{aligned}$$

If we choose

$$\begin{aligned} \tilde{\mu}(x,\tilde{t}) &= \mu(x,t) + \mu(x,t-1) \\ \tilde{\sigma} &= \sqrt{2}\sigma \\ \tilde{K} &= -\tfrac{1}{\beta}\log\left[e^{-\beta K}\left\{1 + e^{-\beta\mu(x-1,t-1)+\beta\mu(x,t-1)}\right\}\right] \end{aligned} \tag{4.18}$$

we get the same kind of model but now with half its length, but $\tilde{K}$ becomes t and x dependent. We can approximate the mean value of $\tilde{K}$ with a Taylor-expansion:

$$\begin{aligned} \langle\tilde{K}\rangle &= K - \frac{1}{\beta}\langle\log\left[e^{-\beta K}\left\{1 + e^{-\beta\mu(x-1,t-1)+\beta\mu(x,t-1)}\right\}\right]\rangle \\ &= K - \frac{1}{\beta}\int_{-\infty}^{+\infty} dx \int_{-\infty}^{+\infty} dy \frac{1}{2\pi\sigma^2} e^{-\frac{(x-\mu)^2}{2\sigma^2}} e^{-\frac{(y-\mu)^2}{2\sigma^2}} \log\left(1 + e^{-\beta(x-y)}\right) \\ &= K - \frac{1}{\beta}\int_{0}^{\infty} dr \int_{0}^{2\pi} d\theta \frac{r}{2\pi\sigma^2} e^{-\frac{r^2}{2\sigma^2}} \log\left(1 + e^{-\beta r\sqrt{2}\cos\theta}\right) \end{aligned}$$

Now look at the term $\log\left(1 + e^{-\beta r\sqrt{2}\cos\theta}\right)$ for not too big r. (For large r the contribution to the integral will be very small due to the term $e^{-\frac{r^2}{2\sigma^2}}$). Writing $\alpha = \beta r\sqrt{2}\cos\theta$ we get:

$$\log\left(1 + e^{-\alpha}\right) = \log 2 + \log\left(1 + \left\{\frac{1}{2}e^{-\alpha} - \frac{1}{2}\right\}\right)$$

If we use the Taylor expansions

$$\log(1+\epsilon) = \sum_{k=1}^{\infty} -\frac{(-\epsilon)^k}{k} \quad \text{and} \quad e^{\epsilon} = \sum_{k=0}^{\infty} \frac{\epsilon^k}{k!}$$

we can write

$$\log\left(1 + e^{-\alpha}\right) = \log 2 - \frac{\alpha}{2} + \frac{\alpha^2}{8} - \frac{\alpha^4}{192} + \frac{\alpha^6}{2880} + \mathcal{O}(\alpha^8)$$

This gives for the expectation of $\tilde{K}$:

$$\tilde{K} = K - \frac{1}{\beta}\left(\log 2 + \frac{(\beta\sigma)^2}{4} - \frac{(\beta\sigma)^4}{16} + \frac{(\beta\sigma)^6}{24}\right) \tag{4.19}$$

For the parameters we used most, the new parameters are listed in table (4.12). Although in the renormalized model the energy associated with a kink is not constant, but fluctuates, we assume that this has little effect on the step free energy. We have the following reason for that: The fluctuations in $\tilde{K}$ do not fluctuate much. In the set

Table 4.12:

	old parameters	renormalized parameters
length	10000000	5000000
energy of a transverse step	K	K-0.715
mean impurity energy	0.1	0.2
variance in impurity energy	0.3	0.424

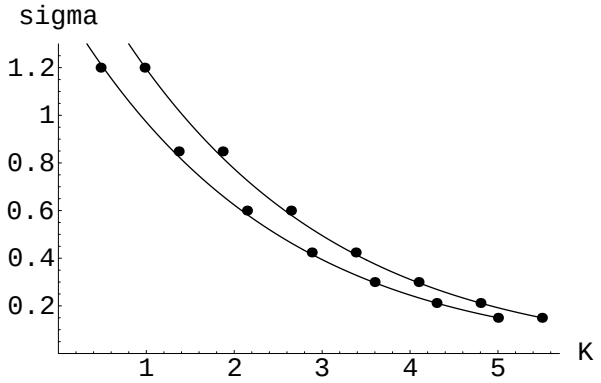

Figure 4.36: renormalization flow lines: Points on the same line will give approximately (see text) the same step free energy. The mean impurity energy is implicitly present in this figure, because an increase in σ by a factor $\sqrt{2}$ coincides with a simultaneous increase of the mean impurity energy μ by a factor 2

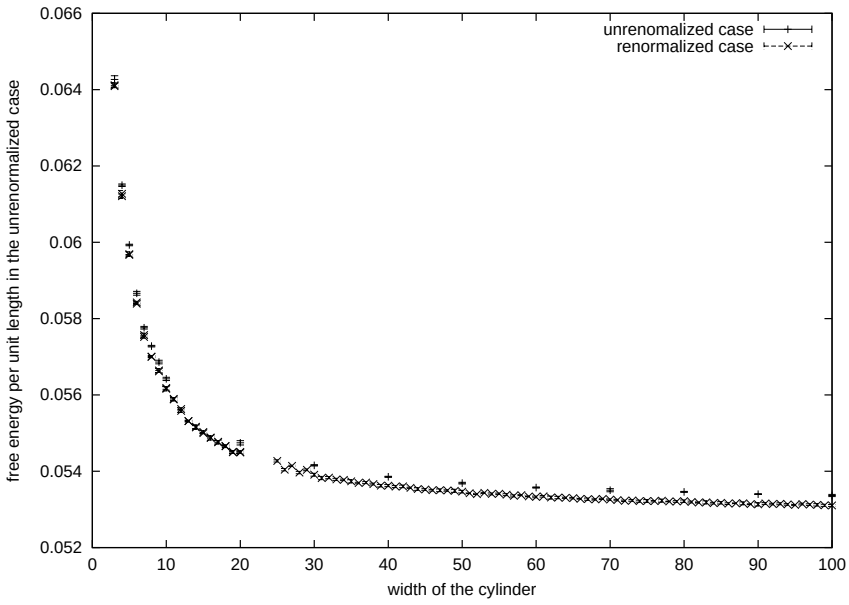

Figure 4.37: unrenormalized case: $K = 5$, $\mu = 0.1$ and $\sigma = 0.3$ renormalized case: $K = 4.284$, $\mu = 0.2$, $\sigma = 0.424$

of parameters we used most, with $\beta = 1$ and $\sigma = 0.3$ the rms of $\tilde{K}$ is 0.21 which is twice as small as the fluctuations in the impurity energy $\tilde{\mu}$. Furthermore the model will also with fluctuations in $\tilde{K}$ remain in the same equivalence class. Therefore we neglect fluctuations in $\tilde{K}$ in the renormalized model. On this way we get different sets in parameter space which are connected by renormalization, see Figure (4.36). We see that the energy of a transverse step becomes smaller, and therefore in the renormalized model the step looks less stiff. That is exactly what is expected because in the case with $K \gg 1$ the probability to have a kink to the right (or left) in the renormalized case is twice as big as in the unrenormalized case.

This calculations is restricted to values of K which are not too small, because otherwise two successive transverse steps must be taken into account. This follows also from numerical simulations. We performed calculations for the original model with $K = 2$ and $K = 5$, and also for the renormalized parameters. The results are plotted in Figure 4.37 and 4.38

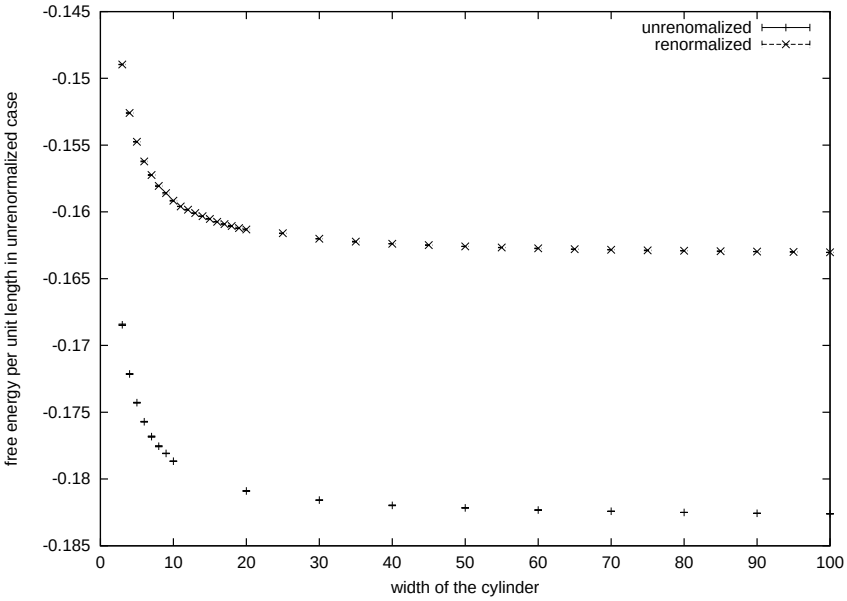

Figure 4.38: unrenormalized case: $K = 2$,$\mu = 0.1$ and $\sigma = 0.3$ renormalized case: $K = 1.284$, $\mu = 0.2$, $\sigma = 0.424$

Chapter 5

appendix

5.1 Proof of the reverse of summation in (2.9)

In the theory, on page 9, we would like to reverse the order of summation. The rather straightforward calculation is shown below.

$$\sum_{(ij)}\left(\sum_{a=1}^{n} s_i^a s_j^a\right)^2 = \sum_{i=1}^{N}\sum_{j=i+1}^{N}\sum_{a=1}^{n}\sum_{b=1}^{n} s_i^a s_j^a s_i^b s_j^b$$

$$= \tfrac{1}{2}\sum_{i=1}^{N}\sum_{j=1}^{N}\sum_{a=1}^{n}\sum_{b=1}^{n} s_i^a s_j^a s_i^b s_j^b - \tfrac{1}{2}\sum_{i=1}^{N}\sum_{a=1}^{n}\sum_{b=1}^{n}\left(s_i^a s_i^b\right)^2$$

$$= \tfrac{1}{2}\left(2\sum_{(ab)}\sum_{i=1}^{N}\sum_{j=1}^{N} s_i^a s_j^a s_i^b s_j^b + \sum_{a=1}^{n}\sum_{i=1}^{N}\sum_{j=1}^{N}\left(s_i^a s_j^a\right)^2\right) - \tfrac{1}{2}\sum_{i=1}^{N}\sum_{a=1}^{n}\sum_{b=1}^{n} 1$$

$$= \sum_{(ab)}\left(\sum_{i=1}^{N} s_i^a s_i^b\right)^2 + \tfrac{1}{2}\sum_{a=1}^{n}\sum_{i=1}^{N}\sum_{j=1}^{N} 1 - \tfrac{1}{2}\sum_{i=1}^{N}\sum_{a=1}^{n}\sum_{b=1}^{n} 1$$

$$= \sum_{(ab)}\left(\sum_{i=1}^{N} s_i^a s_i^b\right)^2 + \tfrac{1}{2}nN^2 - \tfrac{1}{2}Nn^2$$

5.2 Proof of equation (2.12)

We would like to prove the following equation we use on page 9.

$$\text{to prove:}\quad \sum_{\{\mathbf{s}\}}\exp\left[\sum_{(ab)} c_{ab}\sum_{i=1}^{N} s_i^a s_i^b\right] = \left(\sum_{\{\mathbf{s}\}}\exp\left[\sum_{(ab)} c_{ab} s_a s_b\right]\right)^N$$

where the first summation, $\sum_{\{\mathbf{s}\}}$, goes over all the 2^{nN} configurations of the spin-variables s_i^a, which are ± 1, and the second summation goes over the 2^n configurations of the spin-variables S_a which are also ± 1, and c_{ab} is a constant dependent on a and b.

For $N = 1$ the equation is evidently true. For $N > 1$ one can write:

$$\sum_{\{\mathbf{s}\}} \exp\left[\sum_{(ab)} c_{ab} \sum_{i=1}^{N} s_i^a s_i^b\right] = \sum_{\{\mathbf{s_1}\}} \sum_{\{\mathbf{s_2}\}} \dots \sum_{\{\mathbf{s_N}\}} \exp\left[\sum_{(ab)} c_{ab} \left(s_1^a s_1^b + s_2^a s_2^b \dots s_N^a s_N^b\right)\right]$$
$$= \sum_{\{\mathbf{s_1}\}} \exp\left[\sum_{(ab)} c_{ab} s_1^a s_1^b\right] \sum_{\{\mathbf{s_2}\}} \exp\left[\sum_{(ab)} c_{ab} s_2^a s_2^b\right] \dots \sum_{\{\mathbf{s_N}\}} \exp\left[\sum_{(ab)} c_{ab} s_N^a s_N^b\right]$$
$$= \left(\sum_{\{\mathbf{s_1}\}} \exp\left[\sum_{(ab)} c_{ab} s_1^a s_1^b\right]\right)^N = \left(\sum_{\{\mathbf{S}\}} \exp\left[\sum_{(ab)} c_{ab} S^a S^b\right]\right)^N$$

The last equality sign stresses the equivalence of the replica by removing the replica-index. Although nothing specials happens, it looks like we loose many degrees of freedom. This is due to the fact that taking the N'th power of a summation, is equivalent to the product of N times the summation with for each summation another index.

5.3 Proof of equation (2.44)

We have that:

$$\exp\left[ink_j L\right] = \prod_{\substack{\beta=1 \\ \beta\neq j}}^{N} \prod_{\alpha=1}^{n-1} \frac{ik_\beta - ik_j - 2\alpha\kappa}{ik_\beta - ik_j + 2\alpha\kappa} \tag{5.1}$$

We can add a factor $\exp\left[2\pi i n_j\right]$ with $n_j \in \mathbb{N}$ to the right-hand-side, because the factor is equal to 1. Taking differences of the logarithms of both sides for adjacent momenta gives:

$$in\left(k_{j+1} - k_j\right) L = 2\pi\left(n_{j+1} - n_j\right) i +$$
$$\sum_{\substack{\beta=1 \\ \beta\neq j \\ \beta\neq j+1}}^{N} \sum_{\alpha=1}^{n-1} \log\left[\frac{ik_\beta - ik_{j+1} - 2\alpha\kappa}{ik_\beta - ik_{j+1} + 2\alpha\kappa}\right] - \log\left[\frac{ik_\beta - ik_j - 2\alpha\kappa}{ik_\beta - ik_j + 2\alpha\kappa}\right] +$$
$$\sum_{\alpha=1}^{n-1} \log\left[\frac{ik_j - ik_{j+1} - 2\alpha\kappa}{ik_j - ik_{j+1} + 2\alpha\kappa}\right] - \log\left[\frac{ik_{j+1} - ik_j - 2\alpha\kappa}{ik_{j+1} - ik_j + 2\alpha\kappa}\right]$$

The ground state is obtained if we choose the n_j's as closely spaced as possible, that means $n_{j+1} - n_j = 1$, see [31]

The logarithms are purely imaginary and we can write:

$$in\left(k_{j+1} - k_j\right) L = 2\pi i - \sum_{\beta=1}^{N} \sum_{\alpha=1}^{n-1} 2i \arctan\left[\frac{k_\beta - k_{j+1}}{2\kappa\alpha}\right] - 2i \arctan\left[\frac{k_\beta - k_j}{2\kappa\alpha}\right]$$

Now make an Taylor-expansion of the first arctan. It gives:

$$in\left(k_{j+1}-k_j\right)L = 2\pi i - 2i\sum_{\beta=1}^{N}\sum_{\alpha=1}^{n-1}\frac{2\kappa\alpha}{4\kappa^2\alpha^2+\left(k_\beta-k_j\right)^2}\left(k_j-k_{j+1}\right)$$

Rewriting the previous equation gives:

$$n = \frac{2\pi}{L\left(k_{j+1}-k_j\right)} + \frac{1}{L}\sum_{\beta=1}^{N}\sum_{\alpha=1}^{n-1}\frac{4\kappa\alpha}{4\kappa^2\alpha^2+\left(k_\beta-k_j\right)^2}$$

In the limit $L\to\infty$ and $N\to\infty$ with the wall-density $r = N/L$ constant, we have that:

$$\frac{1}{L\left(k_{j+1}-k_j\right)} \to \rho(k)$$
$$\frac{1}{L}\sum_{\beta=1}^{N} \to \int dk\rho(k)$$

Therefore we can write:

$$2\pi\rho(k) = n - \int_{-k_F}^{+k_F} dk'\rho(k')F_n(k-k') \tag{5.2}$$

with the kernel:

$$F_n(k) = \sum_{\alpha=1}^{n-1}\frac{4\kappa\alpha}{4\kappa^2\alpha^2+k^2} \tag{5.3}$$

The Fermi wave number k_F follows from the relation:

$$\int_{-k_F}^{+k_F} dk\rho(k) = \frac{N}{L} = r \tag{5.4}$$

Our aim is to take the $n\to 0$ limit and therefore we rewrite equation (5.2) as:

$$\int_{-k_F}^{+k_F} dk'\rho(k')G_n(k-k') = 1 \tag{5.5}$$

with

$$\begin{aligned} G_n(k) &= \frac{1}{n}\left(2\pi\delta(k) + \sum_{\alpha=1}^{n-1} \frac{4\alpha\kappa}{k^2 + 4\alpha^2\kappa^2}\right) \\ &= \frac{1}{n}\int_{-\infty}^{+\infty} dy \exp\left[iky\right] \sum_{\alpha=0}^{n-1} \exp\left[-2\alpha\kappa|y|\right] \\ &= \frac{1}{n}\int_{-\infty}^{+\infty} dy \exp\left[iky\right] \frac{1-\exp\left[-2\kappa n|y|\right]}{1-\exp\left[-2\kappa|y|\right]} \end{aligned} \tag{5.6}$$

where we used the geometrical serie for the last equality sign. This expression can be continued to $n \to 0$. We get:

$$\begin{aligned} G_0(k) :&= \lim_{n\to 0} G_n(k) = \int_{-\infty}^{+\infty} dy \exp\left[iky\right] \frac{2\kappa|y|}{1-\exp\left[-2\kappa\,|y|\right]} \\ &= 4\kappa \frac{\partial}{\partial k} \int_{0}^{+\infty} \frac{\sin ky}{1-\exp\left[-2\kappa y\right]} \end{aligned} \tag{5.7}$$

The last equation is only finite for all k if $\kappa < 0$ and we get:

$$G_0(k) = \frac{\partial}{\partial k}\left\{\frac{2\kappa}{k} + \pi \coth\left[\frac{\pi k}{2\kappa}\right]\right\} \tag{5.8}$$

In the low-density limit,$\frac{\kappa}{r} \gg 1$, we can write $G_0(k)$ as

$$G_0(k) = \frac{\partial}{\partial k}\frac{4\kappa}{k} \tag{5.9}$$

In this low-density limit, the momentum-density function $\rho(k)$ is given by:

$$\rho(k) = \frac{\sqrt{k_F^2 - k'^2}}{4\pi\kappa} \tag{5.10}$$

That $\rho(k)$ is indeed a solution of the integral-equation (5.5) in the low-density approximation (and with $n \to 0$) is proved in the rest of this section.

$$I(k) := \int_{-k_F}^{k_F} dk' \rho(k') G_0(k-k') = \frac{\mathbf{P}}{\pi}\int_{-k_F}^{k_F} dk' \frac{\sqrt{k_F^2 - k'^2}}{4\pi\kappa}\frac{\partial}{\partial k}\frac{4\kappa}{k-k'}$$

The partial derivative to k can be replaced by the partial derivative to $-k'$. Then we can perform partial integration. This gives:

$$I(k) = \frac{\sqrt{k_F^2 - k'^2}}{\pi(k'-k)}\Big|_{-k_F}^{k_F} + \frac{\mathbf{P}}{\pi}\int_{-k_F}^{k_F} dk' \frac{1}{k'-k}\frac{k'}{\sqrt{k_F^2-k'^2}}$$
$$= \frac{\mathbf{P}}{\pi}\int_{-k_F}^{k_F}\frac{dk'}{\sqrt{k_F^2-k'^2}} + k\frac{\mathbf{P}}{\pi}\int_{-k_F}^{k_F}\frac{dk'}{(k'-k)\sqrt{k_F^2-k'^2}}$$

The first term can be calculated with the aid of the substitution $k' = k_F \sin\theta$. We obtain that the first term is equal to 1. The second term is finite because we take the principal part. Now we can make the substitution $k' = k_F\frac{1-t^2}{1+t^2}$. This gives for the second term ($I_2(k)$):

$$I_2(k) = \frac{2k}{\pi}\mathbf{P}\int_0^\infty \frac{dt}{(k_F-k)-(k_F+k)t^2}$$

This can be written as:

$$I_2(k) = \frac{k}{\pi}\mathbf{P}\int_0^\infty dt\left\{\frac{1}{\sqrt{k_F-k}-\sqrt{k_F+k}t} + \frac{1}{\sqrt{k_F-k}+\sqrt{k_F+k}t}\right\}\frac{1}{\sqrt{k_F-k}}$$

The pole is now at the point $t = \sqrt{\frac{k_F-k}{k_F+k}}$. But because we take the principal value we can integrate over the singularity and we obtain:

$$I_2(k) =$$
$$\frac{k}{\pi\sqrt{k_F-k}}\left\{\frac{-1}{\sqrt{k_F+k}}\log\left|\sqrt{k_F-k}-\sqrt{k_F+k}t\right| + \frac{1}{\sqrt{k_F+k}}\log\left|\sqrt{k_F-k}+\sqrt{k_F+k}t\right|\right\}\Big|_0^\infty =$$
$$\frac{k}{\pi\sqrt{{k_F}^2-k^2}}\left\{\log\left|\frac{\sqrt{k_F-k}+\sqrt{k_F+k}t}{\sqrt{k_F-k}-\sqrt{k_F+k}t}\right|\right\}\Big|_0^\infty = 0$$

Therefore the momentum density function $\rho(k) = \frac{\sqrt{k_F^2-k^2}}{4\pi\kappa}$ satisfies the integral equation.

Bibliography

[1] S. Surnev, K. Arenhold, P. Coenen, B. Voigtländer, H.P. Bonzel, and P. Wynblatt. Scanning tunneling microscopy of equilibrium crystal shapes. *J. Vac. Sci. Technol. A*, 16(3):1059–1065, May/Jun 1998.

[2] H. van Beijeren and I. Nolden. The roughening transition. In W. Schommers and P. von Blanckenhagen, editors, *Structure and Dynamics of Surfaces II*, Topics in Current Physics 43, chapter 7, pages 259–300. Springer-Verlag, 1987.

[3] G. Wulff. Geschwindikeit das wachstums und die auflösung die krystallflächen. *Z. Krist. Mineral.*, 34:449–530, 1901.

[4] J.L. van Hemmen and R.G. Palmer. The thermodynamic limit and the replica method for short-range random systems. *J.Phys.*, A15:3881–3890, 1982.

[5] D. Sherrington and S. Kirkpatrick. Solvable model of a spin -glass. *Phys. Rev. Lett.*, 35:1792–1796, 1975.

[6] D. Sherrington and S. Kirkpatrick. Infinite-ranged models of spin-glasses. *Phys. Rev.*, B17:4384–4403, 1978.

[7] Walter F. Wreszinski and Silvio R.A. Salinas. *Disorder and Competition in Soluble Lattice Models*. World Scientific, 1993.

[8] M. Mézard, G. Parisi, and M. Virasora. *Spin Glass Theory and Beyond*. World Scientific, Singapore, 1986.

[9] Mehran Kardar. Replica bethe ansatz studies of two-dimensional interfaces with quenched random impurities. *Nuclear Physics*, B290:582–602, 1982.

[10] M. Kardar and D.R. Nelson. Commensurate-incommensurate transitions with quenched random impurities. *Phys. Rev. Lett.*, 55:1157, 1985.

[11] M.J.G. Veltman, B.Q.P.J. de Wit, and G. 't Hooft. Lie-groepen in de fysica, 1997. Available at http://www.phys.uu.nl/~thooft.

[12] H.J.F. Knops. Inleiding in de theorie van phase overgangen en kritieke verschijnselen.

[13] H.A. Bethe. Theorie der metalle. erster teil. eigenwerte und eigenfunktionen der linearen atomkette. *Z. Phys.*, 71:No.3–4,205–226, 1931.

[14] Mehran Kardar. Domain walls subject to quenched impurities (invited). *J. Appl. Phys.*, 61 (8):3601–3604, 1987.

[15] D.A. Huse and C.L. Henley. Pinning and roughening of domain walls in ising systems due to random impurities. *Phys. Rev. Lett.*, 54:2708, 1985.

[16] J Villain. Commensurate-incommensurate transition with frozen impurities. *J. Phys. (Paris), Lett.*, 43:551–558, 1982.

[17] M. Kardar, G. Parisi, and Y.C. Zhang. Dynamic scaling of growing interfaces. *Phys. Rev. Lett.*, 56:889, 1986.

[18] J. Krug. Origins of scale invariance in growth processes. *Advances in Physics*, 46:139–282, 1997.

[19] Viktor Dotsenko. *An Introduction to the Theory of Spin Glasses and Neural Networks*, volume 54 of *Lecture Notes in Physics*. World Scientific, 1994.

[20] Giorgio Parisi. Infinite number of order parameters for spin glasses. *Phys. Rev. Lett.*, 43:1754, 1979.

[21] Giorgio Parisi. Replica and glasses. *arXiv:cond-mat/9907052*, 2000, January 26.

[22] Daniel W Stroock. *A Concise Introduction to the Theory Of Integration*. Birkhäuser, second edition, 1994.

[23] Giorgio Parisi, Federico Ricci-Tersenghi, and Juan J. Ruiz-Lorenzo. Dynamics of the four-dimensional spin glass in a magnetic field. *Phys. Rev. B*, 57:13617, 1998.

[24] David Iñiguez, Giorgio Parisi, and Juan J. Ruiz-Lorenzo. Simulation of 3-d ising spin glass model using three replicas: study of binder cumulants. *J.Phys. A*, 29:4337, 1996.

[25] Francesco Guerra. About the overlap distribution in mean field spin glass models. *Int. J. Mod. Phys. B*, 10:1675–1684, 1996. Also available as http://romagtc.roma1.infn.it/papers/lavori/umezawa.ps.

[26] M. Mézard, G. Parisi, N. Sourlas, G. Toulouse, and M. Virasora. Replica symmetry breaking and the nature of the spin glass phase. *J. Physique*, 45:843–854, 1984.

[27] David Sherrington. Spin glasses. *arXiv:cond-mat*, 9806289, 24 June 1998.

[28] Enzo Marinari, Giorgio Parisi, Federico Ricci-Tersenghi, Juan J. Ruiz-Lorenzo, and Francesco Zuliani. Replica symmetry breaking in short range spin glasses: A review of the theoretical foundations and of the numerical evidence. *cond-mat*, 9906076, Jun 1999.

[29] Stefano Ghirlanda and Francesco Guerra. General properties of overlap probability distributions in disorded spin systems. toward parisi ultrametricity. *arXiv:cond-mat*, 9807333, Jul 1998.

[30] Giorgio Parisi and Federico Ricci-Tersenghi. On the origin of ultrametricty. *arXiv:cond-mat*, 9905189v2, Dec 1999.

[31] H.B. Thacker. Exact integrability in quantum field theory and statistical systems. *Rev. Mod. Phys.*, 53,No.2, April 1981.

[32] Michio Jimbo, Tetsuji Miwa, and Mikio Sato. Density matrix of an impenetrable bose gas and the fifth painlevé transcedent. *Physica 1D*, pages 80–158, 1980.

[33] J.J. Sakurai. *Modern Quantum Mechanics*. Addisin-Wesley, revised edition, 1995.

[34] B. de Wit and J. Smith. *Field Theory in Particle Physics*, volume 1. North-Holland Personal Library, 1986.

[35] C.N. Yang. Some exact results for the many-body problem in one-dimension with repulsive delta-function interaction. *Phys. Rev. Lett.*, 19:1312–1315, 1967.

[36] Haye Hinrichsen. Critical phenomena in nonequilibrium systems. *arXiv:cond-mat/0001070*, January 2000.

[37] E.E. Gruber and W.W. Mullins. *J. Phys. Chem. Solids*, 28:875, 1967.

[38] K. Arenhold, S. Surnev, H.P. Bonzel, and P. Wynblatt. Step energetics of pb(111) vicinal surfaces from facet shape. *Surface Science*, 424:271–277, 1999.

[39] S. Surnev, P. Coenen, Voigtländer, H.P. Bonzel, and P. Wynblatt. Flatness and shape of (111) facets of equilibrated pb crystals. *Physical Review B*, 56(19):12131–121334, 1997.

[40] K. Arenhold, S. Surnev, H.P. Bonzel, and P. Wynblatt. Erratum to 'step energetics of pb(111) vicinal surfaces from facet shape' [surf.sci.424(1999)271]. *Surface Science*, 441:223, 1999.

[41] H.P. Bonzel. Private communication, 2000.

[42] Peter J. Feibelman. Ab-initio step- and kink-formation energies on pb(111), 2000. Submitted to Physical Review B.